

# PETROGENESIS AND GEOCHEMISTRY OF FALL HED METEORITES: THREE EUCRITES AND A HOWARDITE

A THESIS SUBMITTED FOR THE COMPLETION OF  
REQUIREMENTS FOR THE DEGREE OF

BACHELOR OF SCIENCE  
(RESEARCH)

BY

HARSH THAKUR  
UNDERGRADUATE PROGRAMME  
INDIAN INSTITUTE OF SCIENCE



UNDER THE SUPERVISION OF  
PROF. RAMANANDA CHAKRABARTI  
INDIAN INSTITUTE OF SCIENCE, BANGALORE

# Declaration

I declare that this work is my own and was carried out in the Lab group of Prof. Ramananda Chakrabarti at Centre for Earth Sciences, Indian Institute of Science, Bangalore, and in the Lab of Dr. Dwijesh Ray at Physical Research Laboratory, Ahmedabad. It was carried out during my undergraduate for a Bachelor of Science (Research) Degree at the Indian Institute of Science from 2019 to 2023. Wherever I have referred to another author's work, I have rightly attributed it in the references. I have acknowledged the people who have helped me in the lab to prepare the samples as well as to load and run them in the respective machines.



.....  
Harsh Thakur  
Undergraduate Program  
Indian Institute of Science  
Bangalore, PIN: 560012

Signature

.....  
Prof. Ramananda Chakrabarti  
Centre for Earth Sciences

# Acknowledgements

I would like to express my sincere gratitude to my thesis advisors for their guidance during this bachelor's thesis. First and foremost, I would like to thank Prof. Ramananda Chakrabarti for his excellent guidance, support, and encouragement throughout my undergraduate school along with this research process, and also for introducing me to meteorites. I would also like to extend my deepest gratitude to Dr. Dwijesh Ray, who made the work possible with his dedication and optimism and made sure I made the most out of my two stays at PRL, Ahmedabad.

During the initial half of this project at PRL, Ahmedabad, I would also thank Dr. Shivani Baliyan for showing me the ropes in the EPMA Lab and Dr. Dipak Panda for his persistent interactions filled with enthusiasm and humour.

The latter half of this project was carried out at RC Lab at CEaS, IISc, where I would like to thank Gaurav for teaching me the process of sample preparation, Soumyaroop and Pritish for teaching me to use the ICP-MS, and Utpalendu for feedbacks regarding the REE modelling. Many thanks to Rishant and Netra for always listening patiently to the latest in my project. Netra's efforts in suggesting ideas and her help in coding the image segmentation program are highly appreciated. I should also acknowledge Sourav and Biswajit for never failing to clear my doubts through their expertise.

This list cannot be complete without thanking all my friends at CEaS, which, along with the people already mentioned, includes Adityam, Arka, Bhanu Priya, Juzer, Kribina, Sanket, Satwik, Srinivas, and Suchismita. They have always kept a friendly and motivating atmosphere.

# Abstract

The howardite, eucrite, and diogenite (HED) clan of meteorites are ultramafic and mafic igneous rocks and impact-generated fragmental debris originating from a highly differentiated asteroid 4 Vesta. The petrology and geochemistry of HEDs shed light on the igneous processes that formed a crust composed of basalts, gabbros, and ultramafic cumulate rocks. Four fall samples including three eucrites (Lakangaon, Piplia Kalan, and Vissannapeta) and one howardite (Lohawat) were studied under EPMA (Electron Probe Microanalyser) to characterise the mineralogy and petrography in order to comprehend the complex thermal metamorphism history of 4 Vesta. Moreover, the bulk compositions of the samples were measured using an ICP-MS (Inductively Coupled Plasma - Mass Spectrometer) to look into the geochemical trends, and the possibility of a chondritic impactor was also explored. Moreover, two-stage and single-stage modelling were carried out in an attempt to generate the REE (Rare Earth Elements) compositions of basaltic and cumulate eucrites, respectively.

# Contents

<b>Declaration</b>	i
<b>Acknowledgements</b>	ii
<b>Abstract</b>	iii
<b>1 Introduction</b>	1
1.1 The HED (Howardite, Eucrite, Diogenite)	
Parent Body . . . . .	2
1.1.1 The HED-Vesta Connection . . . . .	2
1.1.2 4 Vesta and its Properties . . . . .	4
1.2 The HED Suite of Meteorites . . . . .	6
1.2.1 Eucrites . . . . .	6
1.2.2 Howardites . . . . .	12
1.2.3 Diogenites . . . . .	13
1.3 Magma Ocean . . . . .	14
<b>2 Mineralogy and Petrography</b>	24
2.1 Analytical Techniques . . . . .	24
2.2 Lakangaon Eucrite . . . . .	25
2.2.1 Mineral Chemistry . . . . .	25
2.2.2 Accessory Phases . . . . .	30
2.2.3 Conclusions . . . . .	37
2.3 Piplia Kalan Eucrite . . . . .	38
2.3.1 Mineral Chemistry . . . . .	41

2.3.2 Accessory Phases . . . . .	45
2.3.3 Conclusions . . . . .	48
2.4 Vissannapeta Eucrite . . . . .	49
2.4.1 Mineral Chemistry . . . . .	49
2.4.2 Accessory Phases . . . . .	52
2.4.3 Conclusions . . . . .	56
2.5 Lohawat Howardite . . . . .	56
2.5.1 Polymict Diogenite Breccia . . . . .	57
2.5.2 Cumulate Eucrite Clasts . . . . .	57
2.5.3 Basaltic Eucrite Clasts . . . . .	61
2.5.4 Accessory Phases . . . . .	62
2.5.5 Conclusions . . . . .	64
2.6 Clouding . . . . .	64
2.6.1 Identification of Clouding-Causing Phases . . . . .	66
2.6.2 Conclusions . . . . .	73
2.7 References . . . . .	74
<b>3 Bulk Major and Trace Element Composition</b>	<b>81</b>
3.1 Analytical Methods . . . . .	81
3.2 Whole-Rock Chemistry . . . . .	82
3.2.1 Basaltic and Cumulate Eucrites . . . . .	82
3.2.2 Rare Earth Elements (REE) . . . . .	86
3.2.3 Impact Contamination . . . . .	89
3.3 Partial Melting and Fractional Crystallisation . . . . .	96
3.3.1 Batch Melting and Fractional Crystallisation Modelling . . . . .	99
3.4 Conclusions . . . . .	105
3.5 References . . . . .	105
<b>4 Future Outlooks</b>	<b>111</b>
4.1 Ca Isotopic Analyses . . . . .	111
4.2 Sm-Nd Systematics . . . . .	112

4.3	Oxygen Isotopic Compositions . . . . .	114
4.4	Rb-Sr Chronology of Volatile Depletion . . . . .	116
4.5	In-Situ Trace Element Analyses . . . . .	117
4.6	References . . . . .	119

# Chapter 1

## Introduction

In order to comprehend the genesis and evolution of the Solar System, meteorites can be thought as portals into their past. Most of these samples originate from a variety of small parent bodies (asteroids), but a tiny fraction comes from larger bodies like the Moon or Mars. Our ability to study various regions of the Solar System and the stages of its evolution is made possible by the variety of meteorites in terms of composition and age. Meteorites present us with unique source of information about the earliest conditions of the Solar System, including the materials that were involved in the formation of terrestrial planets.

The beginning of meteoritic classification dates back to the 1860s when G. Rose split his collection of meteorites into chondrites (if chondrules were present) and non-chondrites (if chondrules were absent). Later, Maskelyne classified meteorites into siderites (irons), siderolites (stony-irons) and aerolites (stony). Tshemak modified the Rose classification, followed by Brezina modifying the Tshermak-Rose classification (Weisberg et al., 2006). It was in the 20th century when meteorites were first classified based on their chemical composition by Farrington in 1907. His scheme was then modified by Prior in 1920, which was later improved by Mason in 1962. This was the time when meteorites underwent a transition from being collectables to research samples.

Unlike parent asteroids that underwent melting and differentiation after accretion, chondritic stony meteorites are derived from parent asteroids that formed in the protoplanetary disc. Except for the volatile elements, their elemental compositions are comparable to those of the solar photosphere (Scott and Krot, 2005). During the early Solar System's history, chondrules, which are small, almost spherical igneous particles of ferromagnesian silicates and other minerals, rapidly crystallised from liquid or partially molten droplets. Moreover, refractory inclusions that are rich in calcium and aluminium are among the oldest materials we have discovered in chondritic meteorites (CAIs). Minerals that form at extremely high temperatures, such as spinel, melilite, perovskite, hibonite,

anorthite, and forsterite, are included in these inclusions in meteorites. The isotopic composition of calcium-aluminium inclusions, which are sub-millimetre-sized clasts that formed by melting processes within the gas and dust disc, reflects the presolar precursor dust from which they originated (Brearley and Jones, 1998; MacPherson, 2005). Recent U-corrected Pb-Pb dating of CAIs (from Efremovka and Allende carbonaceous chondrites) and chondrules now suggests that they formed simultaneously, at  $4567.30 \pm 0.16$  Ma for CAIs and over a range of  $4567.32 \pm 0.42$  to  $4564.71 \pm 0.30$  Ma for chondrules. Two CAIs from the Efremovka carbonaceous chondrite have been dated (Connelly et al., 2012).

Primitive achondrites and differentiated achondrites are the two categories for the achondritic stony meteorites (Mittlefehldt et al., 1998; Mittlefehldt, 2005). The primitive achondrites have compositions that are somewhat fractionated from chondritic values and yet show signs of their chondritic ancestry, in contrast to the differentiated achondrites, which have igneous textures that have been altered by impact and/or thermal metamorphism (Mittlefehldt, 2005a). The most extensive collection of extraterrestrial crustal igneous rocks that is now available for investigation is the howardite-eucrite-diogenite (HED) meteorite suite (Mittlefehldt et al., 1998; Mittlefehldt, 2005).

## 1.1 The HED (Howardite, Eucrite, Diogenite) Parent Body

### 1.1.1 The HED-Vesta Connection

Based on the similarities in spectral reflectance between Vesta and the eucrite Nuevo-Laredo, the HED meteorites were first associated with asteroid 4 Vesta (hence referred to as Vesta) by McCord et al. (1970) (Figure 1.2). Further research revealed a number of distinguishing characteristics in the reflectance spectrum of meteorites that may be connected to homologous spectra from asteroids (Gaffey, 1976). It has also been done using oxygen isotopes to identify the genetic links of meteorites. Oxygen isotopes have also been employed as a method for identifying the genetic links among meteorites. Eucrites and diogenites have O isotopic fingerprints of  $\Delta^{17}O = 0.241 \pm 0.016\text{‰}$  ( $2\sigma$ ) and  $\Delta^{17}O = 0.246 \pm 0.014\text{‰}$  ( $2\sigma$ ), respectively. According to these studies (Clayton and Mayeda, 1983, 1996; Wiechert et al., 2004; Greenwood et al., 2014), eucrites and diogenites are derived from a single parent body, but are unable to identify the body.

There is, however, still discussion over the Vesta-HED link. According to Wasson (2013), 52% of the V-type asteroids (basaltic asteroids with reflectance spectra similar to Vesta) do not genuinely belong to the Vesta dynamic family, and as a result, the HEDs are not likely to have originated from Vesta. According to this claim, another

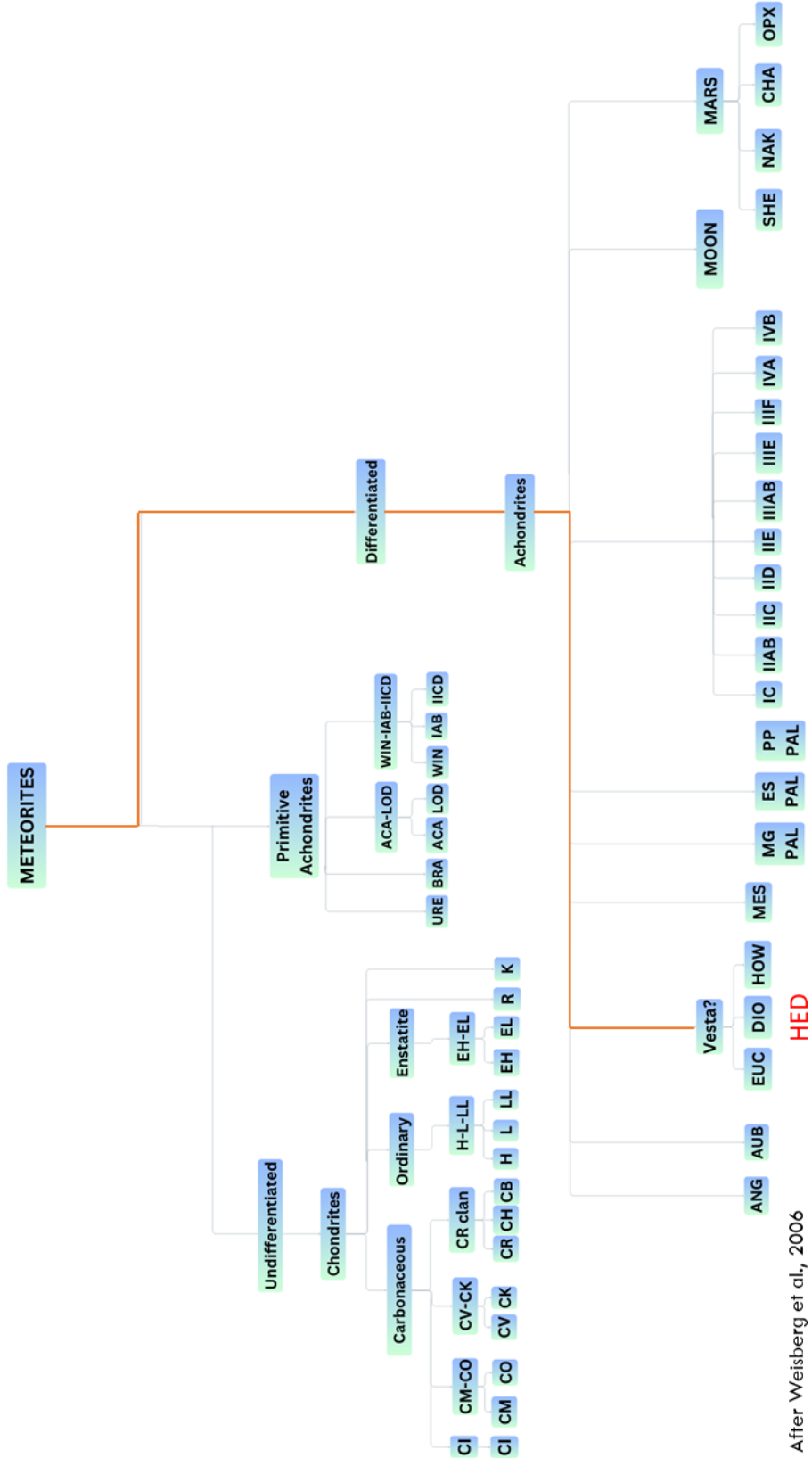


Figure 1.1: Meteorite Classification, after Weisberg et al., 2006. Diagram expressing the systematics of meteorite classification and showing the major meteorite divisions, classes, clans, and groups and relationships among meteorite groups. URE — ureilite, ACA — acapulcoite, LOD — lodranite, ANG — angrite, AUB — aubrite, BRA — brachinitite, WIN — winonaite, HED — howardite-eucrite-diogenite, MES — mesosiderite, MG PAL — main-group pallasite, ES PAL — Eagle Station pallasite, PP PAL — pyroxene pallasite, SHE — shergottite, NAK — nakhlite, CHA — chassignite, OPX — orthopyroxenite.

differentiated asteroid was fragmented and added to the total number of V-type asteroids since the spectra of basaltic V-type asteroids were not sufficiently distinctive to relate all V-type asteroids to Vesta. According to Wasson's (2013) preferred theory, the main group pallasites and IIIAB iron meteorites share a parent body with the HEDs due to similarities in their bulk isotopic compositions of  $^{17}\text{O}$  and  $^{54}\text{Cr}$ . The Wasson (2013) hypothesis is not supported by two significant lines of evidence. Pallasites and HEDs cannot be produced from the same body since the main group pallasites' oxygen isotopic composition differs significantly from that of the HEDs (Greenwood et al., 2015; Greenwood et al., 2014). Second, findings from the Dawn mission strongly support the link between Vesta and HEDs. For instance, measurements of Vesta's Fe/Si and Fe/O weight ratios made by the Gamma Ray and Neutron Detector (GRaND) are comparable to those made by HEDs (De Sanctis et al., 2012b; McSween et al., 2013; Prettyman et al., 2012; Russell et al., 2012).

### 1.1.2 4 Vesta and its Properties

Since Vesta is one of the few planetesimals that has undergone differentiation and has endured intact since its formation early in the Solar System's history, it is of particular interest (Mayne et al., 2009 and references therein). A compelling shift in albedo with rotation was noted by Degewij et al. (1979), who connected this to a corresponding differential in composition and/or surface roughness. Further work by Gaffey backed up these findings (1983, 1997). Using photos from the Hubble Space Telescope, Binzel et al. (1997) created one of the first false-color geological maps of Vesta. Changes in colour on the map correspond to variations in absorption band depth, which represent variations in albedo and, consequently, diversity of geological units, highlighting the distinction between the eastern and western hemispheres. Since Vesta is one of the few planetesimals that has undergone differentiation and has endured intact since its formation early in the Solar System's history, it is of particular interest (Mayne et al., 2009 and references therein).

NASA launched the Dawn space mission on September 27, 2007, with the goal of elucidating the circumstances and processes in the early Solar System through study of Ceres and Vesta, two of the largest asteroids still in tact after their formation. Vesta was chosen as a target for the Dawn mission in part so that researchers could examine the relationship between the asteroid and the HED meteorites. On July 16, 2011, the spacecraft entered Vestan orbit. It remained on orbit for a year, collecting data, before departing for Ceres on September 5, 2012. Yingst et al. (2014) presented a tentative global geological map of Vesta using data from the Dawn mission, greatly enhancing the level of detail of earlier maps and offering a context for Vesta's surface (Fig. 1.3).

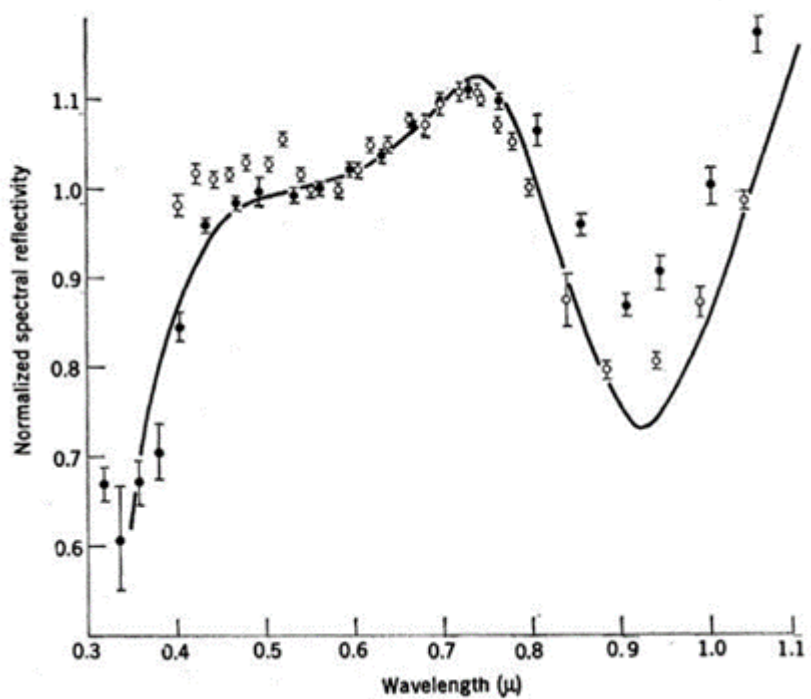


Figure 1.2: Comparison of laboratory measurements of the spectral reflectivity of Nuevo Laredo (solid line) with telescope data for Vesta (open and solid circles). Figure from McCord et al. (1970).

The Framing Camera (FC) on board the Dawn spacecraft provided data at high resolutions that were used to create the most recent geological map. The first map produced had a resolution of 3–9 km/pixel; the second, taken during the Survey orbit, was based on FC data at 200 m resolution and a Digital Terrain Model (DTM) created from orbit image data (Jaumann et al., 2012); and the final iteration used data from the High-Altitude Mapping Orbit (HAMO) with a spatial resolution of 61 m/pixel.

## 1.2 The HED Suite of Meteorites

With the exception of the Earth and the Moon, the HED meteorites have the broadest collection of crustal and sub-crustal rocks that may be studied from any body in the Solar System. Between 2 and 3 percent of all meteorites collected worldwide, 5 percent of all falls, and 60 percent of all achondrites are HEDs (Janots et al., 2012). Over 2767 identified HED achondrites were listed on the Meteoritical Bulletin as of March 2023 (<https://www.lpi.usra.edu/meteor/>).

Most experts believe that a variety of chondritic precursor elements combined to form the HED parent body (Boesenberg and Delaney, 1997; Righter and Drake, 1997a; Ruzicka et al., 1997a; Toplis et al., 2013). For instance, Toplis et al. (2013) proposed that the HED parent body may consist of a mixture of 75% Na-depleted H chondrite and 25% CM chondrite utilising mass-balance and thermodynamic constraints. Models of Vesta’s core size based on siderophile element depletions have been developed (Newsom and Drake, 1982, 1983; Righter and Drake, 1996, 1997). The best estimates place the size of Vesta’s core between 4% and 6% of its mass, with a maximum value of 10% depletion (Ruzicka et al., 1996, 1997a) (Righter and Drake, 1996).

### 1.2.1 Eucrites

The eucrites are separated into basaltic and cumulate eucrites. Also possible are brecciated combinations of these lithologies (Mittlefehldt et al., 1998). A range of crystallisation rates, from quick quenching of near-surface and surface extrusions to delayed crystallisation of deeper magmatic settings, can produce textures that range from being extremely fine to coarse (Duke and Silver, 1967). While brecciation of eucrites as a result of impacts is a common occurrence, brecciation may also be caused by the collapse of a lava tunnel’s top as it cools and contracts or from a’ā lava flows, where a layer of lava fragments builds up at the top and bottom of flows, as seen in Hawaii. According to Ruzicka et al. (1996), the magma ocean on 4 Vesta would have had a higher viscosity, which would have prevented plagioclase from rising to form an anorthositic crust like on the Moon. This is in addition to the minor relative density difference between the magma

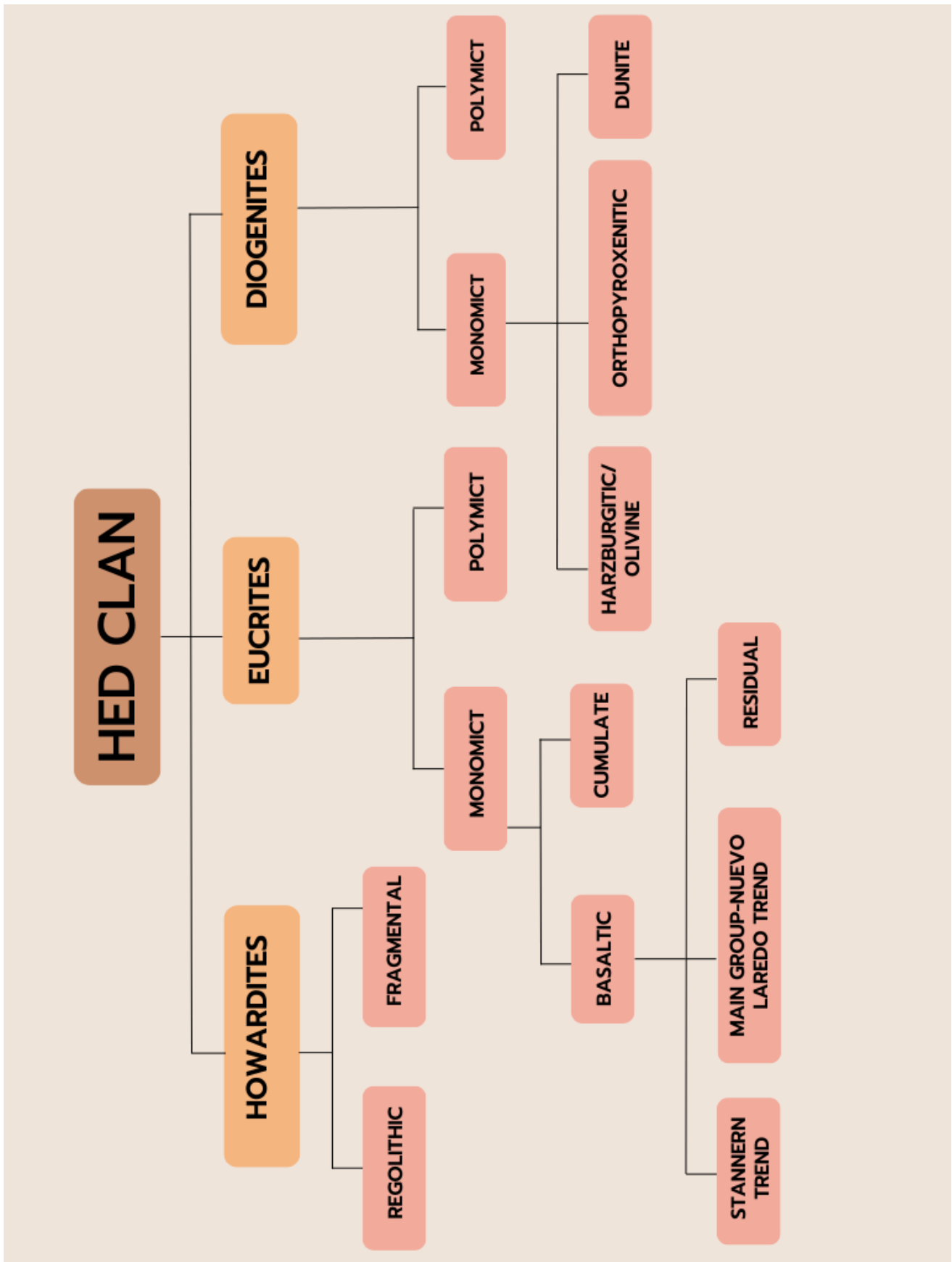


Figure 1.3: Schematic representing the HED clan of Meteorites

ocean and plagioclase. This is demonstrated by the fact that most eucrites generally lack substantial Eu anomalies (Consolmagno and Drake, 1977). Yet, when normalised to a sample from the main-group eucrites, the Stannern-trend eucrites do contain large Eu anomalies (Barrat, et al., 2007). This is explained by the partial melting of the asteroid's crust, which resulted in melts that contaminated main-group eucritic magmas (Barrat et al., 2007).

At 4.56 Ga ago, eucrites began to evolve, and the majority of them underwent metamorphosis at temperatures of about 800°C (Bogard, 2003). These equilibrated basaltic eucrites have undergone metamorphic temperatures, and as a result, their mineral chemistry now reflects those temperatures. For instance, the original core-to-rim zoning in pyroxene, which developed under slow cooling conditions, has changed to a more uniform composition. Eucrites frequently brecciate and heat up, which may be related to impacts (Marchi et al., 2012; Turrini, 2013).

### Cumulate Eucrites

The cumulate eucrites, such as the Moama cumulate eucrite described by Lovering in 1975, are coarse-grained gabbros that often include roughly equal proportions of calcic plagioclase and low-Ca pyroxene, which is typically pigeonite. Based on modal abundances, the cumulate eucrites are further separated into the feldspar- and orthopyroxene-cumulate eucrites (Delaney et al., 1984b). Comparatively to other eucrites, cumulate eucrites have greater Mg/(Mg+ Fe)\*100 ratios (Mg#), lower abundances of incompatible trace elements, and REE patterns with prominent positive Eu anomalies that can be explained by plagioclase accumulation, according to Barrat (2004). The parental melts were unlike those of normal eucrites in that they possessed substantial light REE (LREE) enrichment, according to trace element analyses of pyroxene and plagioclase in cumulate eucrites by Ma and Schmitt (1979), Pun and Papike (1995), Pun et al. (1997), and Hsu and Crozaz (1997).

When compared to non-cumulate eucrites, cumulate eucrites have a restricted range in Fe/Mg and Wo values but a wide range in Mn/Fe with low Fe (Mayne et al., 2009). Furthermore, the Or (Orthoclase:  $KAlSi_3O_8$ ) concentration of plagioclase in any of the 29 unbreciated eucrites investigated (Mayne et al., 2009), including three with a cumulate texture, was no higher than  $Or_5$ . Overall plagioclase compositions, for the 29 unbreciated eucrites, are calcic and range of An<sub>73–96</sub> (Anorthite:  $CaAl_2Si_2O_8$ ) (Mayne et al., 2009), comparable to the ranges of Delaney et al. (1984c) and Mittlefehldt (1998), of An<sub>65–94</sub> and An<sub>75–93</sub>, respectively.

All of the HED meteorites contain low-Ca pyroxenes, and basaltic eucrites have pigeonite, which indicates that the lava cooled very quickly. For example, pigeonite converts

into orthopyroxene when cooling occurs more slowly (Mittlefehldt et al., 1998). Typically, the pyroxenes have an equigranular texture. Minor minerals include chromite, and accessories can include troilite, phosphate, ilmenite, silica polymorphs, and metal (Mittlefehldt et al., 1998). As a whole, most eucrites exhibit a variety of chromite/ulvöspinel compositions, although the compositions of individual meteorites are consistent (Mittlefehldt et al., 1998; Mayne et al., 2009). Little inclusions of phosphate from the apatite species also occur as an accessory mineral in the pyroxene (Delaney et al., 1984a). According to Mittlefehldt and Lindstrom (1993), the cumulate eucrite Y-791195 may have originated from a basaltic eucrite magma similar to Sioux County after 80% crystallisation because it has a bulk incompatible element composition that is intermediate between that of Moore County and Serra de Magé. This suggests that Y-91195 is a cumulate from a parent melt that is similar to Nuevo Laredo, as suggested earlier by Warren and Kallemeij (1992).

In addition to providing an estimate of the depth of burial, the thickness of the exsolution lamellae in pyroxene can be used to calculate the most recent cooling rate of the rocks (Miyamoto and Takeda, 1993; Miyamoto et al., 2001; Brizi and Mellini, 1992; Weinbruch and Müller, 1995; Watanabe et al., 1985).

If lamellae growth is diffusion regulated, lamellae width is typically proportional to the inverse square root of the cooling rate. Based on the thickness of the augite exsolution lamellae and the compositional gradients of Ca in pyroxenes, Miyamoto and Takeda (1993) calculated the depth of burial of the Serra de Magé and Moore County cumulate eucrites to be 7-8 km. In cumulate eucrites, pigeonite was the initial pyroxene with augite exsolution occurring later. In certain cases, this progressed to inversion to orthopyroxene with additional augite exsolution (Mittlefehldt et al., 1998). Where pigeonite is Fe-free or Fe-low, its temperature stability field is higher. Pigeonite's crystallisation stability field is related to the magma's Mg content (Yang and Foster, 1972). Pigeonite's low-temperature limit is 900° C where Fe/Mg is around 1. Seldom retained in slowly cooling intrusive igneous rocks, pigeonite may have inverted into orthopyroxene plus augite based on textural evidence (e.g., Nesse, 2004). Papike (1998) advises probing the cores of pyroxenes in the examination of pyroxenes (for REE such as La, Ce, Nd, Sm, Eu, Dy, Er and Yb and other elements such as Sr, Y and Zr), i.e. the parts of the crystals that are least likely to have reacted with any trapped melt or other cumulus phases during subsolidus reactions that would affect any melt modelling studies.

## Basaltic Eucrites

Noncumulate basaltic eucrites are typically monomict brecciated or unbrecciated, made up of fine to medium grained mineral and lithic fragments, and are typically embedded in a fragmental matrix (Mittlefehldt et al., 1998). Low-Ca pyroxenes with plagioclase

ranging from bytownite to anorthite make up the basaltic eucrites (Mittlefehldt et al., 1998). Pigeonite is the pyroxene and typically has exsolved augite (high-Ca pyroxene) lamellae. Individual basaltic eucrites' plagioclase grains can exhibit wide variations in anorthite concentration (Mittlefehldt et al., 1998). Pyroxenes, which make up basaltic eucrites, are Fe-rich, demonstrating their ferroan, more evolved, melt origin.

Brecciated basaltic eucrites can be monomict or polymict; the polymict breccias appear to form a continuous sequence into howardites; Delaney et al. (1983) proposed that howardites include a 10% diogenite component, whereas polymict eucrites contain more than 90% eucritic material (Delaney et al., 1984c). Nonetheless, the frequent appearance of shock structures within minerals supports at least a portion of impact effects. It has been proposed that the observed brecciation may be attributable to both volcanic processes as well as an impact origin (Duke and Silver, 1967). According to evidence from noble gas, polymict eucrites sample a greater variety of lithologies from the HED parent body than monomict breccias (Delaney et al., 1984c). According to a study of the clasts in the Petersburg polymict eucrite breccia (Buchanan and Reid, 1996), the eucritic melts that served as the breccia's parent material were heterogeneous.

Clasts of diogenites, cumulate eucrites, and basaltic eucrites make up polymict eucrites (Mittlefehldt et al., 1998; Delaney et al., 1984c; Duke and Silver, 1967). According to Nockolds et al. (1978), basaltic eucrites exhibit subophitic to ophitic (basaltic) textures, indicating relatively rapid cooling and the simultaneous crystallisation of its parts. Comparing eucrites to diogenites, which are often Mg, Cr-rich, eucrites are typically rich in Na, Al, P, Ca, Ti and incompatible trace elements (Mittlefehldt and Lindstrom, 1993). Due to the fact that basaltic eucrites have Ce and Eu concentrations that are 8 and 50 times higher than diogenites, respectively, these authors have also demonstrated that Ce and Eu are sensitive markers of the amount of eucritic material in polymict breccias. Inhomogeneous sampling, however, can make it difficult to distinguish polymict breccias from howardites because clast compositions can vary in small samples, which can skew the chemical fingerprints, warn Mittlefehldt and Lindstrom (1993). Delaney et al. (1984c) made a similar observation about the heterogeneous nature of polymict eucrite breccias, noting that while their REE patterns are typically close to  $10 \times \text{CI}$  and are similar to the flat REE patterns of eucrites, some samples with low REE abundances ( $\sim 8 \times \text{CI}$ ) tend to have positive Eu anomalies and those samples rich in REE ( $>15 \times \text{CI}$ ) have negative Eu anomalies. According to Delaney et al. (1984c), the observed variations in REE patterns are caused by the mixing of various eucritic clast forms and do not, therefore, represent processes of trace element/major element fractionation.

Studies of polymict brecciated eucrites by Pun and Papike (1996) indicated that the original crystallisation sequence was 1) pigeonite followed by pigeonite and augite, and 2) simultaneous crystallisation of pigeonite and plagioclase; with the onset of plagioclase

crystallisation being accompanied by increasing Ti/Al ratios in the pyroxene rims as Al is taken up by the crystallising plagioclase. A study of 29 unbreciated eucrites (Mayne et al., 2009) provided additional evidence for the two-stage crystallisation process. Pyroxene with variable Cr and Al at relatively constant Ti crystallised before plagioclase, whereas pyroxene co-precipitating with plagioclase had relatively constant Cr with variable Ti and Al. Pyroxene exhibits both tendencies, demonstrating that it crystallised continuously both before and after plagioclase (Mayne et al., 2009).

The ratio of light rare earth elements (LREE) to heavy rare earth elements (HREE) increases in pyroxenes from core to rim due to two factors: 1) Ca-rich pyroxene rims can accommodate more LREE, and 2) More HREEs are accommodated in the early formed pigeonite, resulting in a residual melt that is enriched in LREEs. This trend was also noted by Pun and Papike (1996). The Nb/Yb ratio in unequilibrated pyroxenes, which has a positive correlation with Fe/(Fe + Mg), serves as an example of this trend. The Mn/Fe ratio in pyroxene has been utilised to distinguish planetary origin (Papike et al., 2003), however the 29 unbreciated eucrites investigated by Mayne et al. (2009) have a far wider range (under 20 to almost 45). As their TiO<sub>2</sub> levels rise at high temperatures, eucrite spinels can also provide useful information (Arai et al., 1998). Hence, Ti-enrichment in spinels might be a sign that they were exposed to high metamorphic temperatures (Yamaguchi et al., 1997a; Yamaguchi, 2000). In unbreciated eucrites, ilmenite is also a typical accessory mineral.

Eucrites can be either unequilibrated (unmetamorphosed) or equilibrated (metamorphosed), where any original chemical zoning in pyroxene crystals is equilibrated across the crystal profile. Ordinary eucrites, also known as monomict noncumulate eucrites, include the main-group Nuevo Laredo trend (such as Juvinas) and the Stannern trend (Warren and Jerde, 1987; Keil, 2002). Preliminary studies on the REE patterns of eucrites led Consolmagno and Drake (1977) to hypothesise that the main group of eucrites might have formed from 10% equilibrium partial melting of a chondritic source, while other eucrites, like the Sioux County eucrite, might have formed from 15% partial melt and Stannern, might have formed from a small 4% partial melt. Sioux County, one of the Main Group eucrites, has a Mg# of 40 and refractory lithophile element abundances of  $\sim 10 \times$  CI chondrites (Mittlefehldt and Lindstrom, 1997). Furthermore, Mayne et al. (2009) hypothesised that the main-group-Nuevo Laredo-trend may combine two or more fractionation trends because they observed significant Ti variation at similar Mg# and variation in Hf at similar Sc contents, both of which are indicative of the composition of multiple magma sources (Mayne et al., 2009).

The two most ferroan (low Mg/Fe) eucrites presently known are Lakangaon and Nuevo Laredo (Warren and Jerde, 1987). The main-group eucrites were first thought to be primordial basalts that had been geochemically separated from the bulk composition

of the eucrite parent body during equilibrium partial melting. However, according to Warren and Jerde (1987), the main-group eucrites are a component of the Nuevo Laredo-trend, which may be a part of a fractional crystallisation series that started with the orthopyroxenite cumulates known as diogenites.

### 1.2.2 Howardites

Howardites are polymict breccias composed of fragments of basaltic and cumulate eucrites, and diogenite material, mixed together in a matrix of fine-grained, fragmental-to-glassy material, and sometimes contain chondritic clasts (Duke and Silver, 1967; Delaney et al., 1984c; Mittlefehldt et al., 1998; McSween, 2000). These breccias consist of lithic clasts embedded in a matrix of fine-grained, fragmented crystal, impact melt, and glasses that may or may not be devitrified and include troilite (Bunch, 1975). Howardites have a higher Ca/Al content than diogenites, according to early geochemical studies by McCarthy et al. (1972), which supports the mixed origin of howardites. Howardites most likely originated as regolith at the surface of an asteroid, where continuous bombardment from asteroidal collisions forced the surface rocks to mix together in a process known as "gardening." According to Metzler and Stöffler (1987), the observed lateral and vertical mixing of lithologies to generate the breccias required numerous large-scale cratering.

The lithologic variety is what gives howardites their distinctively spotted colour. Darker clasts are typically impact melt or carbonaceous chondritic in origin. Howardites' component sizes can range from micrometer-sized mineral fragments in the thinnest matrix to centimeter-sized rock clasts (for example in Kapoeta, Pun et al., 1998). Pyroxene clouding in eucrite clasts of howardites may be caused by the exsolution of finely dispersed inclusions, primarily in the form of chromite or ilmenite blebs in rods or lenses (Harlow and Klementidis, 1980). The heterogeneous nature of the REE signatures, of the different clasts comprising howardites, emphasises their mixed origins (see Mittlefehldt, 1979; Laul and Gosselin, 1990). In order to distinguish the polymict eucrites from the howardites, Delaney et al. (1983) used an arbitrary definition of the criterion based on the amount of magnesian orthopyroxenite (diogenite) component in the meteorite. This was due to the high chemical and mineralogical diversity of polymict basaltic achondrites. According to this definition, howardites are polymict breccias where neither the diogenite component nor the eucrite component make up more than 90% of the meteorite's volume. Mafic clasts in howardites typically feature unzoned pyroxenes, but polymict eucrite clasts more frequently have zoned pyroxene, according to Delaney et al. (1983).

A new subclass of howardites called regolithic howardite is proposed by Warren et al. (2009) in their revaluation of the HED meteorite suite since most howardites have extremely low siderophile levels and just a slight enrichment in Ni/Ir, of  $\sim 2.5$  in the

mantle + crust component. According to the authors, the enrichment in solar-wind noble gases and a distinct enrichment in Ni, glasses, and impactor-chondritic clasts (Warren et al., 2009) distinguished the regolithic howardite sub-class from other howardites, which are fragmental breccias with no indication of near surface residence. Only four of the 104 HED meteorites that the research group examined were defined to be regolithic howardites, and another five were thought to be likely regolithic howardites (Warren et al., 2009). Regolithic howardites could be identified by their  $\text{Al}_2\text{O}_3$  contents of 8 to 9 weight percent, which indicates a 2:1 eucrite:diogenite mixing ratio. Furthermore, the authors propose that some howardites represent a much more recently formed (1 Ga), extremely heterogeneous regolith, and that other howardites represent a regolith that formed early in the history of the parent asteroid as a result of a single large impact that contributed the diogenite material. According to Warren et al. (2009), the early developed regolithic howardites were extensively buried or widely dispersed, therefore only the material that had seen repeated impacts considerably increased in siderophile components. The authors also point out that just four of the howardites they have studied—Kapoeta, Jodzie, Bununu, and Bholghati—are obviously gas-rich and that they are also considerably enriched in siderophile elements like Ir (Warren et al., 2009).

### 1.2.3 Diogenites

The diogenites' mineralogy mostly consists of coarse-grained orthopyroxene, with olivine as a minor component and accessory phases such as troilite, metal, silica, chromite, and rare phosphates as additional components (Mittlefehldt et al., 1998; Mittlefehldt, 2005a). Similar in composition to the low-Ca pigeonite in eucrites, the pyroxene is a Mg-rich hypersthene, but it has a distinct crystal structure as a result of slow cooling. While the major element abundances are homogeneous, Mittlefehldt (2005a) records Mg# varying from 66 (ferroan) to 84 (magnesian) within diogenites (average Mg# between 70 and 73). However, the incompatible element abundances exhibit significant variation.

The majority of diogenites are brecciated and have a reduced oxidation state akin to eucrites. Because it would react with silica minerals to create orthopyroxene, magnesium-rich olivine does not coexist stably with them. As diogenites' pyroxene is more Mg-rich than eucrites' and generated through fractional crystallisation, it is likely that these rocks crystallised from less-fractionated magmas and were concentrated as cumulates (McSween, 2000). Also, the bigger, interlocking pyroxene crystals show that diogenites are plutonic rocks (McSween, 2000). Another possibility is that eucrites are the remains of partial melts with little to no fractionation, which were remelted to form additional magma that crystallised as diogenites (McSween, 2000).

While the cumulate eucrites formed later when the magma was cooling more slowly,

the diogenites formed first (Lugmair and Shukolyukov, 1997; Tera et al., 1997). A longer contact with the melt of the main magma chamber and the formation of a more evolved phase assemblage by a higher degree of crystal fractionation are two factors that Domanik et al. (2005) argue account for the unusually high abundance of phosphates (fluorapatite and REE-bearing whitlockite) in two diogenite meteorites, Manegaon and Roda.

The HED suite's taxonomy has been updated as a result of Beck and McSween's (2010) analysis of diogenites. All ultramafic samples are classified as diogenites in this classification and given one of three qualifying prefixes: dunitic for diogenites with 90% olivine, harzburgitic for olivine + orthopyroxene, and orthopyroxenitic for diogenites that contain orthopyroxene. Additionally, brecciated mixes of these rock types are referred to as polymict, (Beck and McSween, 2010).

### 1.3 Magma Ocean

Mason (1962) provided the first petrogenetic synthesis for the HED suite of lithologies, proposing that they were formed by fractional crystallisation during complete melting of a chondritic parent body. Righter and Drake (1997), Ruzicka et al. (1997), and Warren (1997) also supported the magma ocean hypothesis.

As a result, separation of crystals from a magma will be much less efficient on 4 Vesta than on either the Earth or the Moon (Ruzicka et al., 1996), resulting in a higher fraction of crystal suspension during cooling and any segregation due to gravity only occurring at a higher degree of crystallisation. The surface gravity of 4 Vesta is nearly five orders of magnitude less than that on Earth and nearly four orders of magnitude less than that on the Moon (Righter and Drake, 1997b). Plagioclase crystals would need 1 Ma to ascend just 4 km upward, according to Ruzicka et al. (1996), which would prevent the production of an anorthositic floatation crust like the one that formed on the Moon due to its greater specific gravity. By studying the spectral properties of 4 Vesta, no proof of an anorthosite crust has yet been discovered (De Sanctis et al., 2013).

According to Taylor et al. (1993), on a low-pressure body, a magma ocean would have experienced turbulent convection, preventing crystals that formed close to the magma chamber roof from settling down until the chamber was packed with them. Intriguingly, Taylor et al. (1993) note that while silicate melts travel from hot to cold regions on giant planets, where they crystallise, asteroids have essentially uniformly high temperatures up until the top kilometre. Also, the asteroids' low confining pressure would have facilitated dyke propagation (Taylor et al., 1993). The magma ocean of 4 Vesta would produce a lower mantle rich in pyroxene and olivine and an approximately basaltic (eucritic) upper mantle due to the absence of a major density difference and the existence of turbulent

convection (Ruzicka et al., 1996; Taylor et al., 1993).

The bulk geochemistry of HED meteorites indicates that while 4 Vesta is depleted in volatile elements it has chondritic refractory element abundances (Consolmagno and Drake, 1977; McSween et al., 2011) and that it is relatively reduced (McSween et al., 2011).

While Ghosh and McSween (1998) presented a concept of radiogenic melting throughout practically the whole range of depths, due to the decay of  $^{26}\text{Al}$ , Ikeda and Takeda (1985) proposed a model in which the eucrites formed from a magma ocean only affecting the outer portion of the parent asteroid. A magma ocean on the HED parent body is further supported by Schiller et al. (2011) in their analysis of the mass-independent abundance of  $^{26}\text{Mg}$  in diogenites, which revealed the Mg-isotopic evolution of a large-scale differentiating magma body as evidenced by the rising  $^{27}\text{Al}/^{24}\text{Mg}$  during the brief lifetime of the  $^{26}\text{Al}$  nuclide. These investigations also demonstrate that the HED parent body nearly fully solidified within 2-3 Ma of the magma ocean's initiation.

Diogenites were most likely generated as cumulates from depleted mantle melts where the depletion event was the development of basaltic eucrite melts, according to modelled mineral/melt diogenite partitioning from REE data collected from SIMS (Secondary Ion Mass Spectrometry (Papike, 1996). Diogenites could be orthopyroxene cumulates formed by fractional crystallisation in a magma ocean on the HED parent body, and main-group eucrites may be residual liquids produced within the same chemically evolving magma system, according to a study of major and trace elements in diogenites and eucrites and modelling of magmatic processes Ruzicka et al. (1997a).

Mittlefehldt et al. (2008) modelled both old and new diogenite data to determine whether they were compatible with a global magma origin on the HED parent asteroid. They came to the conclusion that a melt component was necessary to form a better match with the data and that a more complex petrogenesis for 4 Vesta than the existing global melting models was required. Further research by Ghosh (2010) reveals that, according to the magma ocean model, it took around 2 Ma for non-cumulate eucrites to igneous crystallise and about 5 Ma for the residual liquid to completely cool below its solidus.

## References

- Arai, T., Takeda, H., Lofgren, G. E. & Miyamoto, M. (1998). Metamorphic transformations of opaque minerals in some eucrites. Antarctic Meteorite Research 11, 71-91.
- Barrat J.-A. 2004. Determination of parental magmas of HED cumulates: The effects of interstitial melts. Meteoritics & Planetary Science 39(11):1767-1779.

- Barrat, J-A., Yamaguchi, A., Greenwood, R. C., Bohn, M., Cotten, J., Benoit, M. & Franchi, I.A. (2007a). The Stannern trend eucrites: Contamination of main group eucritic magmas by crustal partial melts. *Geochimica et Cosmochimica Acta* 71, 4108-4124.
- Beck, A. W. & McSween, H. Y. Jr. (2010). Diogenites as polymict breccias composed of orthopyroxenite and harzburgite. *Meteoritics & Planetary Science* 45, 850- 872.
- Binzel, R. P., Gaffey, M. J., Thomas, P. C., Zellner, B. H., Storrs, A. D. & Wells, E. N. (1997). Geologic mapping of Vesta from 1994 Hubble Space Telescope Images. *Icarus* 128, 95-103.
- Boesenber, J. S. & Delaney, J. S. (1997). A model composition of the basaltic achondrite planetoid. *Geochimica et Cosmochimica Acta* 61, 3205-3225.
- Bowman, L. E., Spilde, M. N. & Papike, J. J. (1997). Automated energy dispersive spectrometer modal analysis applied to the diogenites. *Meteoritics & Planetary Science* 32, 869-875.
- Brearley, A. J. & Jones, R. H. (1998). Chondritic Meteorites. In: J. J. Papike (ed.), Planetary Materials, Reviews in Mineralogy Mineralogical Society of America, Washington, Volume 36, pp. 3-1–3-398.
- Brizi, E. & Mellini, M. (1992). Kinetic modelling of exsolution textures in igneous pyroxenes. *Acta Vulcanologica*, Marinelli Volume 2, 87-93.
- Buchanan, P. C. & Reid, A. M. (1996). Petrology of the polymict eucrite Petersburg. *Geochimica et Cosmochimica Acta* 60, 135-146.
- Bunch, T. E. (1975). Petrography and petrology of basaltic achondrite polymict breccias (howardites). Lunar Science Conference 6th, Lunar and Planetary Institute, Houston, Texas, USA, 469-492.
- Clayton R. N. and Mayeda T. K. 1983. Oxygen isotopes in eucrites, shergottites, nakhlites, and chassignites. *Earth and Planetary Science Letters* 62(1):1-6.
- Clayton R. N. and Mayeda T. K. 1996. Oxygen isotope studies of achondrites. *Geochimica et Cosmochimica Acta* 60(11):1999-2017.
- Connelly, J. N., Bizzaro, M., Krot, A. N., Nordlund, Å., Wielandt, D.& Ivanova, M. A. (2012). The Absolute Chronology and Thermal Processing of Solids in the Solar Protoplanetary Disk. *Science* 338, 651-655.
- D.W. Mittlefehldt, T.J. McCoy, C.A. Goodrich, A. Kracher, in Planetary Materials, Reviews in Mineralogy, ed. by J.J. Papike, vol. 36 (Mineral. Soc. Am., Washington, 1998), p. 195
- De Sanctis, M. C., Ammannito, E., Capria, M. T., Capaccioni, F., Combe, J. P., Frigeri, A., ... & Russell, C. T. (2013). Vesta's mineralogical composition as revealed by

the visible and infrared spectrometer on Dawn. *Meteoritics & Planetary Science*, 48(11), 2166-2184.

De Sanctis, M. C., Ammannito, E., Capria, M. T., Tosi, F., Capaccioni, F., Zambon, F., Carraro, F., Fonte, S., Frigeri, A., Jaumann, R., Magni, G., Marchi, S., McCord, T. B., McFadden, L. A., McSween, H. Y., Mittlefehldt, D. W., Nathues, A., Palomba, E., Pieters, C. M., Raymond, C. A., Russell, C. T., Toplis, M. J. & Turrini, D. (2012). Spectroscopic Characterization of Mineralogy and Its Diversity Across Vesta. *Science*, 336, 697-700.

Degewij J., Tedesco E., and Zellner B. 1979. Albedo and color contrasts on asteroid surfaces. *Icarus* 40(3):364-374.

Delaney, J. S., O'Neill, C. & Prinz, M. (1984a). Phosphate Minerals in eucrites. *Lunar and Planetary Science 15th*, Lunar and Planetary Institute, Houston, Texas, USA, 208-209.

Delaney, J. S., O'Neill, C. & Prinz, M. (1984b). Two magma types in the eucrite Bouvante. *Lunar and Planetary Science Conference 15th*, Lunar and Planetary Institute, Houston, Texas, USA, 210-211.

Delaney, J. S., Prinz, M. & Takeda, H. (1984c). The Polymict Eucrites. *Proceedings of the Fifteenth Lunar and Planetary Science Conference, Part 1.Journal of Geophysical Research*, Vol. 89, Supplement, Lunar and Planetary Institute, Houston, Texas, USA.

Delaney, J. S., Takeda, H., Prinz, M., Nehru, C. E. & Harlow, G. E. (1983). The nomenclature of polymict basaltic achondrites. *Meteoritics* 18, 103-111.

Domanik, K. J., Sideras, L. C. & Drake, M. J. (2005). Olivine and Ca-phosphate in the diogenites Manegaon and Roda. *Lunar and Planetary Science 36, #2128*, Lunar and Planetary Institute, Houston, Texas, USA (CD-ROM).

Duke, M. B., & Silver, L. T. (1967). Petrology of eucrites, howardites and Mesosiderites. *Geochimica et Cosmochimica Acta*, 31(10), 1637-1665.

Gaffey, M. J. (1976). Spectral reflectance characteristics of the meteorite classes. *Journal of Geophysical Research*, 81(5), 905-920.

Gaffey, M. J. (1983, January). The asteroid (4) Vesta: Rotational spectral variations, surface material heterogeneity, and implications for the origin of the basaltic achondrites. In 14th Lunar and Planetary Science Conference (Vol. 497, p. 14).

Gaffey, M. J. (1997). Surface lithologic heterogeneity of Asteroid 4 Vesta. *Icarus* 127, 130-157.

Ghosh, A. & McSween, H. Y. Jr. (1998). A thermal model for the differentiation of asteroid 4 Vesta, based on radiogenic heating. *Icarus* 134, 187-206.

Ghosh, A. (2010). A thermal evolution model of a magma ocean on asteroid 4 Vesta. *Lunar and Planetary Science* 41, #2570, Lunar and Planetary Institute, Houston, Texas, USA (CD-ROM).

Greenwood, R. C., Barrat, J. A., Scott, E. R., Haack, H., Buchanan, P. C., Franchi, I. A., ... & Burbine, T. H. (2015). Geochemistry and oxygen isotope composition of main-group pallasites and olivine-rich clasts in mesosiderites: Implications for the “Great Dunite Shortage” and HED-mesosiderite connection. *Geochimica et Cosmochimica Acta*, 169, 115-136.

Greenwood, R. C., Barrat, J. A., Yamaguchi, A., Franchi, I. A., Scott, E. R., Bottke, W. F., & Gibson, J. M. (2014). The oxygen isotope composition of diogenites: Evidence for early global melting on a single, compositionally diverse, HED parent body. *Earth and Planetary Science Letters*, 390, 165-174.

Harlow, G. E. & Klementidis, R. (1980). Clouding of pyroxene and plagioclase in eucrites: Implications for post-crystallization processing. *Lunar and Planetary Science* 11, Lunar and Planetary Institute, Houston Texas, USA, 1131-1143.

Hsu W. and Crozaz G. 1997. Mineral chemistry and the petrogenesis of eucrites: II. Cumulate eucrites. *Geochimica et Cosmochimica Acta* 61(6):1293-1302.

Ikeda, Y., & Takeda, H. (1985). A model for the origin of basaltic achondrites based on the Yamato 7308 howardite. *Journal of Geophysical Research: Solid Earth*, 90(S02), C649-C663.

Janots E., Gnos E., Hofmann B., Greenwood R., Franchi I., Bermingham K., and Netwing V. 2012. Jiddat al Harasis 556: A howardite impact melt breccia with an H chondrite component. *Meteoritics & Planetary Science* 47(10):1558-1574.

Jaumann R., Williams D. A., Buczkowski D. L., Yingst R. A., Preusker F., Hiesinger H., Schmedemann N., Kneissl T., Vincent J. B., Blewett D. T., Buratti B. J., Carsenty U., Denevi B. W., De Sanctis M. C., Garry W. B., Keller H. U., Kersten E., Krohn K., Li J.-Y., Marchi S., Matz K. D., McCord T. B., McSween H. Y., Mest S. C., Mittlefehldt D. W., Mottola S., Nathues A., Neukum G., O’Brien D. P., Pieters C.

Keil, K. (2002). Geological history of asteroid 4 Vesta: The “smallest terrestrial planet”. *Asteroids* iii, 573.

Laul, J-C. & Gosselin, D. C. (1990). The Bholghati howardite: Chemical study. *Geochimica et Cosmochimica Acta* 54, 2167-2175.

Lovering, J. F. (1975). The Moama eucrite – a pyroxene-plagioclase adcumulate. *Meteoritics* 10, 101-114.

Lugmair, G. W. & Shukolyukov, A. (1997). 53Mn-53Cr isotope systematics of the HED parent body. *Lunar and Planetary Science* 28, #1240, Lunar and Planetary Insti-

tute, Houston, Texas, USA (CD-ROM).

Ma, M-S. & Schmitt, R. A. (1979). Genesis of the Cumulate Eucrites Serra de Mage and Moore County: A Geochemical Study. *Meteoritics* 14, 81-89.

MacPherson, G. J. (2005). Calcium-Aluminium-rich Inclusions in Chondritic Meteorites. In: Davis, A. M. (ed.). *Meteorites, Comet, and Planets*. Vol. 1., Treatise on Geochemistry. Elsevier-Pergamon, Oxford, pp 201-246.

Marchi, S., McSween, H. Y., O'Brien, D. P., Schenk, P., De Sanctis, M. C., Gaskell, R., Jaumann, R., Mottola, S., Preusker, F., Raymond, C. A., Roatsch, T. & Russell, C.T. (2012). The Violent Collisional History of Asteroid 4 Vesta. *Science* 336, 690 – 694.

Mason, B. (1962). *Meteorites*. Wiley, New York, 274 pp.

Mason, B. (1963). The Hypersthene Achondrites. *American Museum Novitates* 2155, 1- 14.

Mayne, R. G., McSween, H. Y. Jr., McCoy, T. J. & Gale, A. (2009). Petrology of the unbreciated eucrites. *Geochimica et Cosmochimica Acta* 73, 794-819.

McCarthy, T. S., Ahrens, L. H. & Erlank, A. J. (1972). Further evidence in support of the mixing model for howardite origin. *Earth and Planetary Science Letters* 15, 86-93.

McCord, T. B., Adams, J. B. & Johnson, T. V. (1970). Asteroid Vesta: Spectral reflectivity and compositional implications. *Science* 168, 1445-1447.

McSween Jr, H. Y., Binzel, R. P., De Sanctis, M. C., Ammannito, E., Prettyman, T. H., Beck, A. W., ... & Dawn Science Team. (2013). Dawn; the Vesta-HED connection; and the geologic context for eucrites, diogenites, and howardites. *Meteoritics & Planetary Science*, 48(11), 2090-2104.

McSween, H. Y. Jr. (2000). *Meteorites and Their Parent Planets*. 2nd Ed. Cambridge University Press, New York, 310 pp.

McSween, H. Y. Jr., Mittlefehldt, D. W., Beck, A. W., Mayne, R. G. & McCoy, T. J. (2011). HED Meteorites and Their Relationship to the Geology of Vesta and the Dawn Mission. *Space Science Reviews* 163, 141-174.

Metzler, K. & Stöffler, D. (1987). Polymict impact breccias on the eucrite parent body: 1. Lithic clasts in some eucrites and howardites. *Lunar and Planetary Science* 29, Lunar and Planetary Institute, Houston, Texas, USA, 641-642.

Mittlefehldt, D. W. & Lindstrom, M. M. (2003). Geochemistry of eucrites: Genesis of basaltic eucrites, and Hf and Ta as petrogenetic indicators for altered Antarctic eucrites. *Geochimica et Cosmochimica Acta* 67, 1911-1935.

Mittlefehldt, D. W. (1979). Petrographic and chemical characterization of igneous lithic clasts from mesosiderites and howardites and comparison with eucrites and diogen-

ites. *Geochimica et Cosmochimica Acta* 43, 1917-1935.

Mittlefehldt, D. W. (2005a). Achondrites. In: Davis, A. M. (ed.). Meteorites, Comet, and Planets. Vol. 1., Treatise on Geochemistry. Elsevier-Pergamon, Oxford, pp 291-324.

Mittlefehldt, D. W. (2008). Meteorite dunite breccia MIL 03443: A probable crustal cumulate closely related to diogenites from the HED parent body. *Lunar and Planetary Science* 39, #1919, Lunar and Planetary Institute, Houston, Texas, USA (CD-ROM).

Mittlefehldt, D. W., McCoy, T. J., Goodrich, C. A., & Kracher, A. (1998). Non-Chondritic Meteorites from Asteroidal Bodies. In J. J. Papike (ed.), *Planetary Materials, Reviews in Mineralogy Volume 36* Mineralogical Society of America, pp 4-2 - 4- 195.

Miyamoto, M. & Takeda, H. (1993). The thickness of eucritic crust in the HED parent body. *Lunar and Planetary Science* 24, Lunar and Planetary Institute, Houston, Texas, USA, 999-1000.

Nesse, W. D. (2004) *Introduction to Optical Mineralogy*. Oxford University Press, New York, 348p.

Newsome, H. E. & Drake, M. J. (1982). The metal content of the eucrite parent body: Constraints from the partitioning behaviour of tungsten. *Geochimica et Cosmochimica Acta* 46, 2483-2489.

Nockolds, S. R., Knox, R. W. & Chinner, G. A. (1978). *Petrology for Students*. Cambridge University Press, Great Britain, pp 435.

Papike, J. J. (1998). Comparative planetary mineralogy: Chemistry of melt-derived pyroxene, feldspar, and olivine. In: Papike, J.J. (ed.), *Planetary Materials, Reviews in Mineralogy Volume 36*, Mineralogical Society of America , pp 7-01 to 7-11.

Papike, J. J., Karner, J. M. & Shearer, C. K. (2003). Determination of planetary basalt parentage: A simple technique using the electron microprobe. *American Mineralogist* 88, 469-472.

Prettyman, T. H., Mittlefehldt, D. W., Yamashita, N., Lawrence, D. J., Beck, A. W., Feldman, W. C., McCoy, T. J., McSween, H. Y., Toplis, M. J., Titus, T. N., Tricarico, P., Reedy, R. C., Hendricks, J. S., Forni, O., Le Corre, L., Li, J-Y., Mizzon, H., Reddy, V., Raymond, C. A. & Russell, C. T. (2012). Elemental Mapping by Dawn Reveals Exogenic H in Vesta's Regolith. *Science* 338, 242-246.

Pun, A. & Papike, J. J. (1995). Ion microprobe investigation of exsolved pyroxenes in cumulate eucrites: Determination of selected trace-element partition coefficients. *Geochimica et Cosmochimica Acta* 59, 2279-2289.

Pun, A. & Papike, J. J. (1996). Unequilibrated eucrites and the equilibrated Juvinas

eucrite: Pyroxene REE systematics and major, minor and trace element zoning. American Mineralogist 81, 1438-1451.

Pun, A., Keil, K., Taylor, G. J. & Weiler, R. (1998). The Kapoeta howardite: Implications for the regolith evolution of the howardite-eucrite-diogenite parent body. Meteoritics & Planetary Science 33, 835-851.

Pun, A., Papike, J. J. & Layne, G. D. (1997). Subsolidus REE partitioning between pyroxene and plagioclase in cumulate eucrites: An ion microprobe investigation. Geochimica et Cosmochimica Acta 61, 5089-5097.

Righter K. and Drake M. J. 1997. A magma ocean on Vesta: Core formation and petrogenesis of eucrites and diogenites. Meteoritics & Planetary Science 32(6):929-944.

Righter, K. & Drake, M. J. (1996). Core Formation in Earth's Moon, Mars, and Vesta. Icarus, 124, 513-529.

Righter, K. & Drake, M. J. (1997a). A magma ocean on Vesta: Core formation and petrogenesis of eucrites and diogenites. Meteoritics and Planetary Science 32, 929-944.

Russell, C. T., Raymond, C. A., Coradini, A., McSween, H. Y., Zuber, M. T., Nathues, A., De Sanctis, M. C., Jaumann, R., Konopliv, A. S., Preusker, F., Asmar, S. W., Park, R. S., Gaskell, R., Keller, H. U., Roatsch, T., Scully, J. E. C., Smith, D. E., Tricarico, P., Toplis, M. J., Christensen, U. R., Feldman, W. C., Lawrence, D. J., McCoy, T. J., Prettyman, T. H., Reedy, V., Sykes, M. E. & Titus, T. N. (2012). Dawn at Vesta: Testing the Protoplanetary Paradigm. Science 336, 684-686.

Ruzicka, A., Snyder, G. A. & Taylor, L. A. (1996). Asteroid 4 Vesta as the HED parent body: Implications for a metallic core and magma ocean crystallization. Lunar and Planetary Institute Technical Report 96-02, Part 1, 23-24.

Ruzicka, A., Snyder, G. A. & Taylor, L. A. (1997a). Formation of eucrites and diogenites in a magma ocean on the HED parent body. Lunar and Planetary Science 28, #1426, Lunar and Planetary Institute, Houston, Texas, USA (CD-ROM).

S. C., Mittlefehldt, D. W., Mottola, S., Nathues, A., Neukum, G., O'Brien, D. P., Pieters, C. M., Prettyman, T. H., Raymond, C. A., Roatsch, T., Russell, C. T., Schenk, P., Schmidt, B. E., Scholten, F., Stephan, K., Sykes, M. V., Tricarico, P., Wagner, R., Zuber, M. T. & Sierks, H. (2012). Vesta's Shape and Morphology. Science 336, 687-690.

Schiller, M., Baker, J., Creech, J., Paton, C., Millet, M-A., Irving, A., & Bizzarro, M. (2011). Rapid Timescales for Magma Ocean Crystallization on the Howardite-Eucrite-Diogenite Parent Body. Astrophysical Journal Letters, 740:L22 (6 pp).

Scott, E. R. D. & Krot, A. N. (2005). Chondrites and their Components. In: Davis, A.M. (ed.). Meteorites, Comet, and Planets. Vol. 1., Treatise on Geochemistry. Elsevier-Pergamon, Oxford, pp 143-200.

- Taylor, G. J., Keil, K., McCoy, T., Haack, H. & Scott, E. R. D. (1993). Asteroid Differentiation: Pyroclastic Volcanism to Magma Oceans. *Meteoritics* 28, 34- 52.
- Toplis M. J., Mizzone H., Monnereau M., Forni O., McSween H. Y., Mittlefehldt D. W., McCoy T. J., Prettyman T. H., De Sanctis M. C., Raymond C. A., and Russell C. T. 2013. Chondritic models of 4 Vesta: Implications for geochemical and geophysical properties. *Meteoritics & Planetary Science* 48(11):2300-2315.
- Turrini, D. (2013, preprint). The primordial collisional history of Vesta: crater saturation, surface evolution and survival of the basaltic crust. *Planetary and Space Science*.
- Warren, P. H. & Jerde, E. A. (1987). Composition and origin of Nuevo Laredo Trend eucrites. *Geochimica et Cosmochimica Acta* 51, 713-725.
- Warren, P. H. (1997). Magnesium oxide-iron oxide mass balance constraints and a more detailed model for the relationship between eucrites and diogenites. *Meteoritics & Planetary Science*, 32(6), 945-963.
- Warren, P. H., & Kallemeyn, G. W. (1992). Further evidence for geochemical diversity, and possible bimodality, among cumulate eucrites (abstract). *Meteoritics* 27, 303-304.
- Wasson, J. T. (2013). Vesta and extensively melted asteroids: Why HED meteorites are probably not from Vesta. *Earth and Planetary Science Letters* 381, 138-146.
- Watanabe, S., Kitamura, M. & Morimoto, N. (1985). A transmission electron microscope study of pyroxene chondrules in equilibrated L-group chondrites. *Earth and Planetary Science Letters* 72, 87-98.
- Weinbruch, S. & Müller, W. F. (1995). Constraints on the cooling rates of chondrules from the microstructure of clinopyroxene and plagioclase. *Geochimica et Cosmochimica Acta* 59, 3221-3230.
- Weisberg M. K., McCoy T. J., and Krot A. N. 2006. Systematics and evaluation of meteorite classification. *Meteorites and the early solar system II* 19.
- Wiechert, U. H., Halliday, A. N., Palme, H. & Rumble, D. (2004). Oxygen isotope evidence for rapid mixing of the HED meteorite parent body. *Earth and Planetary Science Letters* 221, 373-382.
- Yamaguchi, A. (2000). Spinel in basaltic eucrites: implications for crystallization and metamorphic history. *Meteoritics & Planetary Science* 35, A174 (abstr.).
- Yamaguchi, A., Taylor, G. J., Keil, K. & Bogard, D. D. (1997a). Evidence for a large cratering event on the HED parent body (Vesta) 4.5 Ga ago. *Meteoritics & Planetary Science* 32, A144-A155.
- Yang, H-Y. & Foster, W. R. (1972). Stability of iron-free pigeonite at atmospheric pressure. *American Mineralogist*, 57, 1232-1241.

Yingst, R. A., Mest, S. C., Berman, D. C., Garry, W. B., Williams, D. A., Buczkowski, D., ... & Schenk, P. M. (2014). Geologic mapping of Vesta. *Planetary and Space Science*, 103, 2-23.

# **Chapter 2**

## **Mineralogy and Petrography**

### **2.1 Analytical Techniques**

All petrographic characterisation, textural observation, and back-scattered electron (BSE) image analysis of all the polished thick and thin sections were conducted using a Field Emission Probe Microanalyser (FE-EPMA; JEOL 8530F, Japan) with Energy Dispersive X-ray Spectrometer (EDS) and five Wavelength Dispersion Spectrometer (WDS). As opposed to the simultaneous collection employed in EDS, X-rays are filtered by wavelength rather than the energy in a WD spectrometer. Due to its superior wavelength resolution and lower detection limits, a WD detector outperforms an ED detector in quantitative analysis. It is possible to measure the abundance of elements having an atomic number larger than five (Boron) to within 1%. (Reed, 2005). The examination of various elements uses a variety of diffraction crystals. Lithium fluoride (LIF), pentaerythritol (PET), and thallium acid phthalate are common crystals (TAP). The minerals were analysed, and the images were taken using a typical accelerating voltage of 15 keV and 15 nA sample current and beam size of 1 micron. Natural and synthetic mineral standards are used for calibration and include Si (Diopside), Mg (Olivine), Ti (Rutile), Al (Kyanite), Fe (Magnetite), Cr ( $\text{Cr}_2\text{O}_3$ ), Mn (Rhodonite), Na (Albite), K (Orthoclase), P (Apatite), S (Pyrite), Ni (Ni metal), Co (Co metal). Prior to the microprobe analysis, all section mounts were gold coated and then imaged at 40x-140x magnification. The SEM images were pieced together to make a complete map of each section mount.

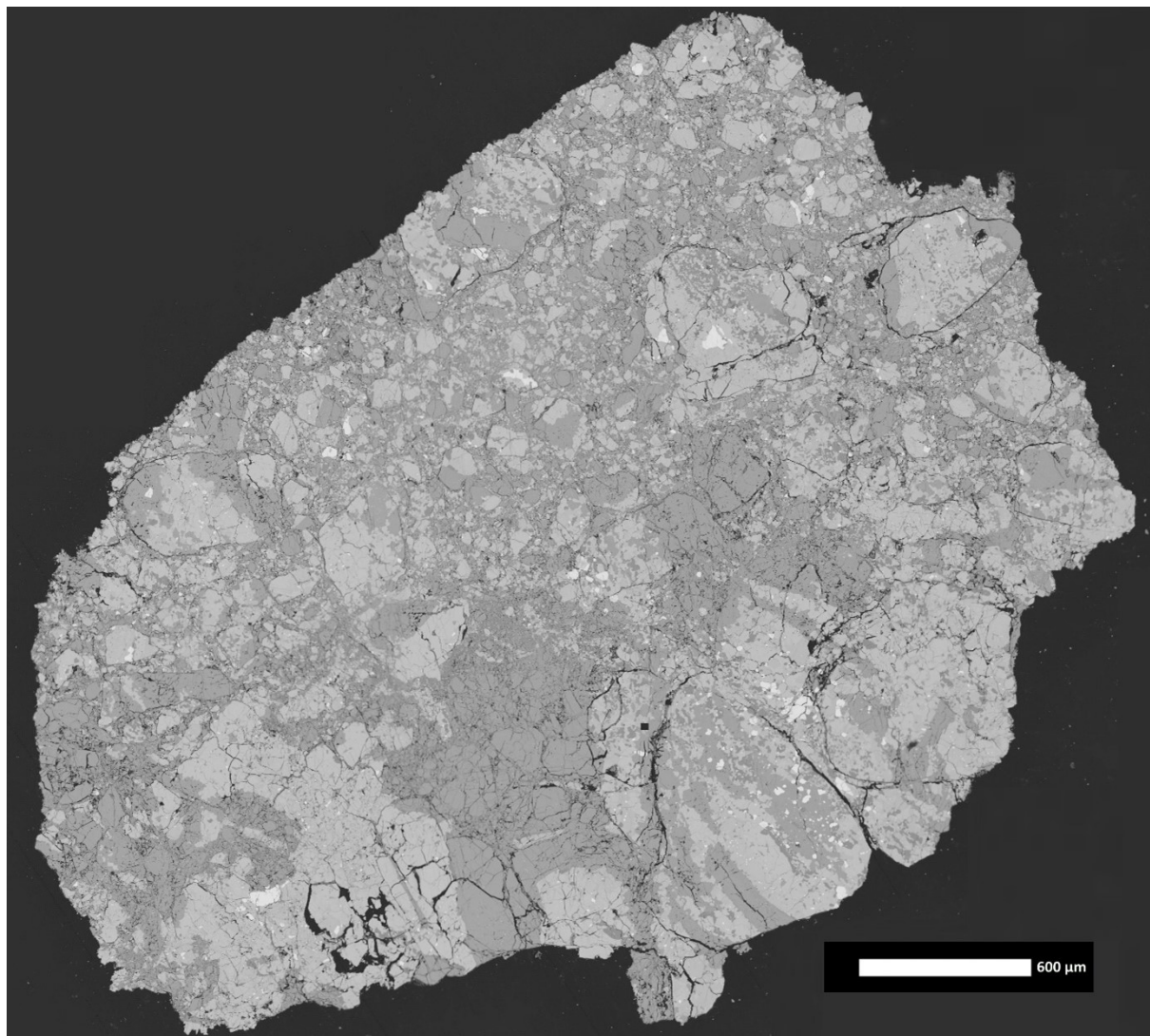
## 2.2 Lakangaon Eucrite

Lakangaon fell on November 24, 1910, in the Nimar region of British India, near present-day Khandwa district, Madhya Pradesh, India, and is one of 261 approved meteorites classified as Eucrite-mmict as of date. After explosions, a dust trail, and a fireball, two shards of a stone were retrieved, weighing a total of 213 g. Lakangaon is a lesser-known eucrite than other eucrites; hence it has not drawn as much attention. Mason et al. (1979) included Lakangaon in their study of pyroxene-plagioclase achondrites, with Hsu and Crozaz (1996) later including it in their study of cumulate vs non-cumulate eucrites. Pyroxenes (both Ca-poor and Ca-rich types) and varied plagioclase are the main components of Lakangaon (mostly bytownite). Warren et al. (1985) deemed Lakangaon as the most Fe-rich eucrite, perhaps because it crystallised later than most Eucrites, as McCarthy et al. (1974) suggested by observing it to be more Fe-O rich.

Though the Lakangaon was described as Fe-rich eucrite in literature, detailed petrography and mineral chemistry were never discussed and explored in detail. Two thick sections of Lakangaon were analysed during the course of this study. Lakangaon, a brecciated basaltic eucrite, is dominated by mafic pyroxene and felsic plagioclase grains. Other accessory minerals include quartz, ilmenite, chromite, and troilite. The overall mineral modes of both thick sections include 36% pyroxene, 59.4% plagioclase + silica, and the accessory minerals like ilmenite, Chromite, and troilite make up 0.9% (Fig. 2.1). There were six major clasts, with a range of mineral composition (Fig. 2.2). The range for pyroxenes, plagioclase, and silica is from 35-60%, 10% to 40%, and a mere 5% to 20%, respectively (Table 2.1). Pyroxenes are typically exsolved in nature; however, zonation is apparently absent. Plagioclase feldspar is mostly calcic and occurs within the clasts as well as in the matrix. Texturally, the clasts resemble brecciated, gabbroic texture. The clasts are mostly subrounded to irregular in shape. Chromite and spinel mainly occur as isolated grains and also as inclusion in pyroxene. Ilmenite also occurs as individual grains, composite grains with chromite or zircon. Silica is present as inclusion, intergrowth with pyroxene and or plagioclase.

### 2.2.1 Mineral Chemistry

The pyroxenes are plotted in the Di-Hd-En-Fs quadrilateral, and their composition ranges from ferrosilite to pigeonite to augite. The compositional trend of pyroxene is linear, as can be seen in Fig. 2.3. The figure also shows the pyroxene trends for Piplia Kalan, Vissannapeta, and various lithologies of Lohawat, for comparison. Pigeonite primarily occurs as exsolution lamellae within the ferrosilite as well as in augite. The fine exsolution texture resulted in intermediate composition primarily due to beam overlap on



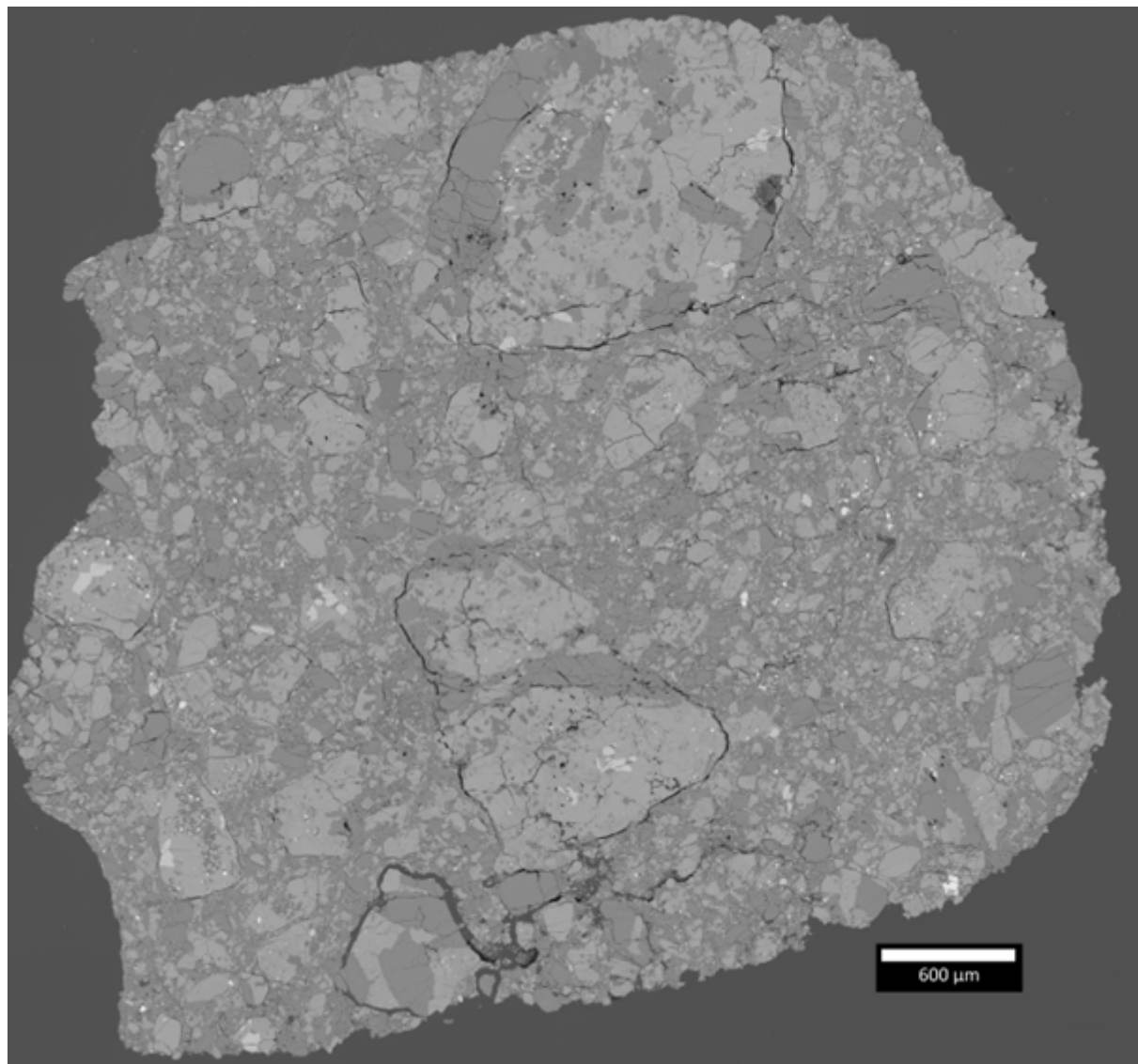


Figure 2.1: Compiled Mosaic of Back-scattered Electron images of both the Lakangao thick sections, taken at 140x. Several major and minor clasts are seen.

	Clast A	Clast B	Clast C	Clast D	Clast E	Clast F
Pyroxene	58%	57.50%	40.60%	60.20%	47.50%	36.60%
Plagioclase	9.70%	19.50%	40.30%	21.10%	37%	34.40%
Silica	19.50%	15%	9.40%	11%	4.80%	21.60%
Accessory minerals (Ilmenite, chromite, troilite, zircon)	4%	1.30%	3%	1.50%	1.80%	2.90%

Table 2.1: The volume percentage of minerals in individual clasts (Calculated using ImageJ software). Pyroxenes and plagioclase together take up 70-75% of every clast. Also, Clast E shows very low silica content.

both pyroxenes, which often became challenging to discriminate the low-Ca and high-Ca compositional ranges. The pyroxene trend for Lakangaon in this pyroxene quadrilateral matches precisely with the Nuevo Laredo trend. The deformed texture of the exsolved pyroxenes is a common sight; the exsolution lamellae width ranges from  $< 0.1 \mu\text{m}$  to  $4 \mu\text{m}$  (Fig. 2.4). The data for pyroxene is presented in Table 2.2.

Takeda and Graham (1991) defined six types of eucrites primarily based on their pyroxenes, where type 1 is a pristine basalt which has suffered very limited subsequent metamorphism, while type 6 has been reheated and extensively metamorphosed (Table 2.3). According to this analysis, Lakangaon falls in type 5 eucrite. The type 5 eucrites contain exsolved pigeonites with homogeneous host composition. For example, Juvinas, Haraiya and Chervony Kut (Takeda et al., 1983b) show no remnants of the original Fe-dominated zoning in their pyroxenes. The pigeonite in Juvinas is clouded extensively and contains precipitated chromites up to  $1.5 \times 0.2 \mu\text{m}$  in size. However, as observed in this study, Lakangaon is only clouded with troilite (Fig. 2.5). More about clouding in plagioclase and pyroxene alongwith the method used to distinguish the clouding-causing minerals, has been discussed in section 2.6 of this chapter.

Plagioclase occurs as separate aggregates as well as plagioclase laths in pyroxenes in Lakangaon (Fig. 2.5). The range is  $\text{An}_{82.19-89.99}$ , and the plagioclase data falls in the bytownite-anorthite field in the plagioclase ternary diagram (Fig. 2.6).

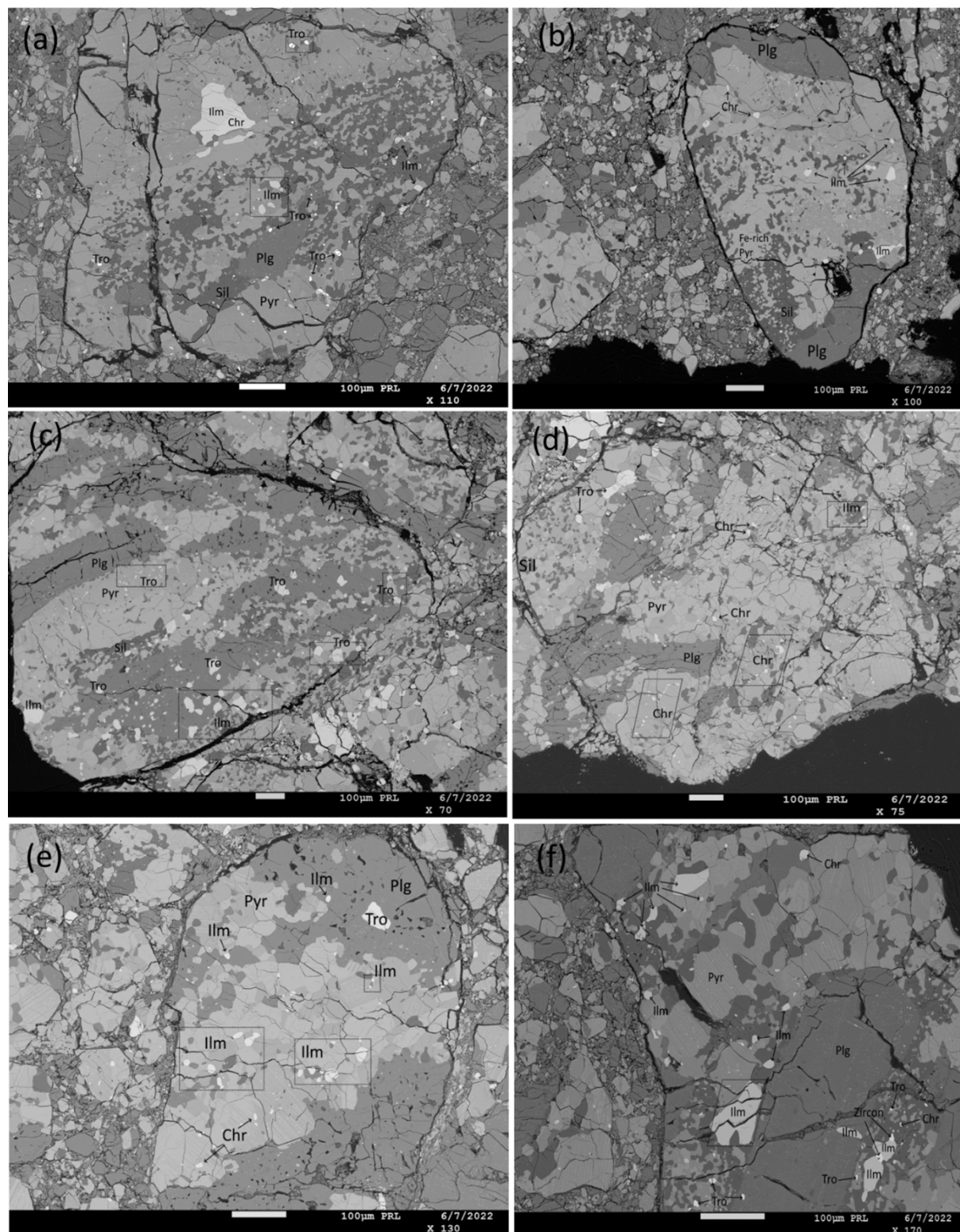


Figure 2.2: Back-scattered electron images of individual clasts of Lakangaon thick section one. Pyr: pyroxene; Plg: plagioclase; Ilm: ilmenite; Tro: troilite; Chr: chromite; All clasts are characteristically dominated by pyroxene + plagioclase with small silica aggregates.

	Pyroxene High- Fe/Low-Ca	Pyroxene High-Ca	Pyroxene High-Ca	Pyroxene High-Fe/ Low-Ca
SiO <sub>2</sub>	50.46	51.06	51.39	50.22
TiO <sub>2</sub>	0.16	0.26	0.30	0.16
Al <sub>2</sub> O <sub>3</sub>	0.17	0.51	0.35	0.23
Cr <sub>2</sub> O <sub>3</sub>	0.04	0.189	0.24	0.14
FeO	37.48	20.69	24.68	29.49
MnO	0.47	0.32	0	0.88
MgO	9.62	8.33	9.02	9.29
CaO	2.48	19.49	15.22	8.87
Total	100.88	100.86	101.20	99.28

Table 2.2: Representative mineral chemistry (wt.%) of pyroxenes from Lakangaon.

### 2.2.2 Accessory Phases

The accessory phases in Lakangaon include silica, ilmenite, chromite, troilite, and zircon. Silica composition is pure silica. Ilmenite (Fig. 2.7) is present as relatively large inclusions in pyroxenes as well as plagioclase, sometimes also in association with silica, in various shapes and sizes (up to  $150 \mu\text{m} \times 100 \mu\text{m}$ ), from subhedral to euhedral to wide elongated (bottle-like) shape. Ilmenite is homogeneous in composition throughout the sample, with 45% FeO and 53% TiO<sub>2</sub> and a very less amount of other oxides (Table 2.5).

Chromite occurs in Lakangaon as inclusions in pyroxenes, plagioclase and also in silica. It is relatively smaller in size as compared to ilmenite, mostly anhedral, and most grains are of the size  $2 \mu\text{m}$  to  $10 \mu\text{m}$ , with some grains up to  $75 \mu\text{m}$  in association with ilmenite (Fig 2.8(c)). The composition of the chromite found in Lakangaon is around 45% FeO with 35% Cr<sub>2</sub>O<sub>3</sub>, 14% TiO<sub>2</sub> and less than 1% MnO (Table 2.5). When plotted on a Cr/(Cr+Al) vs Fe/(Fe+Mg) plot, the chromite data falls on the boundary line between the Mg-Al chromite and chromite region (Fig. 2.8). Cr/(Cr+Al) ratio for Lakangaon ranges from 89.02 to 91.96 with the average of 90.34 which marks it as chromite. Troilite occurs as very fine inclusions in pyroxenes and causes clouding, as discussed in the previous section (Fig. 2.9(b)). Also, as previously discussed, it is pure

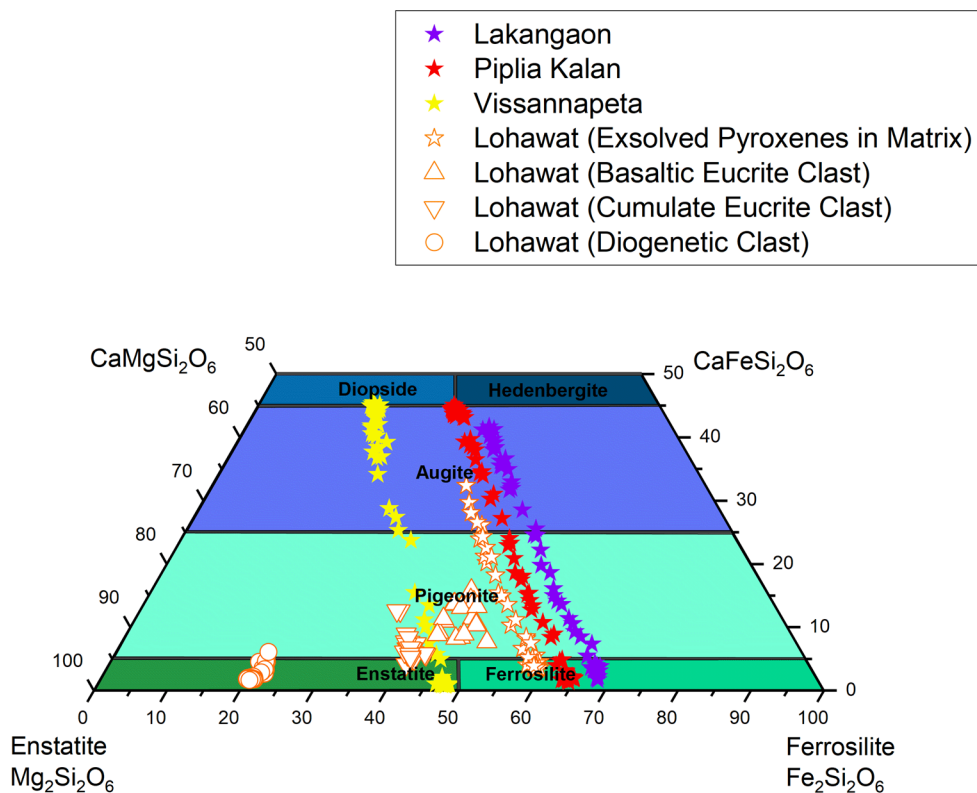


Figure 2.3: Pyroxene ranges for Lakangaon, Piplia Kalan, Vissannapeta and different lithologies of Lohawat.

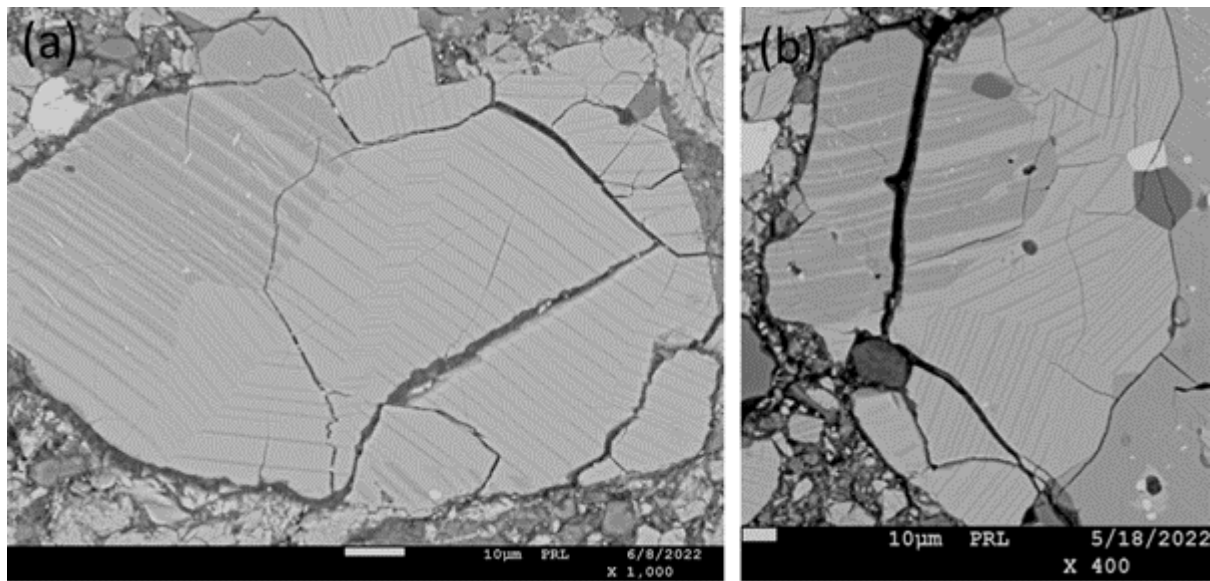


Figure 2.4: (a) The boundary between two grains of pyroxene, one Ca-rich augite (dark-gray) and the other Fe-rich pigeonite (light-gray). Note the similarity of the orientation of the exsolution lamellae (assumed to be parallel to in both grains), suggesting a topotactic relationship during nucleation and growth. The exsolution lamellae in the Ca-rich pyroxene are generally much wider than those in the Fe-rich pyroxene. (b) Pyroxenes deformed at multiple places.

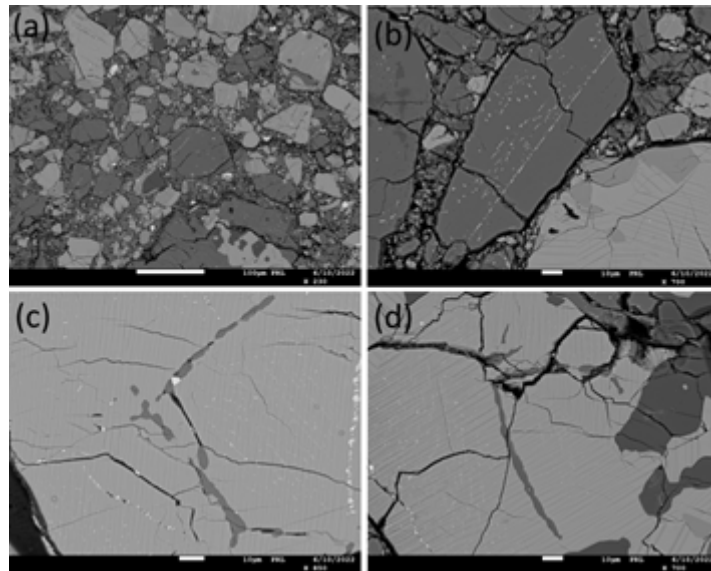


Figure 2.5: (a) Cataclastic arrangement of plagioclase and pyroxenes; plagioclase (dark gray) & pyroxenes (light gray). (b) Minor clast of plagioclase with pyroxene clouding. (c) and (d) Plagioclase laths in pyroxene.

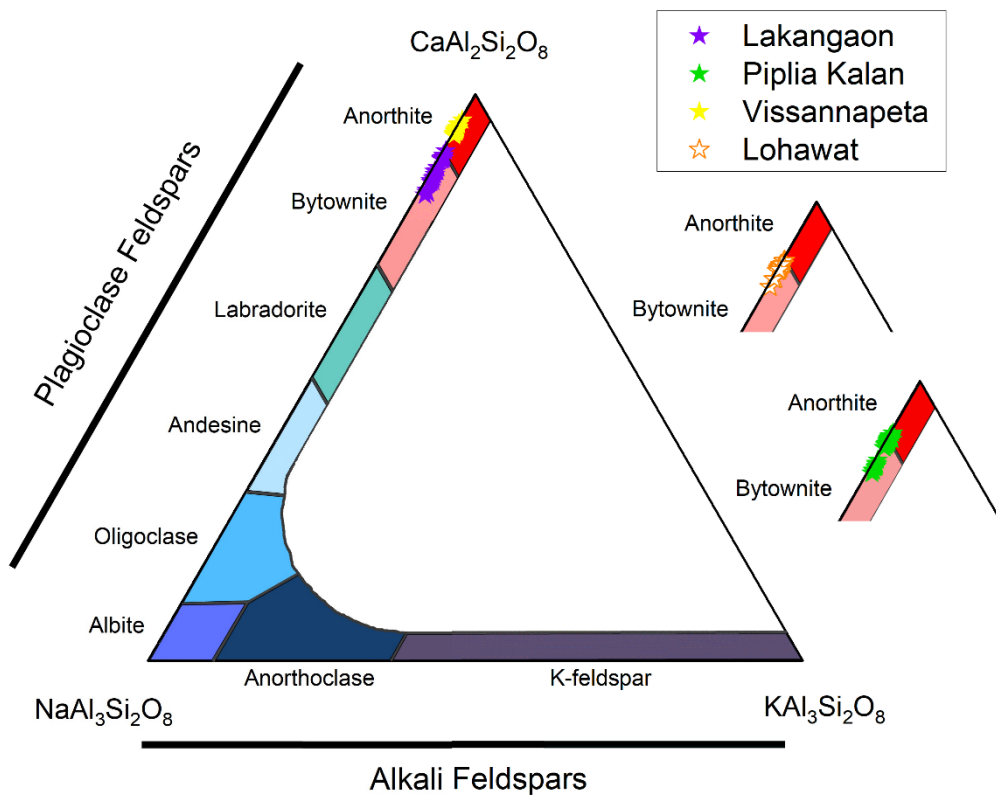


Figure 2.6: Plagioclase ternary diagram for Lakangaon, Piplia Kalan, Vissannapeta, and Lohawat. Lakangaon and Lohawat lie strictly in the Bytownite region, whereas Piplia Kalan barely touches the Anorthite region, with the majority of the points lying in the anorthite region. However, Vissannapeta lies entirely in the Anorthite region of the plagioclase ternary diagram.

Type	1	2	3	4	5	6
Chemical zoning	Extensive zoning if fully preserved	Metastable Fe-rich pyroxenes	Fe-Ca trend from core to rim	Homogeneous host and remnant of zoning	Homogeneous host of exsolved pigeonite	Homogeneous host of exsolved pigeonites
Inversion to Opx	None	None	None	None	Stacking fault	Partly inverted
Examples	Y75011, 84 clasts in Y75015, Y74450	Pasamonte	Clast in Y790266	Stannern, Nuevo Laredo	Juvinas, Haraiya, Emmaville, Sioux Co.	Y791186, Y792510
Clouding of Pyroxene	None	None	Trace	Present	Present	Present
Exsolution of augite	TEM Scale	TEM Scale	TEM Scale coarsened	Resolvable by EPMA	Resolvable by EPMA	Resolvable by EPMA

Table 2.3: Some diagnostic features for classification of the degree of homogenisation of eucritic pyroxenes (excluding cumulate eucrites). (Taken from Takeda and Graham, 1991).

FeS with Co, Cr, and Ni below detection limits (Table 5). It is mostly rod and bleb shaped when occurring in clouding ( $< 0.5\mu\text{ m}$ ), and when it exists as a grain, it is mostly anhedral, and its size is  $< 10 \mu\text{m}$ .

In this study, five grains of zircon were also found. All of them were either associated with ilmenite or as isolated grains (Fig 11). The zircon grains in Lakangaon are less than  $10 \mu\text{m}$  in size.

Zircon has strong resistance to mechanical and chemical breakdown over long periods and is well known to be host of incompatible elements, such as U, Th, Hf, and rare earth elements (REE) (Sawka, 1988, Bea, 1996, O'Hara et al., 2001). Although zircon is a common accessory mineral in terrestrial rocks, zircon in meteorites from asteroids is rare.

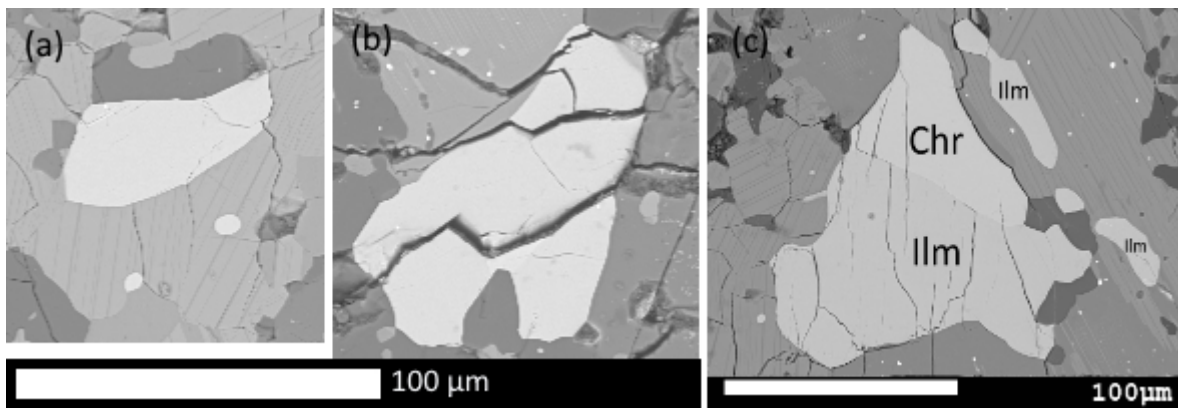


Figure 2.7: (a) Ilmenite in association with silica. (b) A very large grain of ilmenite fractured at multiple places. (c) Chromite is associated with ilmenite, forming a relatively very large grain.

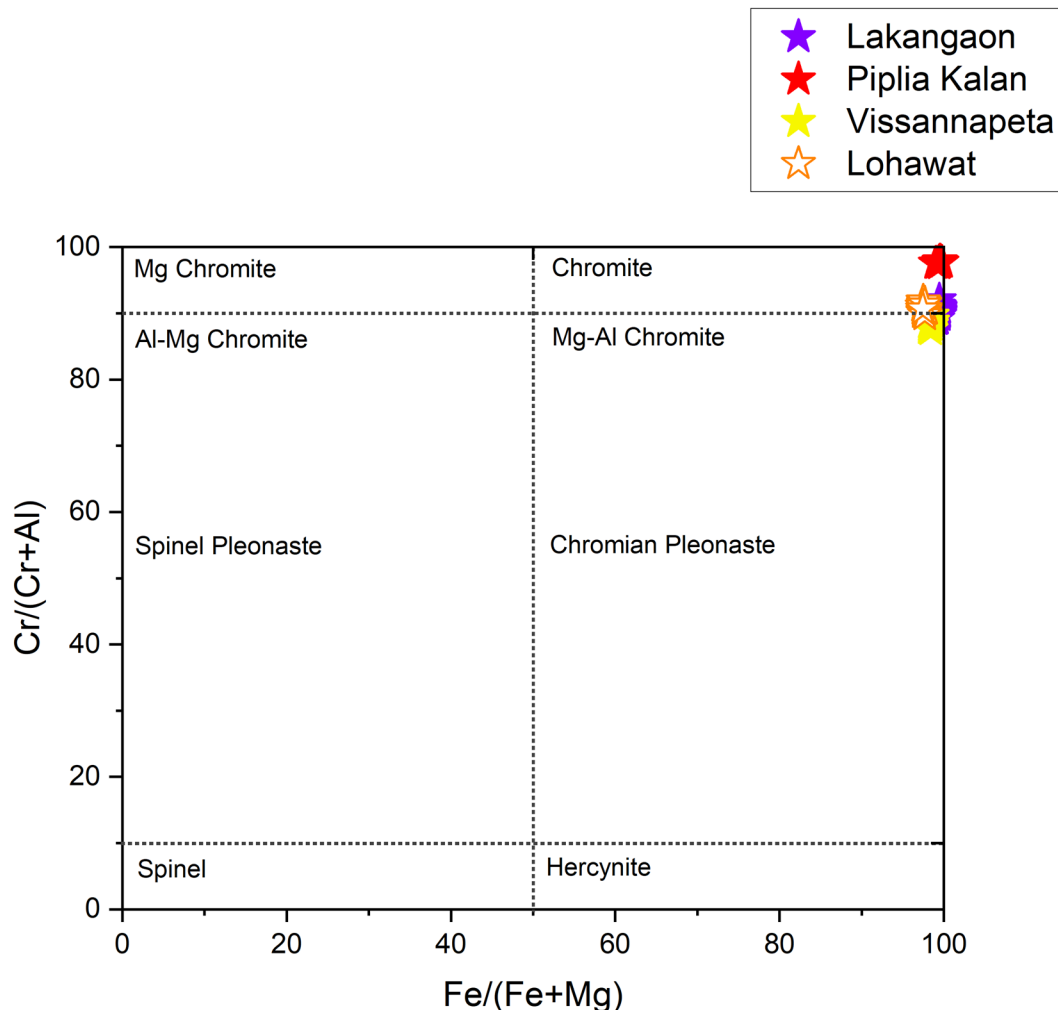


Figure 2.8: (a) Ilmenite in association with silica. (b) A very large grain of ilmenite fractured at multiple places. (c) Chromite is associated with ilmenite, forming a relatively very large grain.

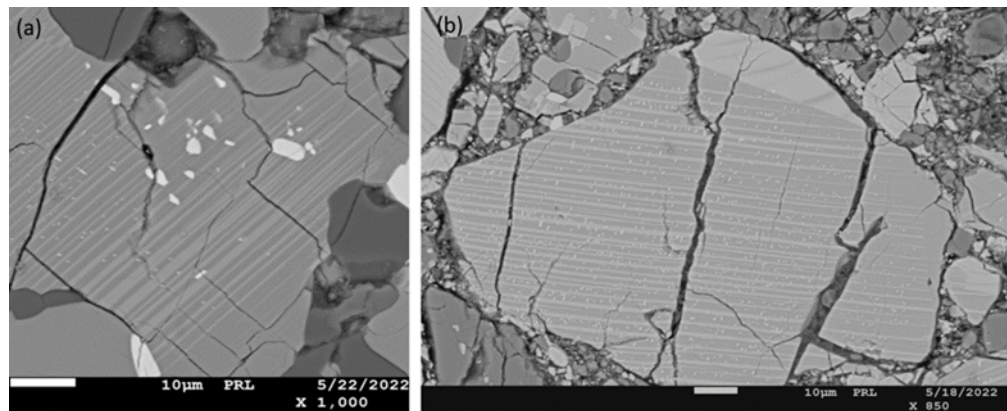


Figure 2.9: (a) Medium-sized inclusions in pyroxene. The bright spots are ilmenite blebs exsolved from the augite lamellae. (b) Very fine inclusions in pyroxene. These inclusions were too small for the EPMA analyses; however, a few fine inclusions are recognised as troilites.

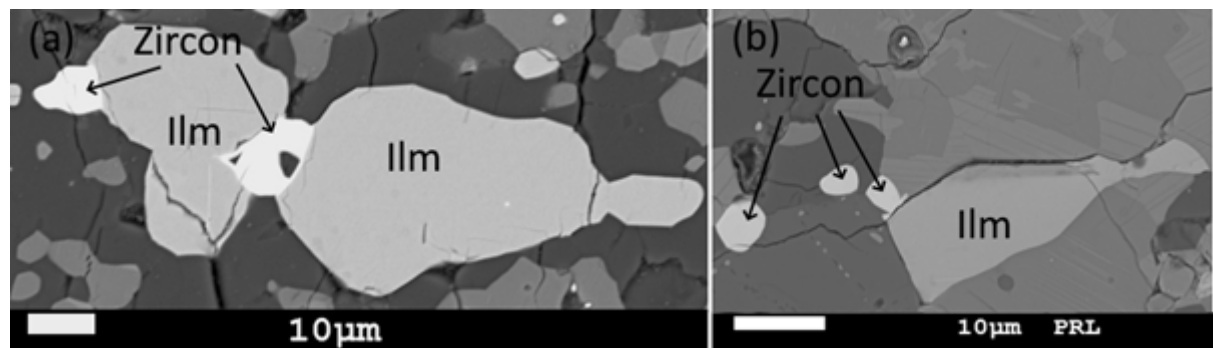


Figure 2.10: (a) Two zircon grains in association with ilmenite. (b) Three zircon grains in close proximity to ilmenite.

Plagioclase	
SiO <sub>2</sub>	47.07
TiO <sub>2</sub>	b.d.
Al <sub>2</sub> O <sub>3</sub>	33.23
Cr <sub>2</sub> O <sub>3</sub>	b.d.
FeO	0.52
MgO	0.11
CaO	18.72
Total	101.01

Table 2.4: Representative plagioclase composition for Lakangaon (where b.d. refers to below detection limit).

	Ilmenite	Chromite	Troilite
SiO <sub>2</sub>	0.12	0.16	b.d.
TiO <sub>2</sub>	53.66	13.93	b.d.
Al <sub>2</sub> O <sub>3</sub>	0.03	4.58	b.d.
Cr <sub>2</sub> O <sub>3</sub>	b.d.	34.59	b.d.
FeO	45.24	45.23	31.81
MnO	0.21	0.81	b.d.
MgO	0.44	0.30	b.d.
CaO	0.47	0.25	b.d.
SO <sub>3</sub>	b.d.	b.d.	68.18
Total	100.24	99.85	100.00

Table 2.5: Representative plagioclase composition for Lakangaon (where b.d. refers to below detection limit).

### 2.2.3 Conclusions

Lakangaon is a basaltic eucrite which falls into the Nuevo Laredo group, as revealed by the chemistry of pyroxenes, and it will be more clear by looking at the bulk rock chemistry and oxygen isotopic data (in the later chapters). Pigeonite is exsolved in augite and ferrosilite. It must have been rapid cooling which preserved this variation of pyroxenes (Yamaguchi et al., 2001). Ilmenite in small amounts is ubiquitous in HED meteorites. It is often associated with chromite. The clouding in pyroxenes is an interesting feature that will be further discussed in Section 2.6 of this chapter.

Troilite, metal, and silica inclusions could have been caused by a reducing agent operating on typical basaltic eucrite pyroxene compositions. The inclusions of troilite and silica in pyroxenes were explained by Zhang et al. (2013) using this fundamental type of reaction, where the reactants were S vapour and eucritic pyroxene instead of fayalite. In Juvinas, Nuevo Laredo, Sioux County, and Stannern, Duke (1963) reported petrographic evidence for the late-magmatic stage reaction of pyroxene to form troilite and silica; nonetheless, he attributed this to late-stage S vapour. He also showed that late-stage ferroan pigeonite and augite are clouded by troilite inclusions, in contrast to the largely inclusion-free pyroxene cores in Pasamonte. Duke (1963) found no evidence for the interaction of pyroxene with S vapour to form troilite in this example, suggesting that the co-crystallisation of these two phases from magma for this meteorite is plausible. Pyroxenes from type 1 unequilibrated eucrites' mesostasis regions may provide compositional evidence for this process. Any evidence of this would have likely been lost during the basaltic eucrite metamorphism, which was prevalent (e.g., Yamaguchi et al. 1996).

Five grains of zircon were also identified in this study. Zircon is a frequent auxiliary mineral in rocks on Earth, although it is very rare in meteorites. The zircons are generally reported in basaltic eucrites, mesosiderites, and an H5 chondrite (e.g., Ireland and Wlotzka, 1992, Misawa et al., 2005). These zircons may have formed through annealing and overgrowth during metamorphic processes. Most basaltic eucrites may have undergone secondary subsolidus reheating processes, as described by Takeda and Graham (1991). Zircons from metamorphosed eucrites may have undergone solid-state recrystallisation during subsolidus reheating events (Hoskin and Black, 2000). Zircons from basaltic eucrites must have originated in melts that were saturated in Zr and Si. These melts can occur as a result of the crystallisation of constituent minerals like clinopyroxene and plagioclase. (Haba et al., 2014).

## 2.3 Piplia Kalan Eucrite

On June 20 1996, a fireball was seen through a cloudy sky after three loud explosions, and then two stones with masses of 30 and 12 kg plummeted 500 metres apart, creating two minor craters in Piplia Kalan, Pali District, Rajasthan, India. Vaya et al. (1996) performed a preliminary petrographic analysis. These stones were recognised as eucrites by Shukla et al. (1997) based on a thorough chemical and petrographic analysis. Piplia Kalan, which is typically categorised as a monomict breccia, is dominated by several lithologies rich in plagioclase and pyroxene that have slightly varied compositions; the plagioclase, for instance, is largely equilibrated. However, a variety of lithologies with a wide range of textures, shapes, and sizes have been documented, most of which are dominated by pigeonite, diopside, and bytownite. Shukla et al. (1997) recognised six distinct lithologies; however, Buchanan et al. (2000) interpreted the meteorite in terms of two major lithologies and one minor lithology. The three lithologies have been observed in the one thick section and two thin sections used in this study.

Piplia Kalan, being a non-cumulate eucrite, is similar to the Lakangaon in the pyroxene and plagioclase ranges, along with the accessory minerals. However, it is quite different from it in terms of texture and lithology. The clasts as well as the inclusions in Piplia Kalan, are bigger in size than that of Lakangaon. Also, the inclusions are spaced further apart, which provided Srinivasan et al. (1997) with enough inclusion-free areas to analyse feldspars which are inclusion-free and have a relatively low Mg-Al ratio. These results are significant because they show that the melting of the eucrite parent body may have been caused by the decay of  $^{26}\text{Al}$  to  $^{26}\text{Mg}$ . Fig. 2.11 shows the mosaic of the samples. The clasts are subrounded and irregular in shape. Pyroxenes are exsolved, and the width of the exsolved lamellae also varies quite significantly. The metallic phases like ilmenite, chromite and troilite also have a great degree of variation in grain size and are very often associated with silica. The overall mineral modes for the thick sections and two thin sections have been presented in Table 2.6, and these include 36% pyroxene, 59.4% plagioclase + silica, and the accessory minerals like ilmenite, chromite, and troilite make up 0.9%.

There are three distinct lithologies in Piplia Kalan. Lithology A consists of ophitic-subophitic blocky grains of plagioclase in random orientation, and pyroxene fills the interstices with a minor amount of silica (Fig. 2.12(a)). Chromite, ilmenite, and troilite, are also present along with Fe-beads (Fig. 2.19(a)). The EPMA data for these Fe-beads read 100% Fe with no nickel or cobalt. The pyroxenes are exsolved (mainly augite lamellae in a pigeonite host) with lengths up to 90  $\mu\text{m}$ . Mineral modes are given in Table 2.7. Type A lithology clearly exhibits non-cumulate eucritic texture with abundant inclusions.

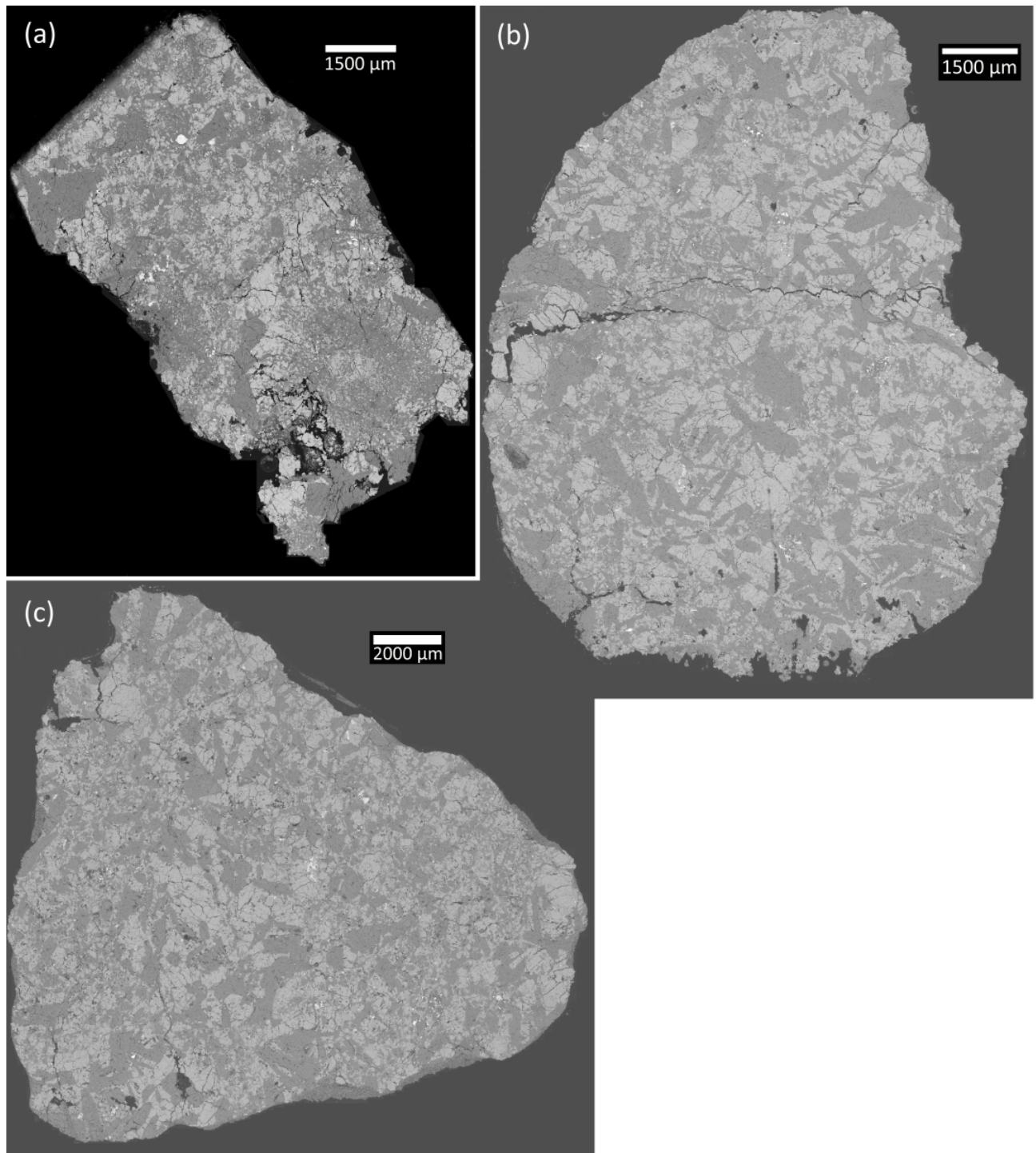


Figure 2.11: Stitched Back-scattered Electron Images (BSE) of the studied one thick section (a) and two thin sections ((b) and (c)) of Piplia-Kalan.

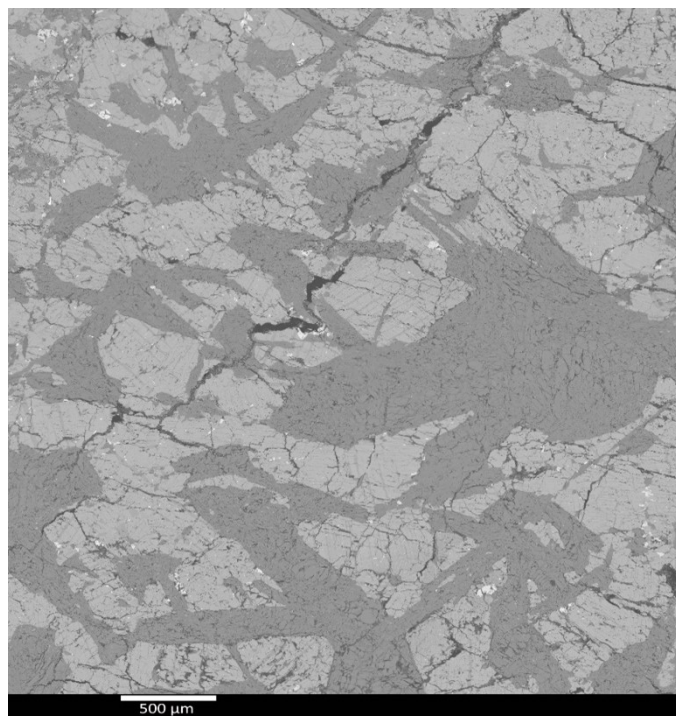


Figure 2.12: Coarse grains of plagioclase (average around 300  $\mu\text{m}$ ) from Lithology A. The shape is blocky with relatively sharp edges and average length-to-width ratio of about 8-10.

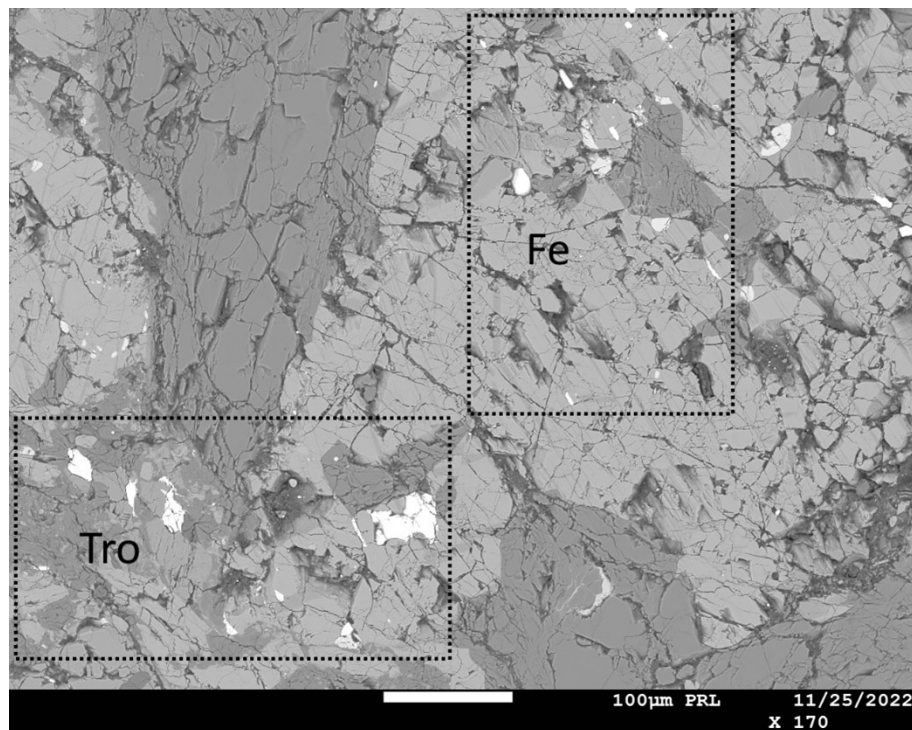


Figure 2.13: The bright-white phases in the top-right and bottom-left boxes show Fe-beads and troilites, respectively, in lithology A of Piplia Kalan. Fe beads are small in size (2-15  $\mu\text{m}$  in width).

	Thick_A	Thin_A	Thin_B
Pyroxene	51.3%	55.9%	52.1%
Plagioclase and Silica	45.9%	42.4%	42.2%
Accessory minerals (Ilmenite, chromite, troilite, zircon)	2.7%	1.6%	5.6%

Table 2.6: Mineral modes in different sections of Piplia Kalan (one thick section and two thin sections).

Type B lithology has grains that are finer than that of lithology A (Fig. 2.14), although the constituent minerals are almost the same; i.e. pyroxene (orthopyroxene and clinopyroxene), plagioclase, silica, ilmenite, chromite, and troilite. However, Fe-beads were not found in lithology B. Augite was seen as exsolved lamellae in low-Ca pyroxene with lengths of up to 80  $\mu\text{m}$ . Lithology B also shows similarity to basaltic non-cumulate eucritic texture.

Type C lithology (Fig. 2.15) clasts have an equigranular texture which closely resembles terrestrial hornfels. Pyroxenes and plagioclase are granular, with sizes ranging from 20  $\mu\text{m}$  to 50  $\mu\text{m}$ . Plagioclase and silica also occur as laths in random orientation and contain equant-shaped pyroxene inclusions (Fig 2.16). Almond (1964) identified feldspar phenocrysts with scalloped edges found in some of these metavolcanic rocks. These crystals, which are similar to those in Piplia Kalan's lithology C, were formed when nearby pyroxenes were recrystallised into equant grains. Abundant metallic inclusions are also present, which are many times smaller (3-15  $\mu\text{m}$ ) than the grains of pyroxene and plagioclase, with a few in the range of 30-40  $\mu\text{m}$ .

### 2.3.1 Mineral Chemistry

Pyroxenes in Piplia Kalan are generally augite exsolution lamellae in pigeonite host (Fig. 2.16 (a)), but the opposite is also observed (Fig. 2.16(b)). The width of exsolved lamellae in the pyroxenes of Piplia Kalan varies greatly (from <1  $\mu\text{m}$  to 15  $\mu\text{m}$ ). This can be seen in pyroxenes grains from different places and also in the same grain (Fig. 2.16 (c)). The pyroxenes are plotted in the Di-Hd-En-Fs quadrilateral (Fig. 2.3), and the compositional trend of pyroxene is linear and similar to Lakangaoon. It is also seen that some pyroxenes are deformed, and the

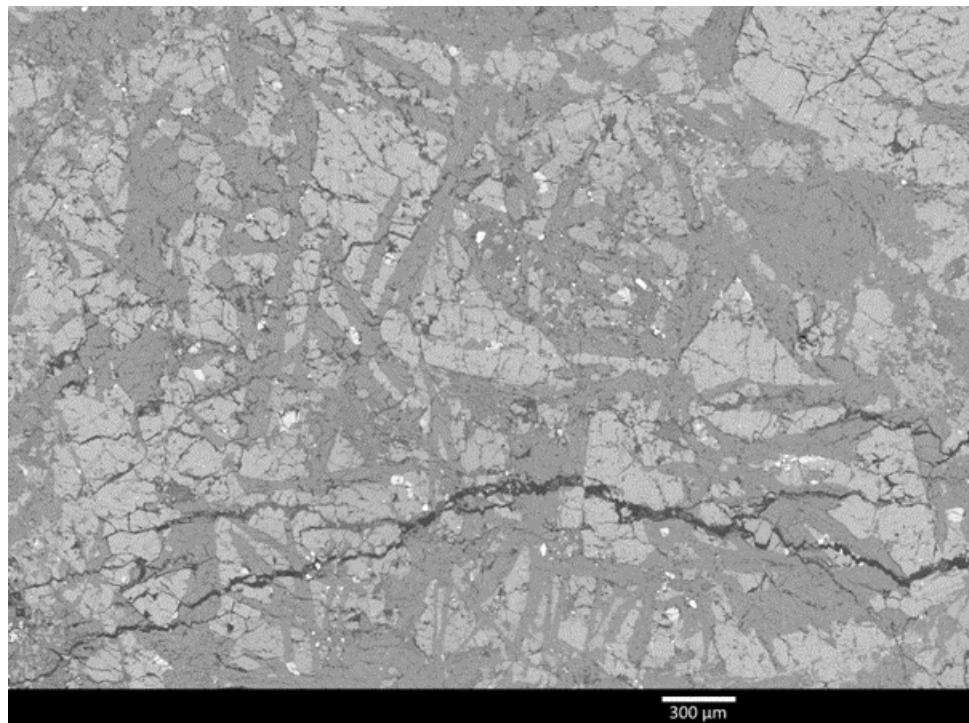


Figure 2.14: Lithology B in Piplia Kalan. The plagioclase laths are thinner as compared to that of Lithology A and are also greater in number. The average length to width ratio of these plagioclase laths is 7.5-8.

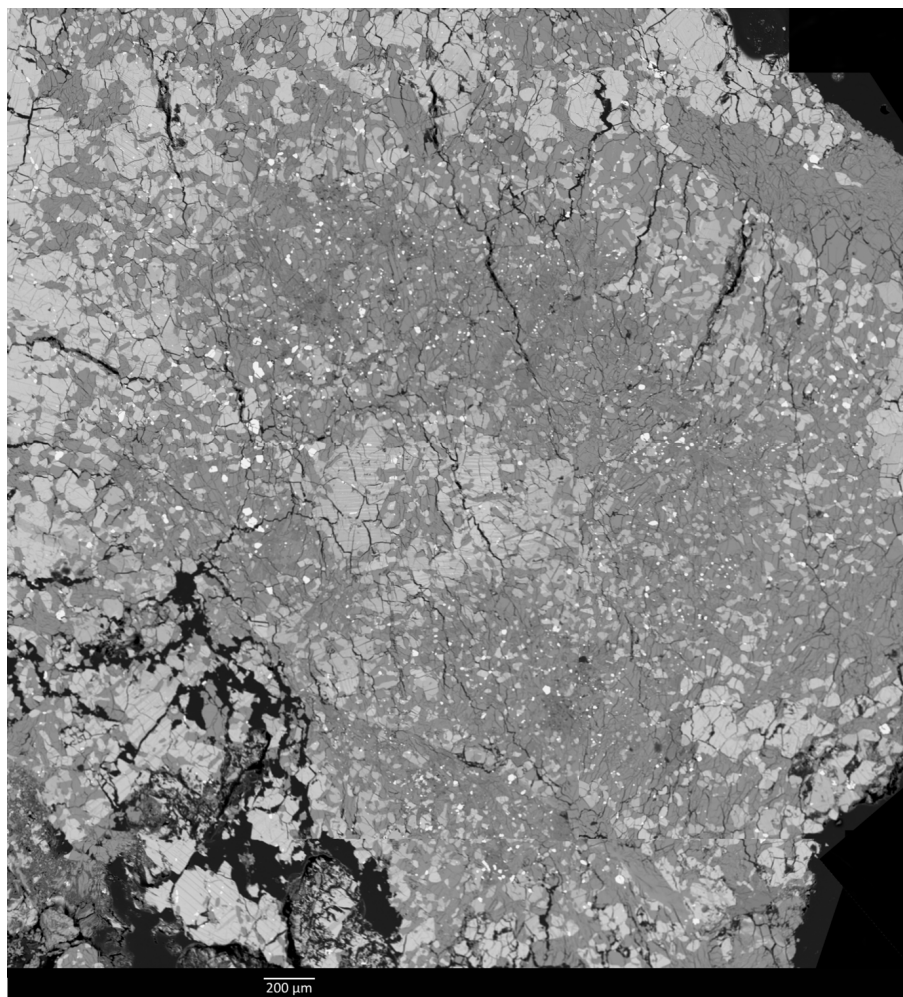


Figure 2.15: Lithology C in Piplia Kalan. The equigranular texture can be clearly observed with some plagioclase and silica laths.

	Lithology A	Lithology B	Lithology C
High-Ca Pyroxenes	14.9%	22.9%	18.6%
Low-Ca Pyroxenes	29.4%	19.74%	13.5%
Plagioclase and Silica	44.6%	43.8%	67.9%
Accessory minerals (Ilmenite, chromite, troilite, zircon)	0.66%	0.82%	0.88%

Table 2.7: Mineral modes in the three lithologies of Piplia Kalan.

exsolution lamellae appear to shift on the other side of the fracture (Fig. 2.16 (d)). The representative data for different types of pyroxenes are given in Table 2.8. Pyroxenes are also clouded by abundant metallic inclusions that are generally oriented along the boundaries between the host pyroxene and the guest pyroxene in the exsolved texture. This type of clouding was observed in metamorphosed tertiary lavas by Hutchison and Bevan (1977). Silica and plagioclase also occur as inclusions that are elongated in shape and size that ranges from  $\sim 10 - 100 \mu\text{m}$ .

Takeda and Graham (1991) defined six types of eucrites primarily based on their pyroxenes, where type 1 is a pristine basalt which has suffered very limited subsequent metamorphism, while type 6 has been reheated and extensively metamorphosed (Table 2.3), as mentioned in section 2.2.1. Yamaguchi et al. (1996) introduced a type 7. Ca-zoning (a type 4 feature) is seen in pyroxene in Haraiya, Jonzac, and Palo Blanco Creek, but some pyroxene grains are partially inverted pigeonite (a type 6 feature). Compared to type 4, this type's Ca-zoning is less visible. Based on these properties and shock features, Basu et al. (2016) classified Piplia Kalan as type 7, which was earlier classified as type 5/6 by Buchanan et al. (2000).

Plagioclase from Piplia Kalan often occur as long and thick ophitic-subophitic block grains in lithology A (Fig. 2.12). In lithology B, the plagioclase is finer than in lithology A but with a similar texture (Fig. 2.14). In lithology C, one can observe equant grains of plagioclase and some plagioclase laths in random orientation (Fig. 2.15). The plagioclase is also clouded with rod and droplet-shaped pyroxene inclusions that are  $1-10 \mu\text{m}$  in size and often for a straight dashed line (Fig. 2.17(a), (b)). The composition of plagioclase is  $\text{An}_{83.69-90.77}$ , and it lies in the Bytownite-Anorthite field in the plagioclase ternary diagram (Fig. 2.6), which is on the lines of basaltic eucrite.

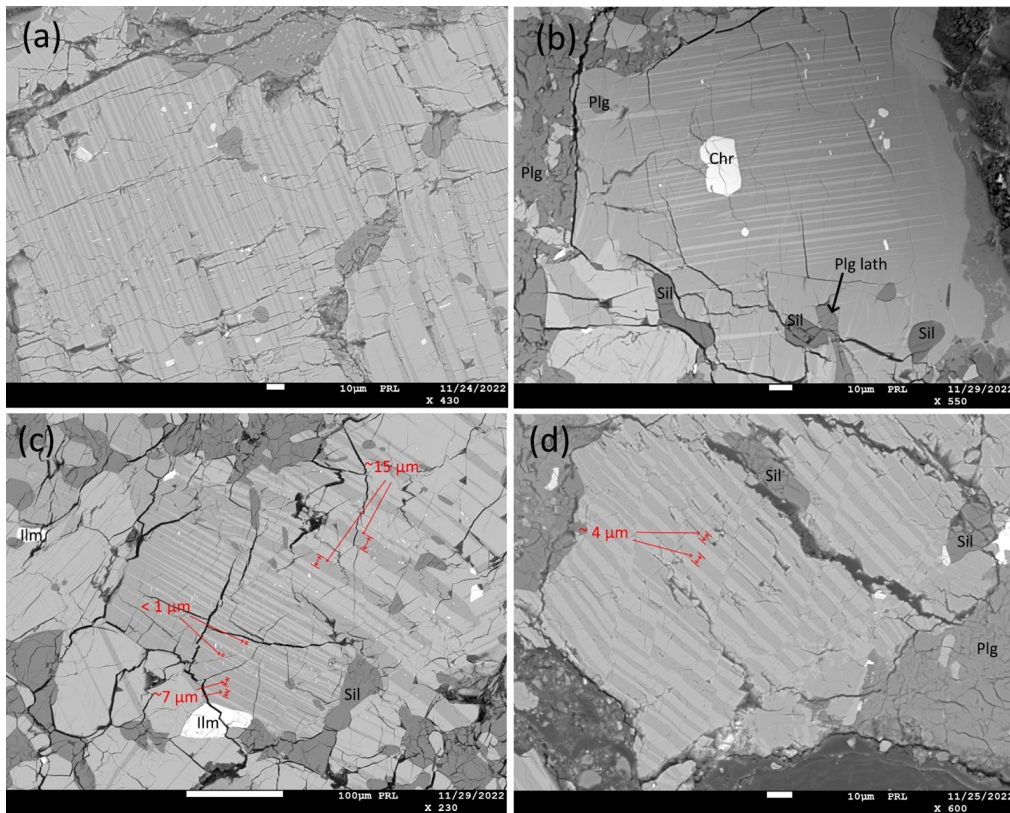


Figure 2.16: (a) Exsolved augite lamellae in pigeonite host. Droplets-shaped plagioclase inclusions and a bit of rod and bleb shaped metallic inclusions are also visible. (b) Pigeonite lamellae in augite host. Plagioclase and Silica are present as round or elongated inclusions alongwith a chromite grain which is subhedral to euhedral in shape. (c) Different thickness of exsolved lamellae is visible in the same grain of pyroxene, which also hosts a subhedral ilmenite inclusion which is in association with a long silica inclusion. Clouding, to some extent, is also visible (d) Pyroxene deformed at multiple places; the exsolution lamellae appear to be shifted and continue on the other side of the deformation line.

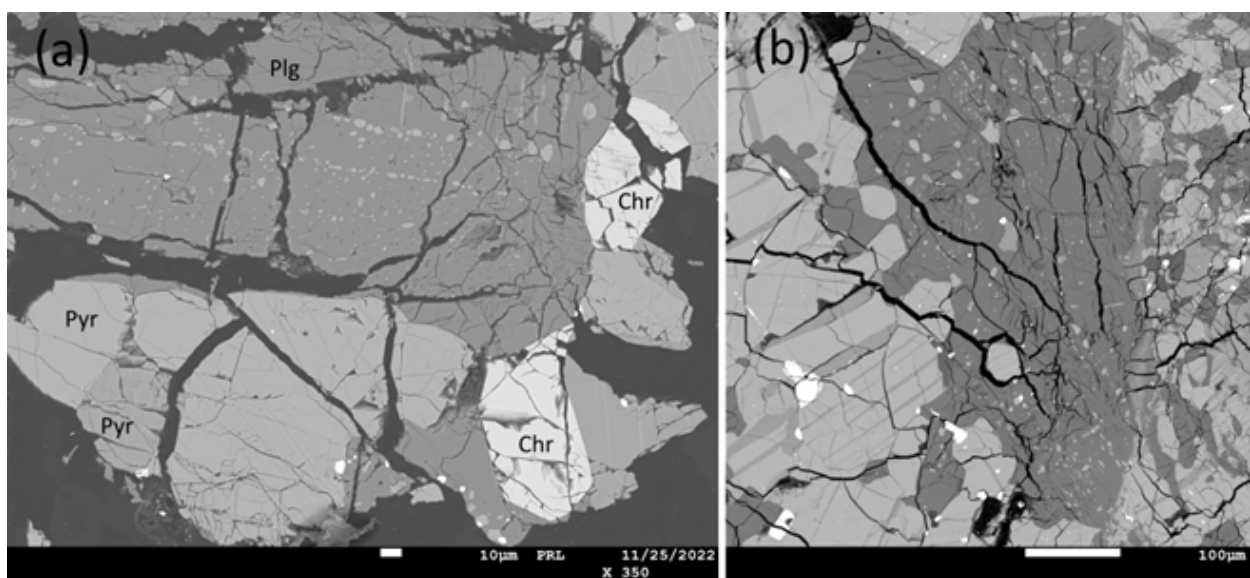


Figure 2.17: (a) Plagioclase grain clouded with pyroxene inclusions. Two grains of chromite are also associated with plagioclase and pyroxene, and all of these are highly fractured. (b) Plagioclase grain which appears to be recrystallised into equant grains. Again, clouding by minuscule pyroxene inclusions and fracturing can be observed.

	Pyroxene High-Fe	Pyroxene Low- Ca
SiO <sub>2</sub>	48.76	50.52
TiO <sub>2</sub>	0.17	0.42
Al <sub>2</sub> O <sub>3</sub>	0.14	0.68
FeO	37.88	17.25
MnO	1.23	0.50
MgO	11.18	9.7
CaO	0.87	21.43
Total	100.22	100.51
Wo	1.89	44.30
En	33.81	27.88
Fs	64.30	27.83

Table 2.8: Representative composition for pyroxenes of Piplia Kalan. Individual oxide percentages have been rounded off to two decimal places.

### 2.3.2 Accessory Phases

Accessory phases in Piplia Kalan include silica, ilmenite, chromite, troilite, and very rare occurrences of Fe-beads. The EPMA data for silica came out to be 100% SiO<sub>2</sub>, and for the Fe-beads, it was 100% FeO (no Nickel or Cobalt was detected). Silica occurs as inclusions in pyroxenes, as well as separate aggregate. The metallic inclusions like ilmenite, chromite, and troilite have been observed to be associated with silica (Fig. 2.18) and also as individual grains that are relatively very big in size as compared to the Lakangaon eucrite (Fig. 2.19).

Troilites are well spread across the sample and are most abundant among the metallic phases. Moreover, it also has the largest size of grains among the metallic phases (Fig. 2.19 (c), (d)). The shape of troilite grains ranges from subhedral to anhedral but at some places where it is strongly associated with silica, the shape is very distorted as the silica seems to have partly recrystallised over the troilite grain (Fig. 2.18 (b)).

Chromite and ilmenite from Piplia Kalan are less abundant than troilite and are also

Plagioclase	
SiO <sub>2</sub>	46.15
Al <sub>2</sub> O <sub>3</sub>	35.05
FeO	0.07
MgO	b.d.
CaO	18.58
Na <sub>2</sub> O	1.17
K <sub>2</sub> O	0.08
Total	101.11
An	89.37
Ab	10.17
Or	0.46

Table 2.9: Representative composition for pyroxenes of Piplia Kalan. Individual oxide percentages have been rounded off to two decimal places; b.d. refers to below detection limit

smaller in size (Fig. 2.17 (a)). Some chromite grains are subhedral to euhedral (Fig. 2.16 (b)), while others are almost anhedral (Fig. 2.19 (a)). When plotted on a Cr/(Cr+Al) vs Fe/(Fe+Mg) plot, the chromite data falls in the chromite region (Fig. 2.8). Cr/(Cr+Al) ratio for Piplia Kalan chromite ranges from 97.48 to 97.87 with the average of 97.66. The data for chromite, ilmenite and troilite has been given in Table 2.10.

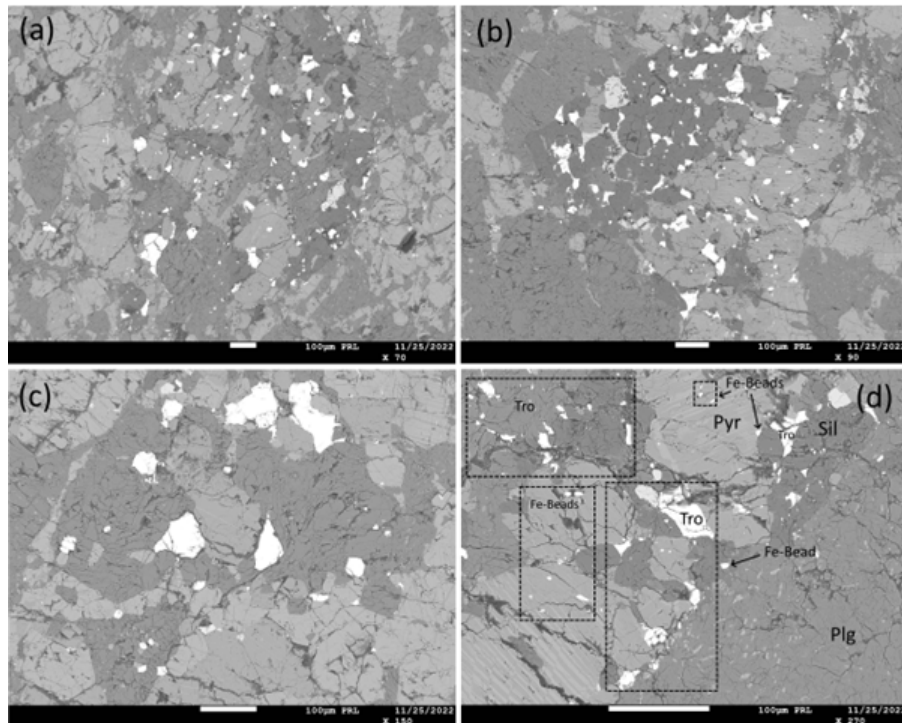


Figure 2.18: Multiple BSE images from different sections of Piplia Kalan thin and thick sections. A blend of troilite ( $\sim 5\text{--}100\ \mu\text{m}$ ) and silica grains can be observed (up to  $500\ \mu\text{m}$ ). In (a), (b), and (c), the bright white phases are troilites. In (d), troilites and Fe-beads have been marked. Pyr: pyroxene; Tro: troilite; Plg: plagioclase; Sil: silica.

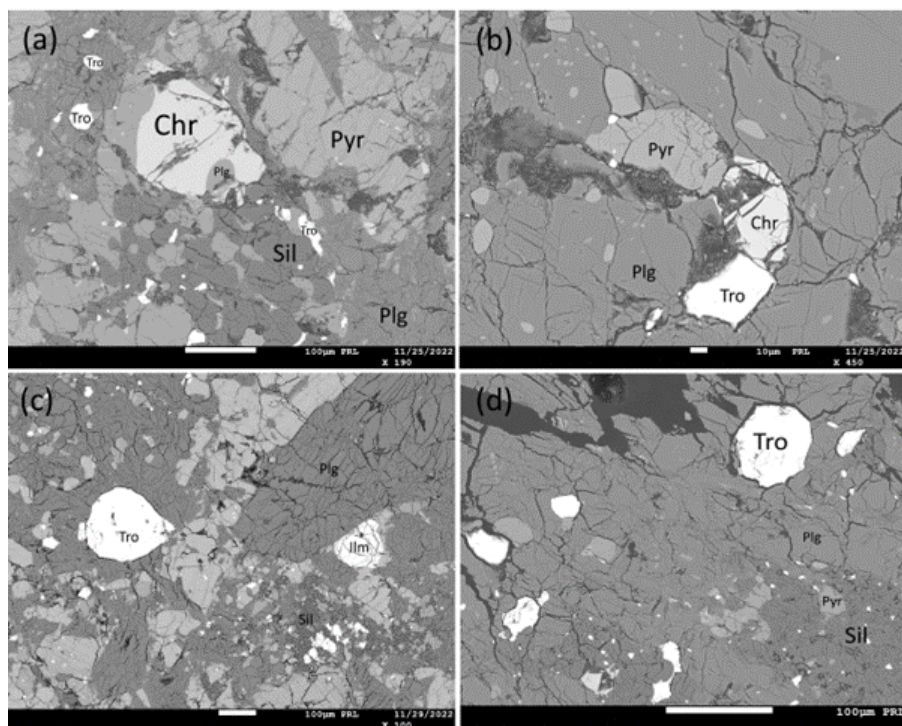


Figure 2.19: (a) Big chromite grain ( $\sim 200\ \mu\text{m}$ ) with plagioclase as an inclusion. Silica aggregates can be observed, and small troilite inclusions ( $\sim 10\ \mu\text{m}$ ) in plagioclase. (b) Pyroxene, chromite, and troilite association, along with the surrounding plagioclase, has undergone immense fracturing. The surrounding plagioclase is also clouded with pyroxene inclusions. (c) A relatively huge troilite grain ( $\sim 200\ \mu\text{m}$ ), almost completely rounded in shape. An ilmenite grain,  $\sim 150\ \mu\text{m}$  in size, can also be seen. (d) All the bright white phases are troilite. Again the size is  $\sim 100\ \mu\text{m}$ .

	Ilmenite	Chromite	Troilite
SiO <sub>2</sub>	0.48	0.10	b.d.
TiO <sub>2</sub>	54.51	20.18	b.d.
Al <sub>2</sub> O <sub>3</sub>	b.d.	2.35	b.d.
Cr <sub>2</sub> O <sub>3</sub>	b.d.	25.40	b.d.
FeO	43.88	50.70	60.72
MnO	0.90	0.80	b.d.
MgO	0.49	0.35	b.d.
CaO	0.17	0.15	b.d.
SO <sub>3</sub>	b.d.	b.d.	39.29
Total	99.94	100.03	100.01

Table 2.10: Representative compositions for ilmenite, chromite and troilite from Piplia Kalan after rounding off to two decimal places (b.d. refers to below detection limit).

### 2.3.3 Conclusions

Piplia Kalan is an equilibrated basaltic eucrite consisting of ophitic-subophitic clasts that come as three different lithologies (Coarse grained lithology A, fine grained lithology B, and very fine-grained lithology with equigranular texture, C). This classification is consistent with the pyroxene compositions of Piplia Kalan, which are more ferroan than typical cumulate eucrites (e.g. Serra de Magé and Vissannapeta). The different grain sizes and textures of the lithologies also tell a story. Type A must have cooled at a greater depth, that too slowly, and went under different pressure, temperature and oxygen fugacity conditions than lithology B and C. Lithology B cooled at shallow depths and formed a finer texture. Sarbadhikari et al. (2016), in their study of the petrogenesis of Piplia Kalan, found that the lithology C was earlier lithology A, which underwent hydrous and silica-melt metasomatism and transformed into dacitic composition. The pieces of evidence for this in lithology C are the remnant grains of coarse augite in a silica-rich matrix and the clouding in pyroxenes.

There are multiple features that Piplia Kalan has undergone extensive metamorphism. Almost all the clasts show signs of having experienced metamorphism and were subjected

to high pressure, high temperature, or both, and thus can be called as metavolcanic. Most clasts have been recrystallised to a lesser or greater extent. The thermal metamorphism must be extensive to produce inclusions of such large size ( up to  $250\ \mu\text{m}$ ). The pyroxenes are also clouded, and it has been discussed in a later section (2.6). The glassy veins that have been observed in all the sections of Piplia Kalan are not recrystallised, and according to Buchanan et al. (2000), this continuity of the glassy veins across different clasts suggests that it formed during a late-stage shock event, which might be the impact that caused Piplia Kalan to shoot off from the Vesta.

Clasts make up a larger component of Piplia Kalan's composition than matrix material. The early brecciation event could have been a low-energy impact which did not cause much shock and brecciation. The other reason could be that Piplia Kalan was at the periphery or at a greater depth of a high-energy impact.

## 2.4 Vissannapeta Eucrite

In Vissannapeta village ( $16^{\circ}55' \text{ N}$ ,  $80^{\circ}45' \text{ E}$ ), Nuzivid Mandal, Krishna district, Andhra Pradesh, India, a meteorite crashed on December 13, 1997, at three in the morning. A single stone weighing 1303.8 g fell with a crash, accompanied by long streaks of bright light in the dark sky. It was a rounded pyramid in shape with the size of  $13 \times 10 \times 7\ \text{cm}$  and was covered with a fusion crust (Fig. 2.20) (Ghosh et al., 2000).

Vissannapeta is extremely brecciated, dominated by pyroxene (~33.7%) and plagioclase (~67.2%) (Fig. 2.20). After the first petrographic study of Vissannapeta by Ghosh et al. (2000), Srinivasan (2002) studied the  $^{26}\text{Al}$ - $^{26}\text{Mg}$  systematics in Vissannapeta, and Mahajan et al. (2019) included Vissannapeta in their study of noble gas, nitrogen composition and cosmic ray exposure history. Other than that, not much has been inspected in the Vissannapeta eucrite. In this study, one thin section of Vissannapeta was used to take a look into its petrogenesis.

### 2.4.1 Mineral Chemistry

The pyroxene in Vissannapeta is dominantly orthopyroxene, and exsolved lamellae of augite are also present (Fig. 2.22). The pyroxene grains are medium to large sized (  $200 - 900\ \mu\text{m}$  in width) and anhedral to subhedral in shape. The width of the exsolved lamellae is up to  $2\ \mu\text{m}$ , and they run parallel to each other. The fractures due to brecciation can be clearly observed, and the exsolution lamellae run right through them. When plotted in a Di-Hd-En-Fs quadrilateral, the pyroxene ranges from augite to pigeonite to enstatite (Fig. 2.3). The representative data for the pyroxenes has been presented in Table 2.11.

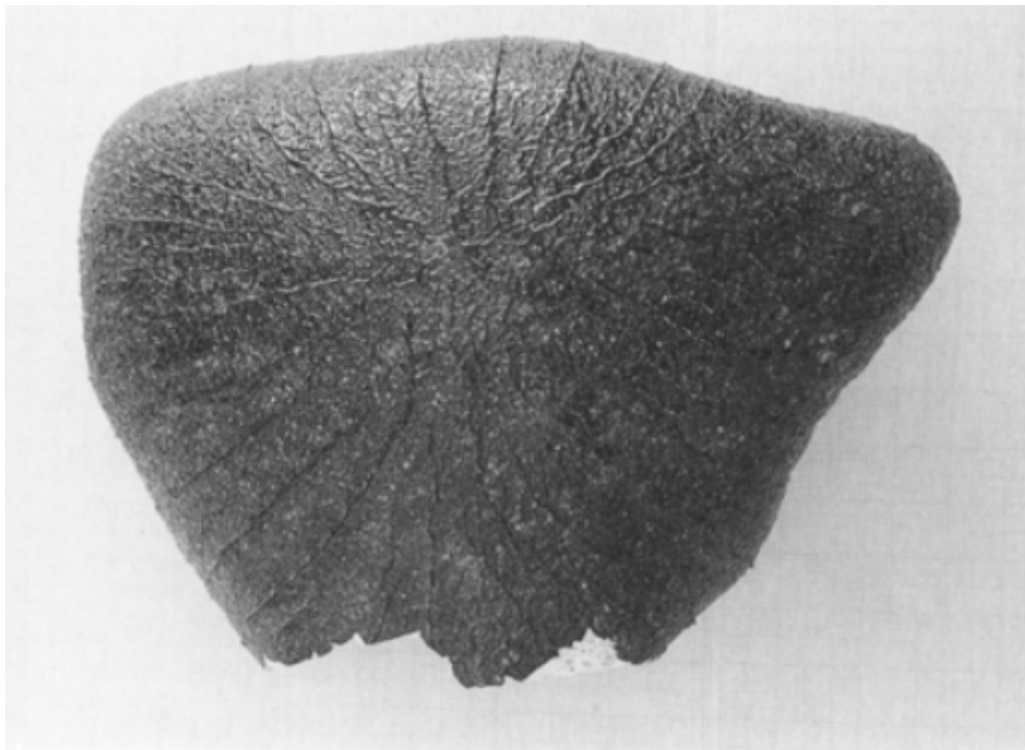


Figure 2.20: Photograph of Vissannapeta, which displays its rounded pyramidal shape and fusion crust full of flow ribs. Taken from Ghosh et al. (2000).

	Pyroxene High-Fe	Pyroxene Low- Ca
SiO <sub>2</sub>	53.05	53.24
TiO <sub>2</sub>	0.03	0.07
Al <sub>2</sub> O <sub>3</sub>	0.46	0.65
FeO	27.94	11.17
MnO	1.08	0.49
MgO	17.40	14.69
CaO	0.49	19.91
Total	100.43	100.28
Wo	1.05	40.58
En	52.04	41.64
Fs	46.90	17.78

Table 2.11: Representative composition for pyroxenes of Vissannapeta. Individual oxide percentages have been rounded off to two decimal places.

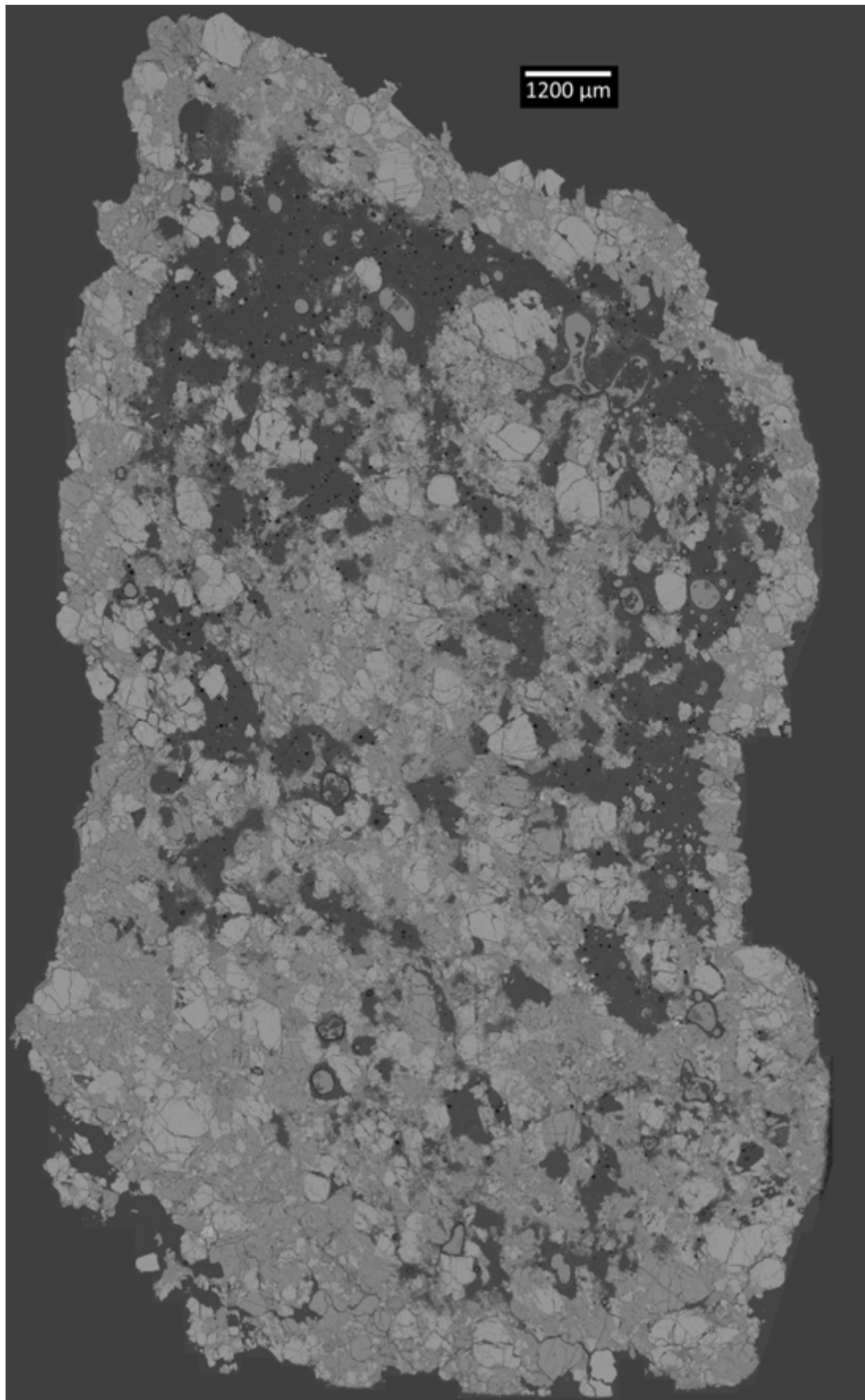


Figure 2.21: Stitched Back-scattered Electron Images (BSE) of the studied thin-section of Vissannapeta.

The compositional trend of Vissannapeta in the pyroxene quadrilateral precisely matches with Serra de Magé (the data for Serra de Magé was taken from Barrat et al. (2007)).

The plagioclase in Vissannapeta is the most calcic among all the analysed samples, with the width of the grains ranging from 500 to 1000  $\mu\text{m}$  (Fig. 2.23). All the points lie in the Anorthite region ( $\text{An}_{92.71-94.74}$ ) (Fig. 2.6). The representative composition for plagioclase is shown in Table 2.9. There are two phases that mark their presence as inclusions in plagioclase grains. One is silica and it occurs as multiple droplets-shaped mostly anhedral inclusions with size ranging from 10 to 80  $\mu\text{m}$  (Fig. 2.23). Another phase is troilite which occurs at very few places in an almost perfectly circular shaped with a width of 1 - 1.5  $\mu\text{m}$  (Fig. 2.25). Table 2.12 provides representative data for plagioclase from Vissannapeta.

Plagioclase	
$\text{SiO}_2$	44.80
$\text{Al}_2\text{O}_3$	34.96
$\text{FeO}$	0.16
$\text{MgO}$	0.02
$\text{CaO}$	19.47
$\text{Na}_2\text{O}$	0.59
$\text{K}_2\text{O}$	0.02
Total	100.01
An	94.74
Ab	5.16
Or	0.10

Table 2.12: Representative composition for pyroxenes of Vissannapeta. Individual oxide percentages have been rounded off to two decimal places.

## 2.4.2 Accessory Phases

The accessory phases in Vissannapeta include silica, chromite, and troilite. Silica is a frequent accessory mineral that is predominantly observed as inclusions in plagioclase

(Fig. 2.23) and sparingly in orthopyroxene. Additionally, it can be observed in the interstices between pyroxene and plagioclase. Data for the silica phase shows 100% SiO<sub>2</sub>. Chromite exists as discrete grains at the interface between pyroxene and plagioclase. The size of chromite grain varies from  $\sim 10\text{-}350 \mu\text{m}$ , and all the chromite grains are extremely brecciated (Fig. 2.24). On the Cr/(Cr+Al) vs Fe/(Fe+Mg) plot, the chromites from Vissannapeta lie in the Mg-Al chromite region (Fig. 2.8). Cr/(Cr+Al) ratio for Piplia Kalan chromite ranges from 87.65 to 89.63 with the average of 88.30.

Troilite, unlike chromite, was not found to exist as large-sized grains in the studied thin section of Vissannapeta. The troilite was very rare and only existed as almost circular inclusions with a diameter of  $\sim 1\text{-}1.5 \mu\text{m}$  (Fig. 2.25) at just one place, and it was not possible to measure the exact composition. It was identified as troilite through the mixed data of pyroxene and troilite that was received from the EPMA. However, Ghosh et al (2000), reported troilite grains in Vissannapeta with sizes up to tens of microns. This can be attributed to sample bias. Ilmenite, on the other hand, was neither observed during this study nor in the study carried out by Ghosh et al. (2000). The oxide percentage data for chromite has been provided in Table 2.9.

Chromite	
SiO <sub>2</sub>	0.08
TiO <sub>2</sub>	0.41
Al <sub>2</sub> O <sub>3</sub>	9.40
Cr <sub>2</sub> O <sub>3</sub>	55.20
FeO	33.10
MnO	0.67
MgO	0.69
CaO	0.14
SO <sub>3</sub>	b.d.
Total	99.69

Table 2.13: Representative compositions for chromite in Vissannapeta.

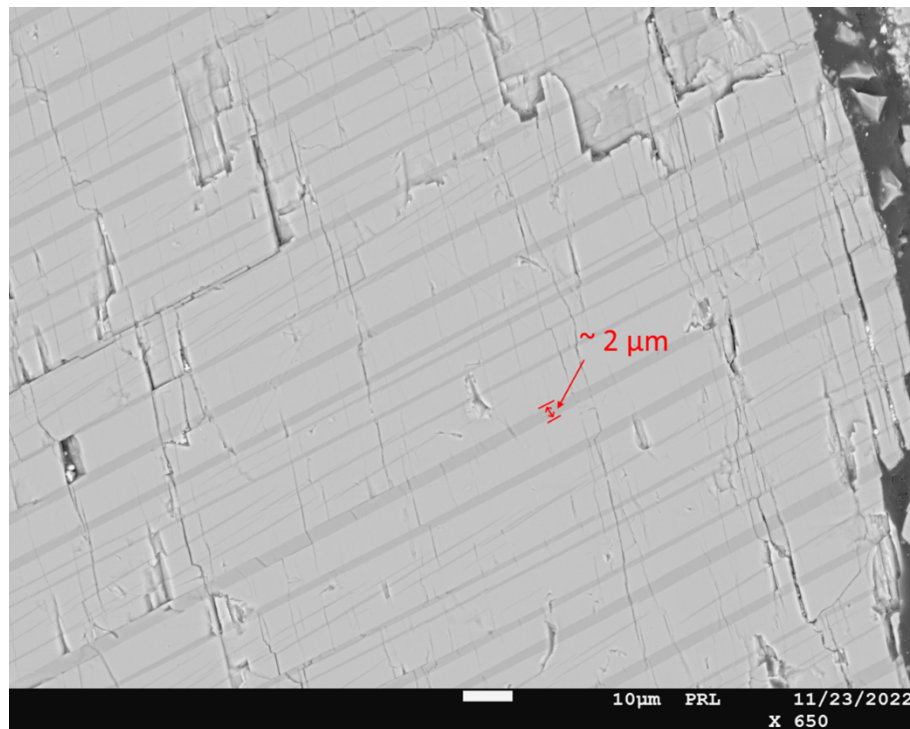


Figure 2.22: Exsolved pyroxenes in Vissannapeta, up to  $\sim 2 \mu\text{m}$  in width. The marked exsolution lamellae get shrunk towards the edge.

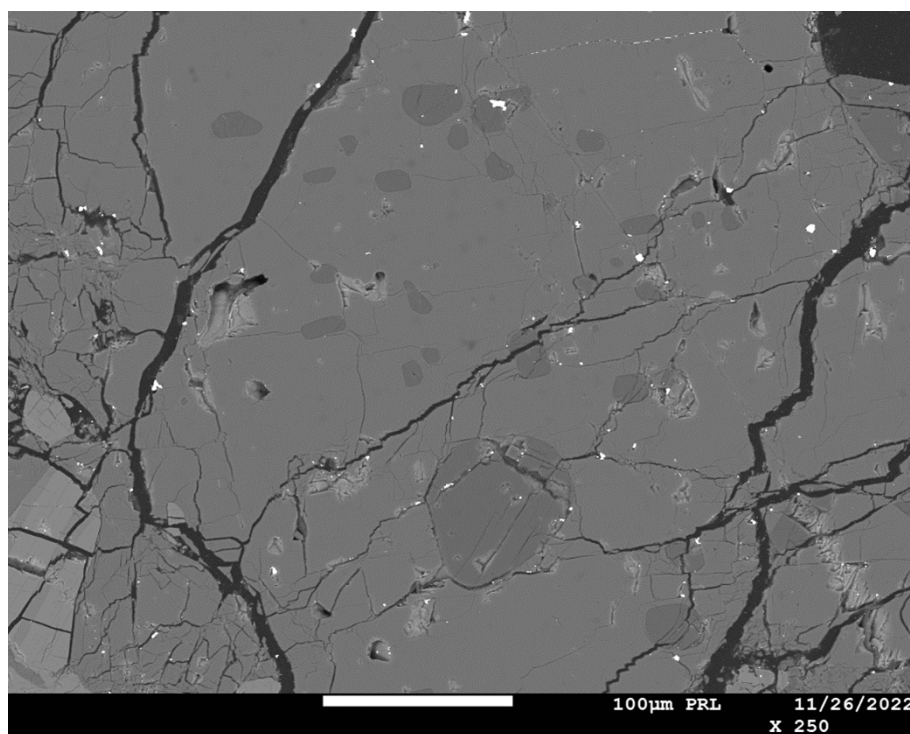


Figure 2.23: Plagioclase grain with multiple silica inclusions (10-80  $\mu\text{m}$ ).

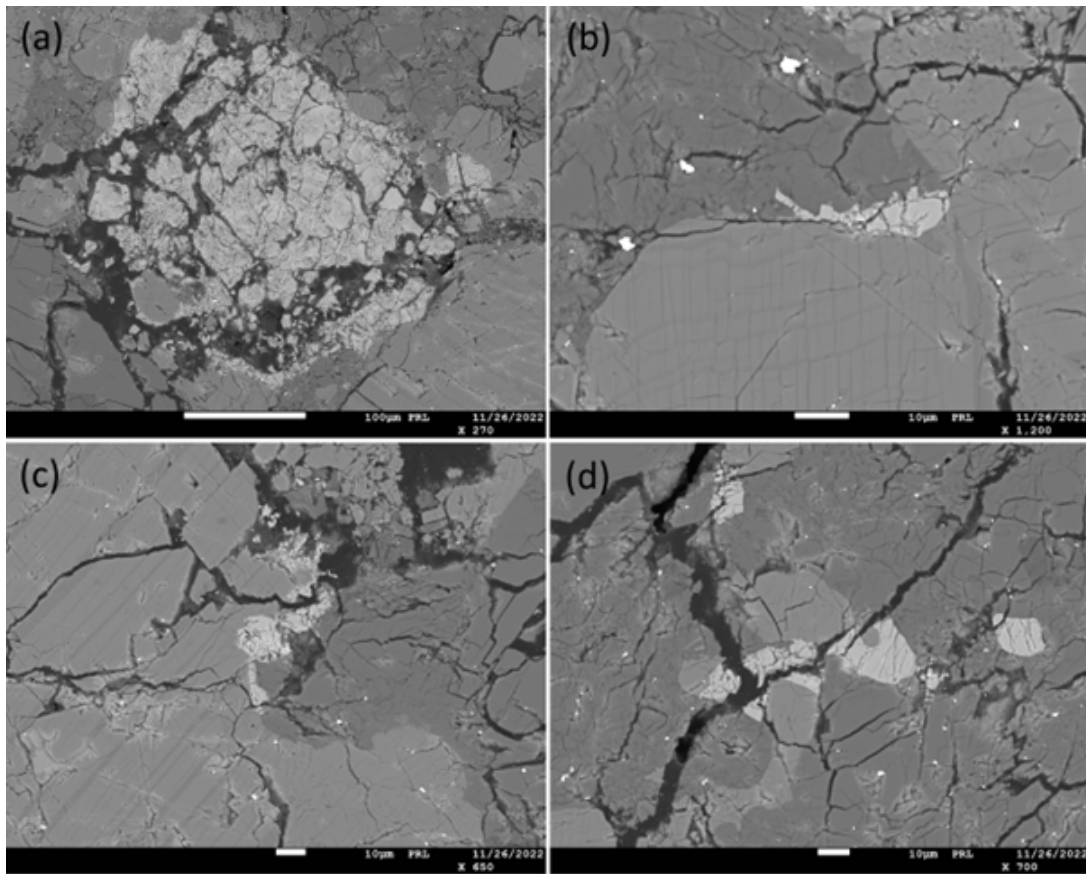


Figure 2.24: BSE images of chromite grains from the Vissannapeta thin section. Note the size difference. Also, due to extreme brecciation, the chromite grains are absolutely shattered. The three bright white spots in (b) is the bit of gold coating that was used on the thin section before loading into the EPMA.

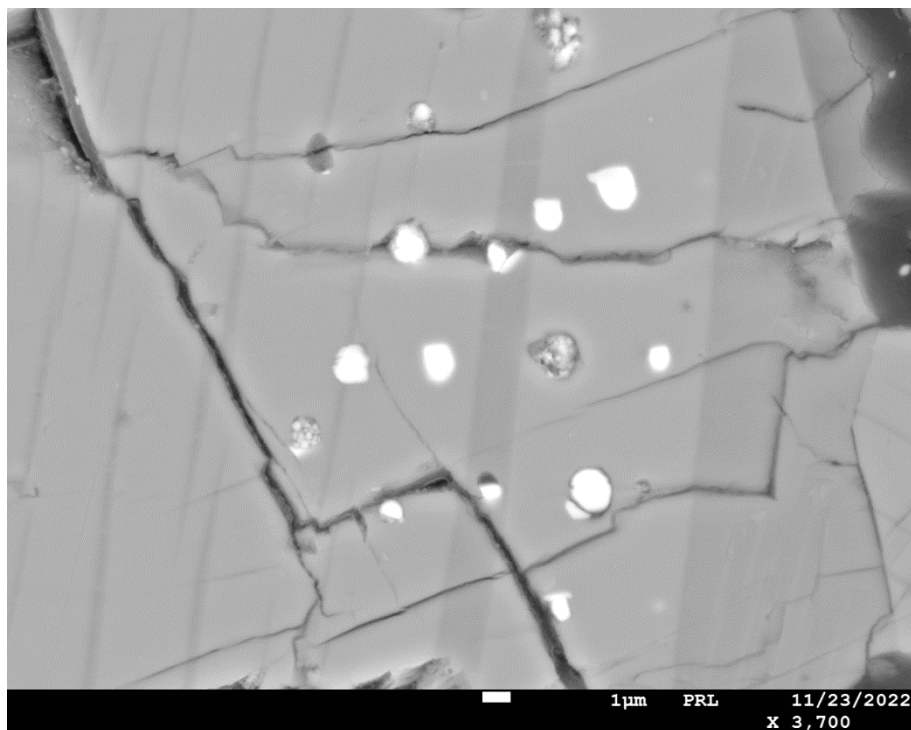


Figure 2.25: Troilite inclusions in exsolved pyroxene. The occurrences of these troilite inclusions are very rare in the thin section studied.

### 2.4.3 Conclusions

The first thing to be observed in the Vissannapeta sample is extreme brecciation and cumulus texture which is enriched in pyroxene component. Pyroxene's severe fractures appear to be linked to Vesta's moderate shock events. The pyroxenes in Vissannapeta are significantly enriched in MgO, and plagioclase is more calcic, as compared to Lakangaon and Piplia Kalan (which are basaltic eucrites) (Fig 2.3) (Fig 2.6). The exsolved lamellae of clinopyroxene in orthopyroxene host, and the existence of silica majorly as inclusions in plagioclase, and the absence of ilmenite, are some of the signature features of cumulate eucrites. Based on these features, Vissannapeta falls under the cumulate eucrite category.

The presence of numerous blebs and lamellae of pyroxene composition suggests that shock-induced melting, recrystallisation, and exsolution have also occurred in Lake Carnegie, even though some plagioclase appears to have retained primary crystallisation features with simple and multiple twinning (Rubin, 1995; 2002; 2004; Wang and Chen, 2006). In certain cases, plagioclase crystals only include lamellae and bleb inclusions in the region of the crystal that is closest to the silica-rich melt, which further supports a petrogenetic link. A grain of chromite that is nearly rimmed by plagioclase provides additional evidence of melting by demonstrating how the plagioclase crystallised first before surrounding the chromite during melting.

## 2.5 Lohawat Howardite

A 40 kg stone crashed onto an open field after a spectacular fireball and loud boom, leaving half-a-meter deep hole. The Geological Survey of India gathered 6.245 kg, although this was only a portion of the material that had been recovered because the meteorite had a mass of  $\sim$ 40 kg and a diameter of around a foot. It is noteworthy that five meteorites—Didwana (H5), Piplia Kalan (eucrite), Lohawat (howardite), Devri Khera (L6), and Itawa Bhopji (L3/5)—fell in Rajasthan over the course of nine years (1991 August to 2000 May) and were relatively close to one another, with Lohawat and Devri Khera falling on the same day and within three hours of one another. Chattopadhyay et al. (1998) released the first report on Lohawat and its major element chemistry, classifying it as a howardite and is one of the 379 registered howardites as on date (Meteoritical Bulletin, MB85).

Lohawat sample's origin was classified as originating from a parent body other than asteroid 4 Vesta because of the sample's high exposure age (107 Ma) and lack of solar gases typically present in that material (Mahajan et al., 2000). Thin section and petrographic examinations revealed that the meteorite's major mineral components were colourless to gray pyroxene, subhedral to anhedral plagioclase, and a small quantity of

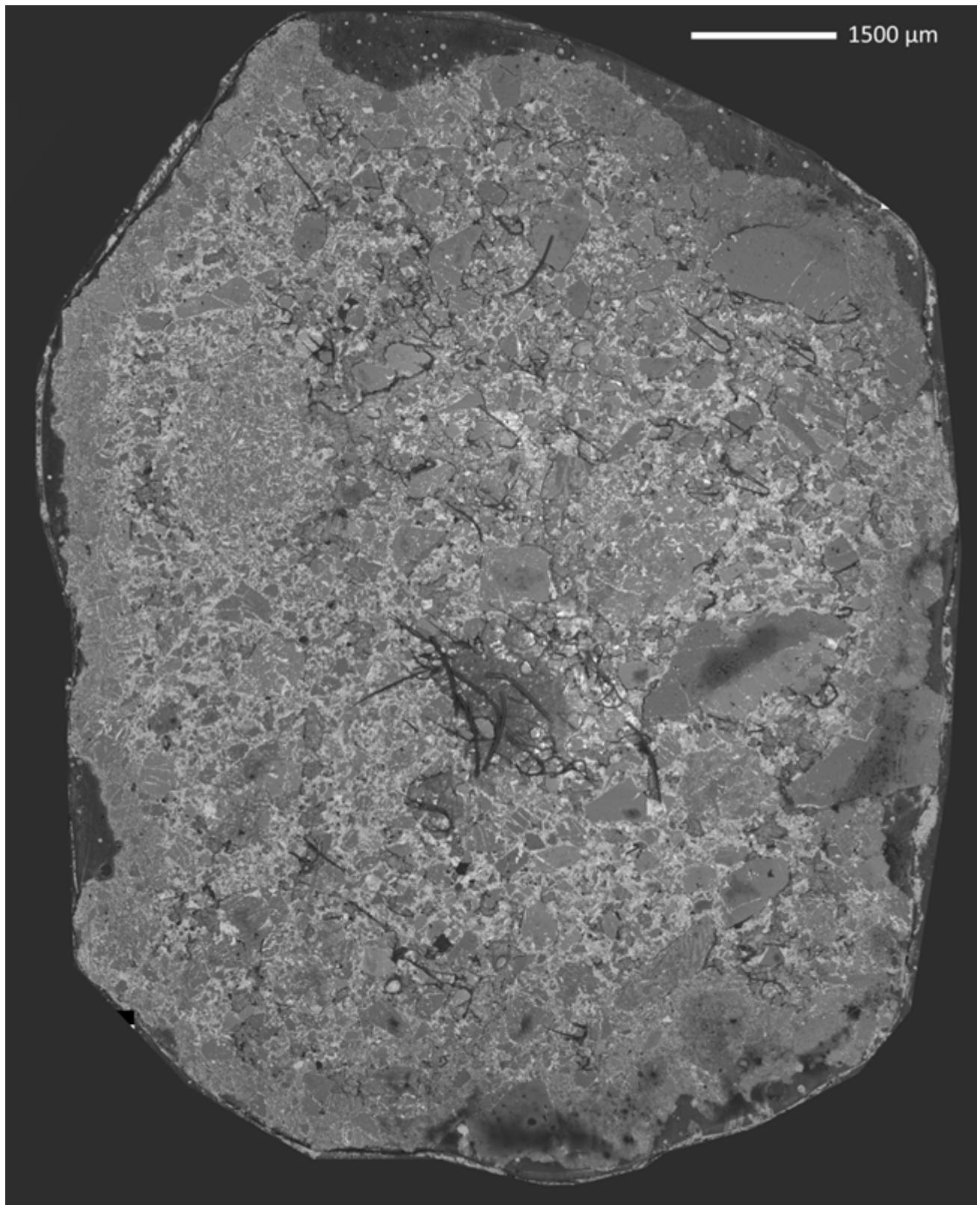
anhedral olivine embedded in a fine to the medium-grained matrix without many inter-growth associations (Chattopadhyay et al., 1998; Singh et al., 1998; Sisodia et al., 2001). Being an impactite, lohawat howardite is made up primarily of igneous lithologies with minor amount of impact-melt rocks and melts. Ray and Ghosh (2022) reported unusual low-Mg clasts in Lohawat and these low-Mg rock fragments appeared to have been ballistically transported regolith fines of granite from some unknown, distant regions where a high-energy impact on eucrite crust could have generated limited parental melt via impact-induced remelting and ultimately produced the low-Mg rocks and acidic melts, respectively. Two thin sections of Lohawat were analysed during this study (Fig. 2.26). One thin section consists of approximately 19.3% plagioclase and silica, with 52.8% pyroxene and 10.9% metallic phases. The other thin section includes about 11.0% plagioclase and silica, 89.6% pyroxene and 2.9% metallic phases. Besides diogenetic clasts, basaltic eucrite clasts and cumulate eucrite clasts were also found in Lohawat samples.

### 2.5.1 Polymict Diogenite Breccia

These clasts consist of mostly diogenites (> 70%) with very few eucrite clasts (~ 10%) and crystalline matrix (silicate-sulphide) (Fig. 2.27(a), (e), (f)). In the diogenite clast, the pyroxenes are Mg-dominated orthopyroxenes (Fe-poor enstatite, with mean composition  $\text{Fs}_{20.99}\text{Wo}_{2.48}\text{En}_{76.53}$ ), with minor clinopyroxene (pigeonite, with mean composition  $\text{Fs}_{44.89}\text{Wo}_{14.43}\text{En}_{40.68}$ ). Some clasts firmly exhibit pigeonite crystallisation from ferrosilite. There are a few euhedral to subhedral grains of ilmenite and chromite as inclusions (~ 25-50  $\mu\text{m}$  in width). The size of diogenite clasts range from 300 to 1500  $\mu\text{m}$ , and in the case of cumulate and basaltic clasts, the size ranges from 50 to 1000  $\mu\text{m}$ . Some small (around 100  $\mu\text{m}$  in width) plagioclase clasts are associated with the diogenite clasts. The cumulate clasts display their typical coarse-grained pyroxene-plagioclase texture.

### 2.5.2 Cumulate Eucrite Clasts

Cumulate eucrite clasts are monomict type in Lohawat, and they are medium to coarse-grained with the aggregates of pyroxene and plagioclase being equigranular, which is the typical texture of a cumulate eucrite clast, similar to terrestrial gabbro except for the blocky banded texture (Fig. 2.27 (a)). The plagioclase is extremely calcic (> An<sub>90</sub>), which is very similar to the plagioclase observed in Vissannapeta, which is another cumulate eucrite, and pyroxene is almost all pigeonite (mean composition  $\text{Fs}_{40.00}\text{Wo}_{6.69}\text{En}_{53.31}$ ) with a small amount of sub-calcic augite (mean composition  $\text{Fs}_{35.64}\text{Wo}_{27.95}\text{En}_{36.40}$ ). Small aggregates of silica are also present and associated with plagioclase.



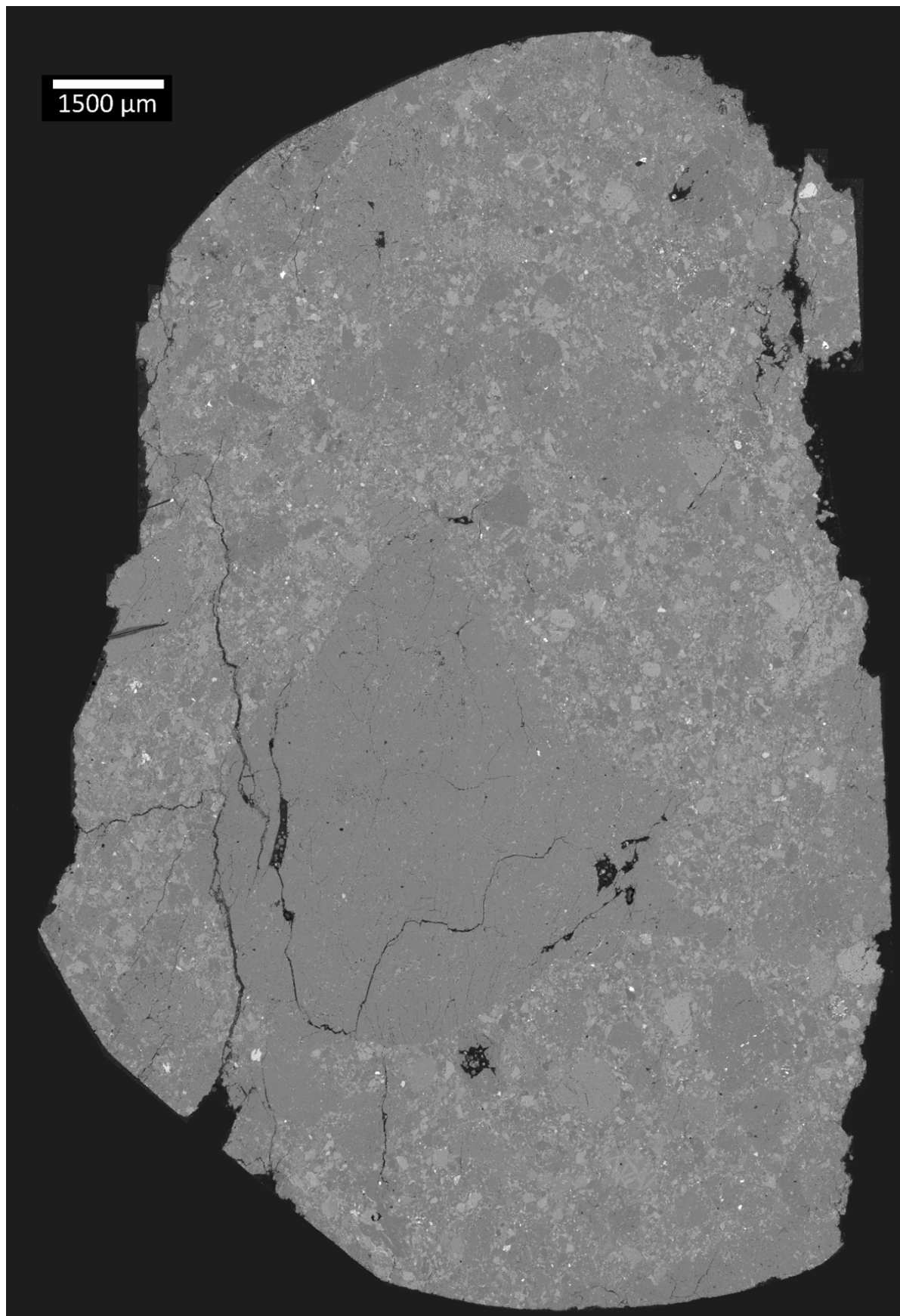


Figure 2.26: Stitched mosaic made from Back-Scattered Electron (BSE) images of Lohawat thin sections.

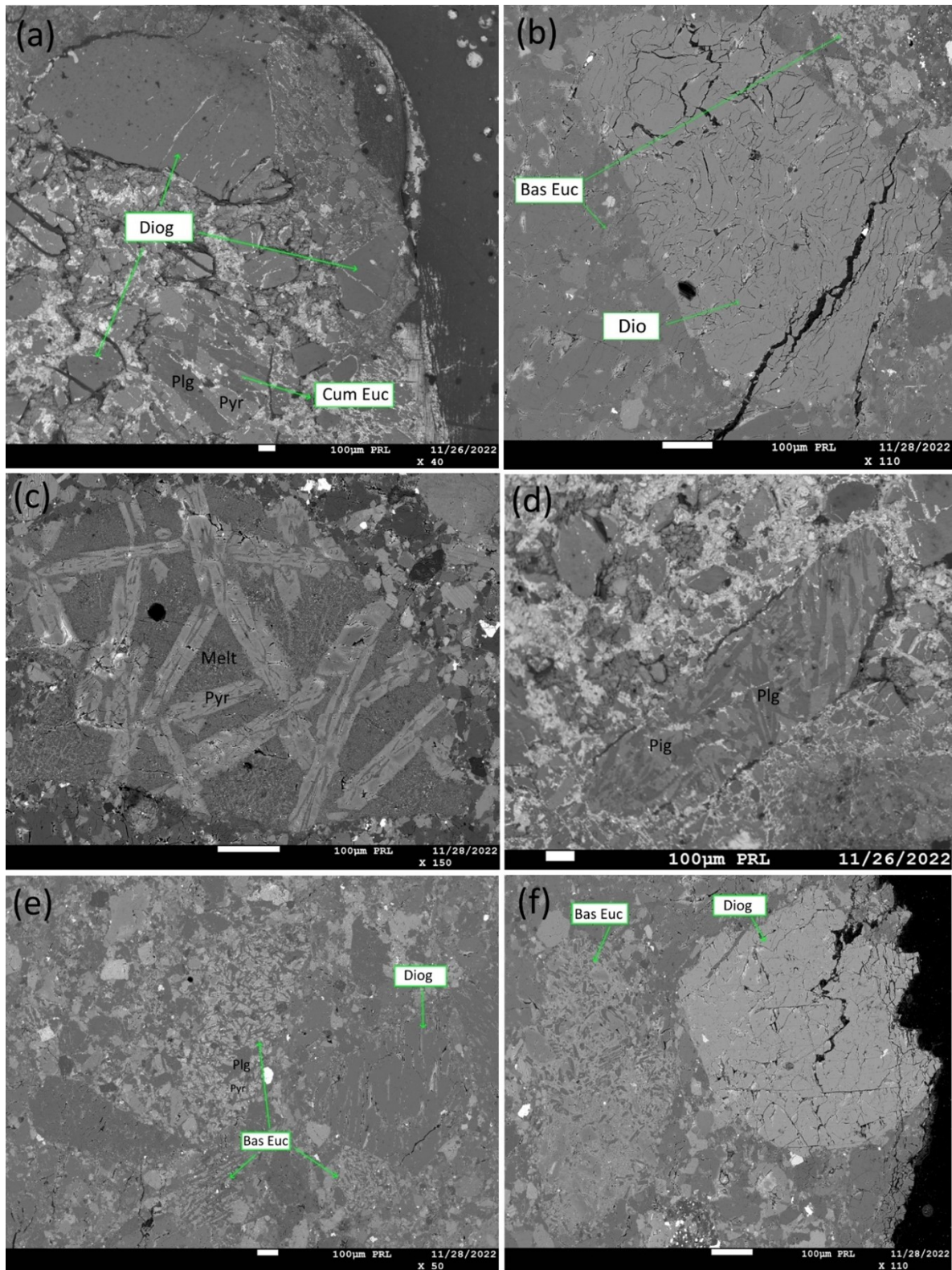


Figure 2.27: BSE images of (a) Diogenite clasts showing polymict breccia texture along with one cumulate eucrite clast displaying coarse gabbroid texture, (b) Diogenite Clast which has several fractures, and two very small ( $50$  and  $150\ \mu\text{m}$ ) basaltic clasts, (c) ophitic texture in a basaltic eucrite clast, and, (d) ophitic-modified coarse feathery texture in basaltic eucrite clast, (e) Diogenite clast and three basaltic eucrite clasts that show a texture that is finer than (d), (f) Basaltic eucrite clast adjacent to a diogenite clast of similar size. Plg: plagioclase; Pyr: pyroxene

	Diogenite Clast	Cumulate Eucrite Clast	Basaltic Eucrite Clast	Exsolved Pyroxenes in Matrix (Host)	Exsolved Pyroxenes in Matrix (Guest)
$\text{SiO}_2$	55.10	51.65	48.35	49.05	49.99
$\text{TiO}_2$	0.12	0.15	0.54	0.56	0.91
$\text{Al}_2\text{O}_3$	0.85	1.11	4.05	0.47	1.20
$\text{NaO}$	0.03	0.02	0.06	0.04	0.10
$\text{FeO}$	14.45	24.27	24.99	34.54	21.69
$\text{MnO}$	0.45	0.73	0.72	1.02	0.71
$\text{MgO}$	27.84	18.23	14.50	12.48	11.23
$\text{CaO}$	1.37	3.68	6.23	2.06	13.75
Total	100.21	99.84	99.45	100.21	99.59
<hr/>					
Wo	2.67	7.66	13.58	4.43	29.70
En	75.37	52.86	43.93	37.42	33.73
Fs	21.96	39.48	42.49	58.15	36.57

Table 2.14: Representative compositions for different pyroxenes from Lohawat.

### 2.5.3 Basaltic Eucrite Clasts

Multiple basaltic eucrite clasts were found in the Lohawat thin sections, and these were more in number than cumulate eucrite clasts (Fig. 2.27(c), (d), (e), (f)). The pyroxene is majorly pigeonite (mean composition  $\text{Fs}_{42.68}\text{Wo}_{16.56}\text{En}_{40.76}$ ). The plagioclase is calcic ( $\sim \text{An}_{81-90}$ ), which is very similar to the plagioclase from Lakangaon and Piplia Kalan, which are other basaltic eucrites. The original igneous texture can be observed as being grains of medium-size, triangular pigeonite phenocrysts encompassing the pigeonite-plagioclase matrix, which is glassy to fine-grained. Zoning can also be observed in pigeonite phenocrysts, and extensive thermal metamorphism must have been the reason for the eradication of primary zoning and equilibration of different phases while forming exsolved lamellae of augite by inversion of pigeonite to orthopyroxene. Fig. 2.27(c) displays ophitic texture in a basaltic eucrite clast, and that type of texture is replaced by a

feathery texture primarily due to shock, which led to fractures through the interface of different phases with different hardness (Fig. 2.27(d)).

The eucritic clasts from Lohawat also put forward a collection of clasts of different metamorphic types, as suggested by Takeda and Graham (1991). These include Type 1, Type 3, Type 5 and Type 6, where Type 1 is pristine basalt which has suffered very limited subsequent metamorphism, through to type 6, which has been reheated and extensively metamorphosed. The characteristics of each type differ from each other, as shown in Table 3. Type 1 basalts are characterised by mesostasis-rich basalts that cooled relatively quickly and include extensively zoned pyroxenes. Pyroxenes do not exhibit clouding or exsolution. The dark, glassy matrix and preservation of considerable Mg-Fe zoning in the pyroxenes suggest that the clast is the least altered basalt as a eucrite (Fig. 2.28(a)). Type 3 clasts are where Fe, as well as Ca enrichment towards the rim, can be observed in the pigeonite zoning (Fig. 2.28(b)). The EPMA gives superior signals for individual phases in type 5, rather than giving mixed data of two pyroxene phases, as the exsolution lamellae are wide enough for the EPMA beam to not overlap on different phases. Exsolved pigeonites with homogeneous host composition make up type 5.

Additionally, the initial Fe-dominated zoning is not seen in the pyroxenes of this type. The type 6 eucrites in this classification system cool down the most slowly. Examples of this kind typically comprise orthopyroxene inverted from pigeonite with a homogeneous host composition comparable to that of type 5 eucrites. Pigeonite must be partially inverted to orthopyroxene in order to meet this type's requirements. Clinopyroxene's transition into orthopyroxene indicates that the type 6 eucrites cool at a pace similar to the cumulate eucrites. The type 6 basaltic clast can be seen in Fig. 2.28(d).

#### 2.5.4 Accessory Phases

The accessory phases in Lohawat are silica, troilite, ilmenite, and chromite. Silica is often found on the edges of the diogenetic clasts and also in the interstices between pyroxene grains. Silica is also seen to be associated with troilite, chromite, or ilmenite, though not always (Fig. 2.19(a)). The shape of silica is not well defined and mostly exists as aggregates, unlike eucrites such as Vissannapeta, where the silica exists mostly as droplet-shaped inclusions. Ilmenite (Fig. 2.29(b), (c)) (up to 30  $\mu\text{m}$  wide) is relatively small as compared to chromite (Fig. 2.29(b)) and troilite (Fig. 2.29(d)), which are up to 50 and 100  $\mu\text{m}$  wide respectively. The shape of these metallic phases is subhedral to anhedral. The representative mineral data for these phases are given in Table 2.14. The chromite data was plotted on a Cr/(Cr+Al) vs Fe/(Fe+Mg) plot (Fig. 2.8). The chromite from Lohawat lies in the chromite region with Cr/(Cr+Al) ranging from 90.03 to 91.53 and with an average of 90.76.

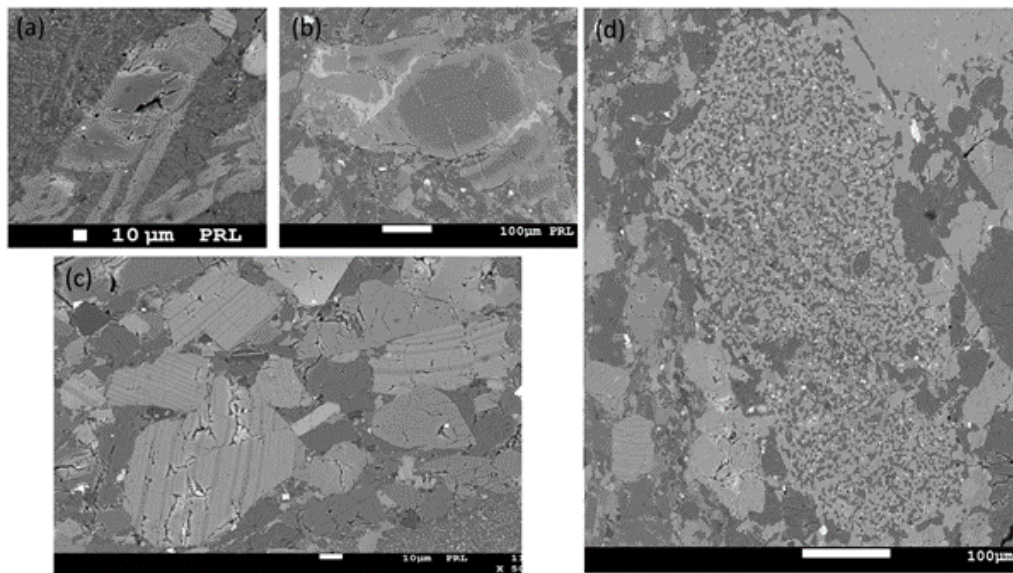


Figure 2.28: BSE images of (a) Type 1 texture of thermally metamorphosed basaltic eucrite which shows the glassy matrix, (b) Type 3 texture where the dark gray is pigeonite, (c) Type 5 eucritic texture consisting of exsolved pyroxenes where the dark gray exsolved lamellae are augites, and the light gray (host) are the pigeonites, (d) Type 6 which is the hornfels texture.

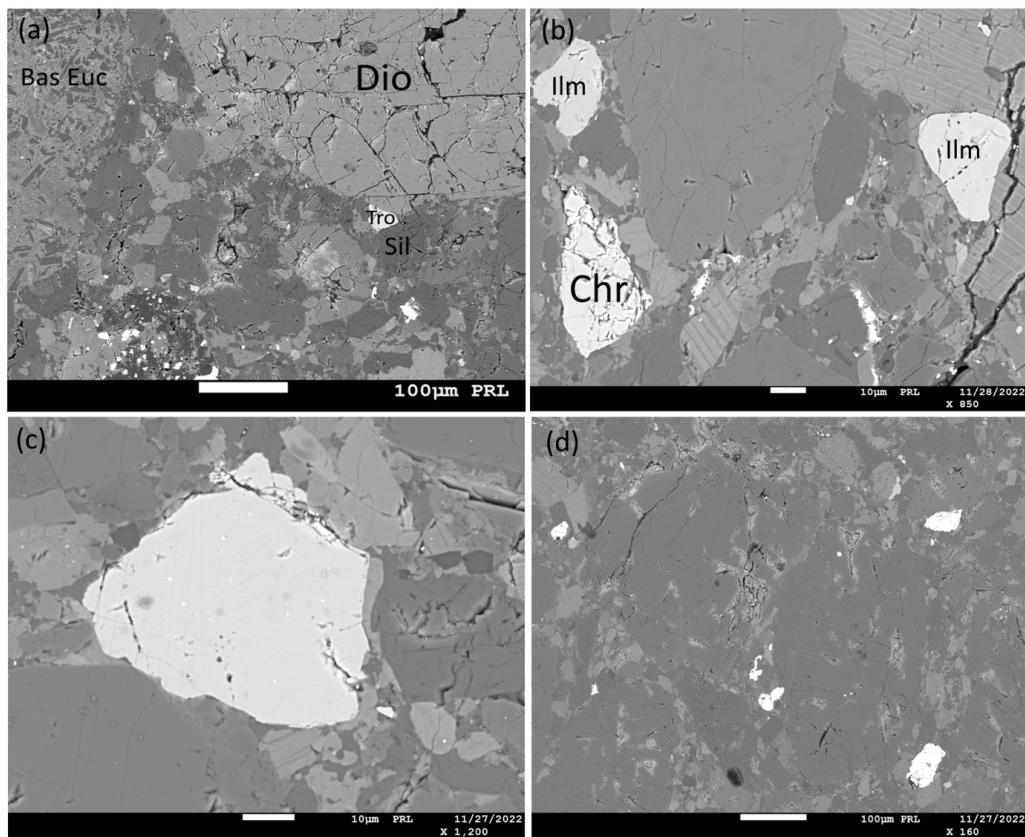


Figure 2.29: BSE images of (a) Silica aggregates along the edges of diogenetic and basaltic eucrite clast. Troilite is also present in association with silica, (b) Ilmenite and chromite grains surrounding a small diogenetic clast. Again, the silica association can be observed, (c) Ilmenite grain with a width of 50 μm. (d) Subhedral to anhedral-shaped troilite grains with sizes ranging from 20 to 100 μm.

	Ilmenite	Chromite	Troilite
TiO <sub>2</sub>	55.44	3.87	b.d.
Cr <sub>2</sub> O <sub>3</sub>	b.d.	51.59	b.d.
FeO	41.61	35.60	57.93
MnO	0.79	0.60	b.d.
MgO	1.29	1.16	b.d.
CaO	b.d.	0.09	b.d.
SO <sub>3</sub>	b.d.	b.d.	41.31
Total	99.11	99.78	99.24

Table 2.15: Representative compositions for different pyroxenes from Lohawat.

### 2.5.5 Conclusions

Howardite polymict breccia is Lohawat. It is made up of a combination of groundmass, diogenetic, and eucritic components. The petrography and geochemistry of eucritic clasts are identical to those of the eucrite in the Piplia Kalan, which is formed of basaltic pyroxene and plagioclase phases. Compared to the eucritic clast pyroxenes, the diogenetic clasts have a greater proportion of Mg-rich and Ca-poor pyroxenes. In Lohawat howardite, there are a lot of clast-rich and clast-poor melt textures, which strongly suggests a heterogeneous degree of melting without any heating event (Ray and Ghosh, 2022). Moreover, Lohawat howardite has certain unique features, such as pigeonite crystallising from ferrosilite, fine exsolution lamellae of augite inside ferrosilite, and olivine and pigeonite exhibiting a corona texture. These characteristics define the pyroxene crystallisation sequence. At a high temperature, high-Mg orthopyroxenes (enstatite) crystallise first, followed by ferrosilite, pigeonite, olivine, and augite (Biggar 1985). Fayalite and pigeonite have similar coronal textures, which shows that fayalite crystallises at a lower temperature than pigeonite (Srivastava, 2013).

## 2.6 Clouding

The very fine disseminated inclusions that are recognised in Lakangaon (Fig. 2.5(b) and Fig. 2.9(a), (b)) and Piplia Kalan (Fig. 2.16(a), (c) and Fig. 2.17(a), (b)) resemble the texture what is known as "clouding in pyroxenes and plagioclase". It has been pre-

viously observed in various eucrites, including ALHA77302, Juvinas, Pasamonte, and Stannern (Harlow and Klimentidis, 1980). Several old studies also suggest that clouding has been noted in most petrographic descriptions but has not been adequately described and interpreted. Tschermak (1885) and La Croix (1926) noted inclusions of small opaque grains. Jerome and Slodzian (1971), using an ion microprobe, recognised a high-silica and pyroxene-like phase in plagioclase and a high-Ti phase and high-Cr phase in pyroxene.

Papike and White (1979) talked about inhomogeneities in Cr distribution in equilibrated eucrite pyroxenes that may indicate the separation of a Cr-rich phase, perhaps chromite. Similarly, the clouding of pyroxene with oriented ilmenite inclusions and plagioclase with pyroxene and some silica grains has been reported by Dymek et al. (1976) for a basaltic clast from the Kapoeta howardite, and he suggested thermal metamorphism and inclusion during crystallisation as the possible explanations. Similarly, Duke and Silver (1967) and Stolper (1977) also suggested that thermal metamorphism is the reason for clouding. The pyroxene of Stannern was observed to be predominantly clouded with ilmenite by Mason et al. (1979). In the case of terrestrial rocks too, similar textural features have been observed, such as clouded plagioclase from metadolerites (e.g., Poldervaart and Gilkey, 1954; Prinz, 1964; Armbrustmacher and Banks, 1974). Buchanan et al. (2001) also described clouding in Piplia Kalan.

Fig. 2.30 includes some more highly magnified images of clouding in pyroxenes and plagioclase of Lakangaon and Piplia Kalan. There is a difference in the clouding in pyroxenes and plagioclase. The phases that cause clouding will be discussed in Section 2.6.1. In pyroxenes, the clouding-causing phases are rod-shaped; most of them are aligned in a direction, and a few are at an angle to that general direction. Also, most inclusions have a bit bright and wide side while the other side is thin and less bright, and it appears like an image of a "meteor shower" (Fig. 2.30(a)). When it comes to plagioclase, the inclusions are mostly anhedral (Fig. 2.30(b)), but in some places, some inclusions with perfect square/rectangular shapes can be seen (Fig. 2.30(c), (d)). A thin, straight line/streak can also be observed, which is entirely made up of these clouding-causing minerals like a dashed line (Fig. 2.30(b), (c)).

Coming from Lakangaon to Piplia Kalan (Fig. 2.31), things get bigger in size: the general size of clasts and grains, as well as the size of clouding-causing inclusions. In the Lakangaon sample, the clouding is extremely intensive, and almost every pyroxene grain is clouded to a lesser or greater extent, whereas in Piplia Kalan, the clouding is much more localised. This might be related to the fact that Lakangaon is among the most Fe-rich eucrite. This can be the reason for more intensive clouding as more Fe As can be seen in Fig. 2.31(b), the pyroxene grain, which is made up of mostly augite, is clouded while the surrounding pyroxene which is mostly pigeonite, looks void of any clouding. Another noticeable feature in the clouded pyroxenes from Lakangaon (Fig. 2.30(a)) is

that the exsolved lamellae of augite are not continuous from one end to another and look shifted and deformed multiple times in between, which might be an act of some micro-fractures that later got healed. Apart from one big crack that goes almost through the grain, a few mini-fractures can also be seen. It is plausible that those micro-fractures were where the inclusions formed, and the micro-fractures eventually healed. In addition to the major fracturing that we see in Piplia Kalan, Fig. 2.31(b) also shows multiple cracks and mini-fractures all over the place. The pyroxene lamellae are also deformed, and the healed micro-fractures could also be the culprit in this case. This phenomenon is called as "healed-cracks" (Metzler et al. 1995). The handful amount of troilite inclusions in just one pyroxene grain in the Vissannapeta may or may not be regarded as clouding as it is not visible throughout the sample. Note that these troilite inclusions are almost perfectly circular (Fig. 2.25), whereas the clouding-causing troilite inclusions in the pyroxenes of Lakangaon are all rod-shaped.

### 2.6.1 Identification of Clouding-Causing Phases

Because these inclusion are extremely small in size (as small as  $0.2 \times 0.05 \mu\text{m}$ ), it becomes incredibly hard to acquire the mineral data using the EPMA, as the inclusions get smaller than the EPMA beam, and then it provides mixed data. Several earlier studies relied on this mixed data to infer and identify the mineral. This method was fine, but in some places, particularly plagioclase, the clouding-causing minerals are multiple, and then one needs to acquire data for many spots to make a safe conclusion about which phases cause the clouding in pyroxene and plagioclase, and is also a tedious task as the beam may not give the mixed signal every time. Here, a different approach has been carried out using the K-means clustering algorithm. Since every phase possess a different gray value in the BSE image and the gray value of surrounding grains of different phases (that are big enough to be accurately measured by the EPMA) is known, it allows us to cluster the gray values that are closely related and assign them to a corresponding phase. The K-means clustering algorithm helps cluster the closely related gray values and gives them a unique label. This way, each phase can have a unique label, and each label can be represented with a different colour, enabling us to clearly distinguish between phases, irrespective of the size of the phase.

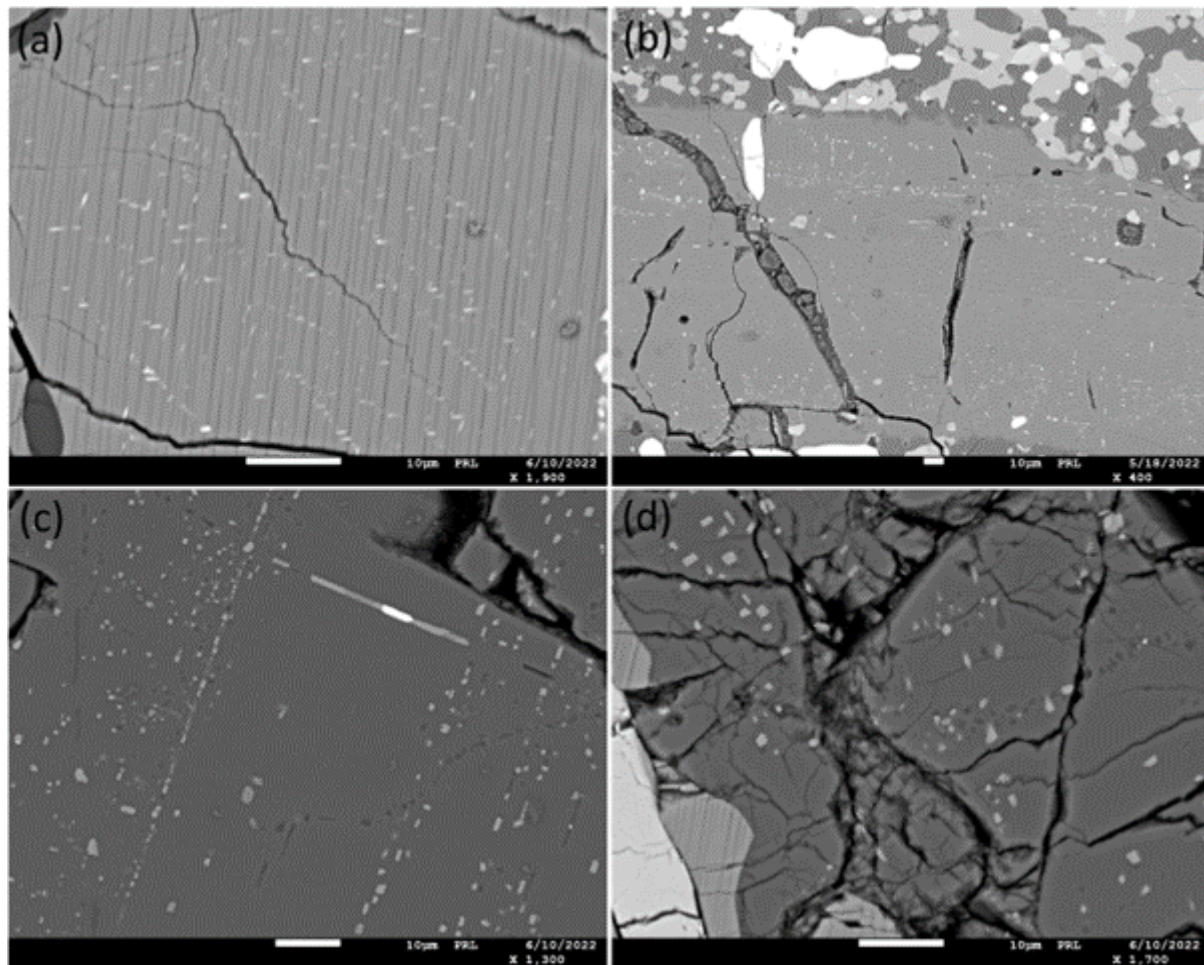


Figure 2.30: BSE images that show clouding in pyroxenes and plagioclase. (a) Pyroxene from Lakangaon; the clouding-causing minerals are thin and rod-shaped and are mostly aligned in one direction. Note that the left end of these inclusions is broader and more bright as compared to the thinner and less bright right end, and thus, the inclusions as a whole look like the pictures of a "meteor shower". The inclusions range from  $0.2 \times 0.05 \mu\text{m}$  to  $1.8 \times 0.5 \mu\text{m}$ . (b) Plagioclase from Lakangaon, which is heavily clouded; this clouding is very different from the clouding of pyroxene, where the variation in the size of clouding-causing inclusions is not huge. The inclusions are bigger in size towards the edge of the plagioclase (average  $\sim 0.6 \times 0.4 \mu\text{m}$ ) and are extremely small around the centre of the plagioclase grain ( $\sim 0.4 \times 0.2 \mu\text{m}$ ). A streak (appears like a finely dotted line) made of very fine inclusions can also be seen going through the centre of the plagioclase grain, (c) & (d) These are also plagioclase from Lakangaon and the clouding pattern here shows inclusions of various sizes (average  $\sim 1.1 \times 1.3 \mu\text{m}$ ), from almost circular to triangular and even rectangular. Again, a vertical streak of inclusions can be seen in (c), whereas (d) shows a horizontal streak made by fine silica inclusions. In (c), the bright white euhedral phase is troilite ( $\sim 5.3 \times 0.1 \mu\text{m}$ ), which has pyroxenes on both sides ( $\sim 11.3 \times 0.1 \mu\text{m}$  on the left side). Notice how even this tiny bit of pyroxene shows both augite and pigeonite. Also, another interesting observation would be that the centre of plagioclase in (d) is void of any fractures and is also void of any clouding.

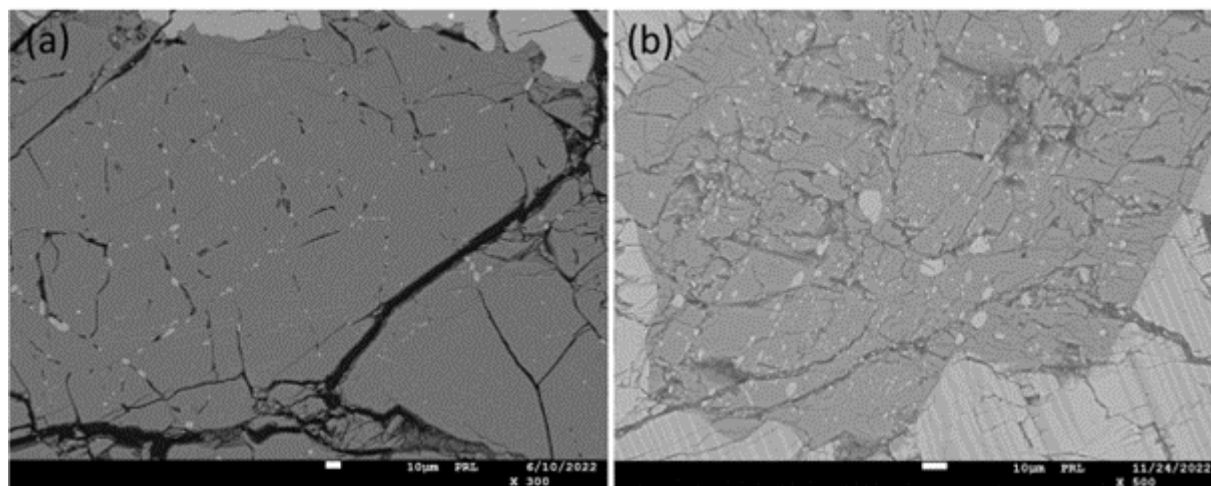


Figure 2.31: (a) Plagioclase from Piplia Kalan which is highly fractured and possesses inclusions that are small-sized (average  $\sim 1.7 \times 0.9 \mu\text{m}$ ) as well as some that are large-sized (average  $\sim 6.0 \times 6.5 \mu\text{m}$ ), (b) Pyroxene from Piplia Kalan which shows clouding where tiny rod-like inclusions are mostly in a particular orientation, and the average size is  $\sim 2.8 \times 1.9 \mu\text{m}$ .

K-means, one of the most used clustering methods, is an unsupervised machine learning algorithm to address a well-known clustering issue. The process uses a predetermined number of clusters to categorise a given data set in a concise manner. Finding k centroids, one for each cluster set, is the major goal. Due to the varied locations producing varying results, these centroids must be placed ingeniously. The best course of action is to place them as far apart from one another as you can. The next step is to locate the closest centroid point for each point that is part of a certain data set. The first phase is finished, and the group is given a label when there are no outstanding points. At this point, k new centroids must be recalculated as the centres of clusters produced by the preceding phase. The new binding between the identical data set points and the closest new central point must be created when these k new middle points are attained. It becomes a loop. This loop causes k centroids to start to shift positions until there are no more adjustments. Large-scale images are typically segmented using the clustering method. This unsupervised learning method, called clustering, divides a set of components into standard groups.

The BSE images are not very straightforward for an unsupervised algorithm because the phases do not always abruptly change gray values; the phases rather fade near the edges of the grain. Moreover, because the pyroxenes that have been dealt with exhibit no zoning and are equilibrated, the boundaries between augite and pigeonite show a smooth change in gray value and not a sharp demarcation. These reasons make it necessary to cleverly manoeuvre the parameters when the automatic segmentation is not perfect.

Fig. 2.32 and Fig. 2.33 show the results of segmenting the BSE images of the Lakangao and Piplia Kalan samples that show clouding, respectively. Along with each image, a respective plot of the counts of pixels vs the gray value has been shown which, almost always demonstrates different phases as unique peaks. Several other images of clouding in Lakangaon and Piplia Kalan sample were analysed although only a total of five have been presented as Fig. 2.32 and Fig. 2.33. To provide the best possible distinction between phases, the label values of different phases were not selected in ascending order (default), but rather the colour for each phase was carefully chosen (cracks and crevices: 1 (navy blue), silica: 3 (sapphire blue), plagioclase: 4 (light blue), augite: 6 (light green), pigeonite: 7 (yellow), chromite: 8 (orange), ilmenite: 9 (red), troilite: 10 (brown)).

In some cases, the peaks of different phases overlap with each other, as can be seen in the plot of Fig. 2.32(b) and Fig. 2.33(b), and it wrongly labels some inclusions of a particular phase. However, this problem only occurs with augite and pigeonite, and the peaks of metallic phases, plagioclase, and silica are clear and do not overlap with each other. This means that even after manual tweaking of the parameters to get the best segmentation possible, the demarcation between augite and pigeonite will be tricky, especially near the edges of the grains, where the pixel values are slightly different from the

centre of the grain. By analysing multiple images through this algorithm, it is understood that the plagioclase in Lakangaon is clouded primarily with pyroxenes (both augite and pigeonite) and secondarily with silica, and a few clusters of inclusions of chromite and troilite are present, especially near a big chromite inclusion and towards the edges of the grain, respectively. The silica inclusions are localised and do not show much spreading. Instead, they mostly occur in a file and make thin, small, straight or curvy lines within the plagioclase. The pyroxenes from Lakangaon are solely clouded with troilite, whereas the pyroxenes from Piplia Kalan are observed to be clouded with ilmenite. The plagioclase from Piplia Kalan, on the other hand, is clouded by pyroxenes (both augite and pigeonite), although some very rare occurrences of tiny chromite inclusions were detected. It was also observed by zooming a lot into the image that a single tiny inclusion consisted of one-half of augite while the other half was pigeonite.

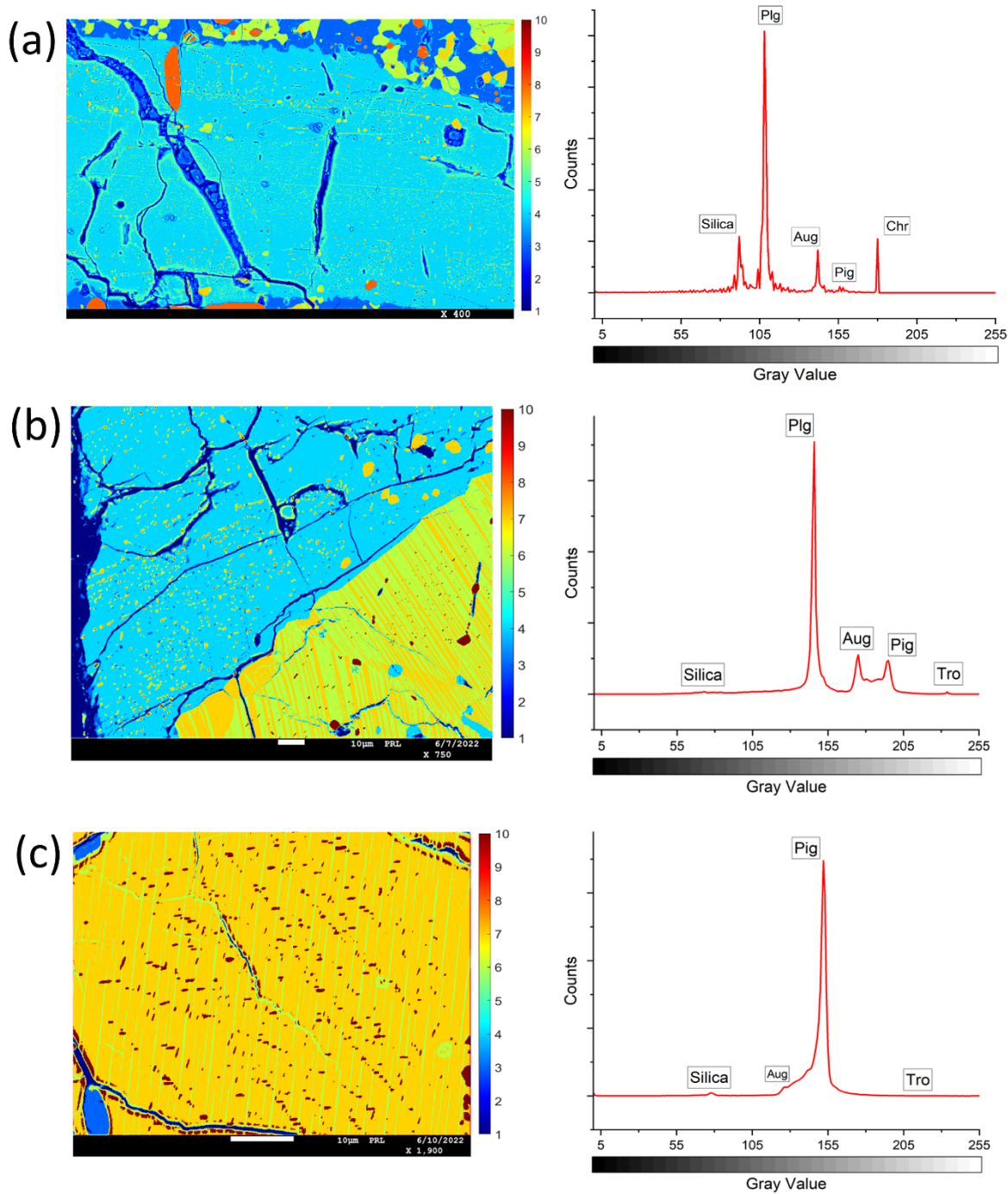


Figure 2.32: (a) The major clouding-causing agent in plagioclase is augite (light green), including the straight line/streak. Some inclusions form two to three curve lines, and these inclusions are silica (sapphire blue). A few inclusions are of pigeonite (yellow). The small inclusions that are in close proximity to the big troilite inclusion ( $\sim 7 \times 5 \mu\text{m}$ ) are also troilite (brown). (b) This image shows clouding in plagioclase as well as in pyroxene. The plagioclase is majorly clouded by plagioclase and silica in about equal proportion, but very few inclusions of troilite are also present together in clusters, especially in the part of plagioclase which is closer to the pyroxene grain. Some pyroxene inclusions in plagioclase exhibit both augite and pigeonite. The exsolved pyroxenes, on the other hand, are solely clouded by troilite in this case. (c) Extensive clouding by troilite in the exsolved pyroxenes (very fine exsolved lamellae of augite in pigeonite) of Lakangaon.

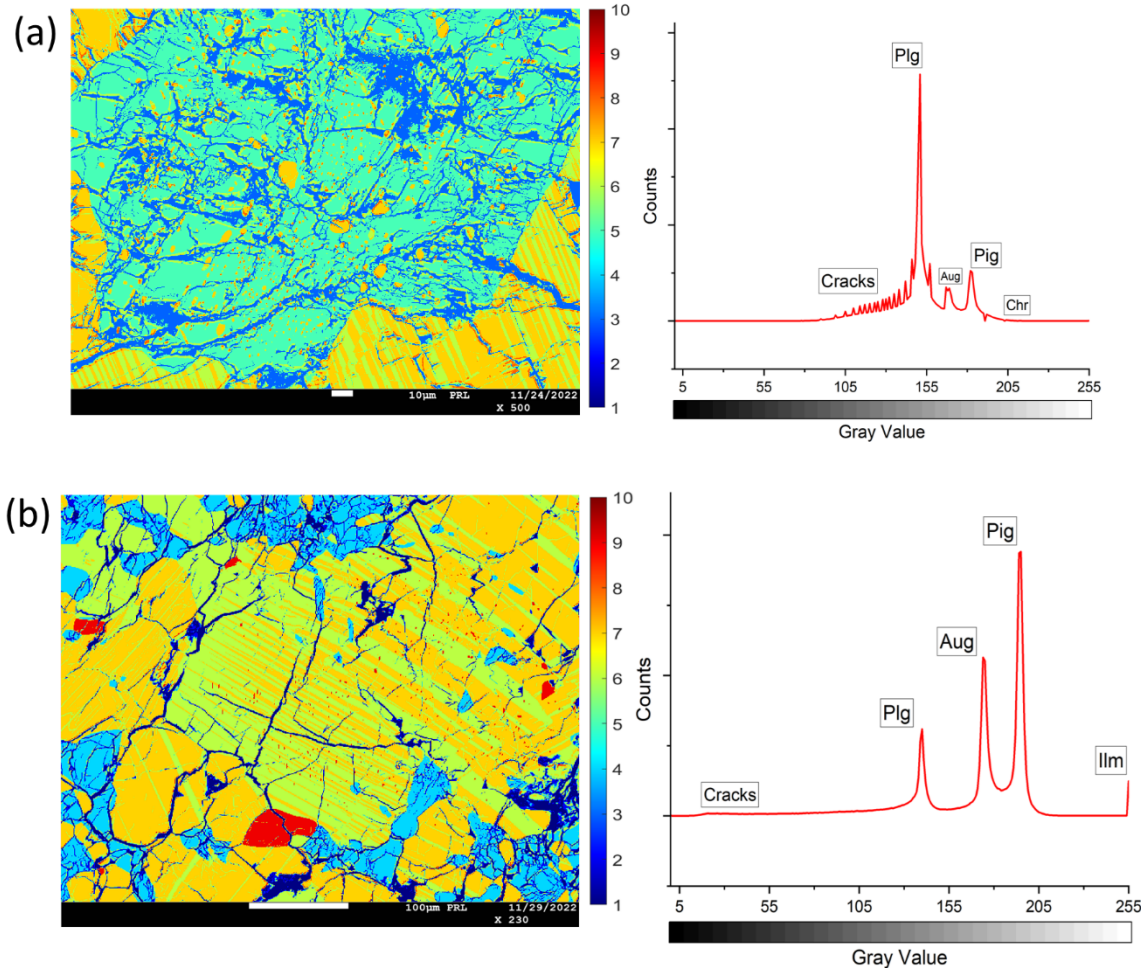


Figure 2.33: (a) Brecciated plagioclase grain (sapphire blue) from Piplia Kalan surrounded by exsolved pyroxenes (light green and yellow). The plagioclase is clouded mostly by pyroxene, although it does possess occasional inclusions of chromite. However, no clouding by silica was detected. (b) Exsolved pyroxenes that are clouded by ilmenite (red) inclusions. The surrounding plagioclase aggregates are small and do not exhibit any clouding.

## 2.6.2 Conclusions

Clouding was observed in two basaltic eucrites (Lakangaon and Piplia Kalan) out of the four samples that were studied. The other two samples consisted of a howardite and a cumulate eucrite, and these are not known to display any clouding in pyroxenes or plagioclase. Out of the four basaltic eucrites (Stannern, Juvinas, Pasamonte, and ALHA 77382) that were analysed by Harlow and Klementidis (1980), the pyroxenes of Stannern and Juvinas were observed to be clouded. ALHA 77302, which did not exhibit any clouding, had a low Fe/(Fe+Mg) ratio of 0.4 (as compared to the value of  $\sim 0.6$  for eucrites), and this was suggested as the reason for it to now show any clouding. Most pyroxenes in Pasamonte also had Fe/(Fe+Mg) ratio of  $\sim 0.5$  and did not exhibit any clouding. However, Pasamonte was marked as a unique eucrite because some areas with Fe/(Fe+Mg) ratio of  $\sim 0.6$  also only showed a trace amount of clouding on extant cracks. It was reasoned that Pasamonte underwent a lesser degree of metamorphism or cooled faster than other eucrites. This brings us to the Fe/(Fe+Mg) ratios for Piplia Kalan and Lakangaon, which are 0.80 (using the values from Shukla et al., 1997) and 0.82 (using the values from Warren and Jerde, 1987), respectively. Harlow and Klementidis (1980) made another observation regarding Pasamonte that although the pyroxenes do not show any clouding, the plagioclase from Pasamonte does. This indicates that plagioclase is more susceptible to clouding than pyroxene. Similarly, the pyroxenes from Piplia Kalan show clouding in significantly fewer pyroxene grains, whereas the plagioclase clouding in both Piplia Kalan and Lakangaon are almost of similar intensity. Dowty (1980) explains that the diffusivity of pyroxene and plagioclase varies due to differences in their structural packing densities. This can ultimately affect the threshold for clouding in eucrites, and this would mean that the clouding in pyroxenes records different P-T-f(O<sub>2</sub>) conditions than what is recorded by the clouding in plagioclase. The clouding of pyroxenes solely by troilite (FeS, with Cr, Co, and Ni below the detection limit) troilite is similar to what Mittlefehldt (2015) and Mittlefehldt et al. (2022) described in QUE 94484. The reason given for this characteristic was that this anomalous eucrite QUE 94484 experienced a reduction by S during crystallisation.

The crystallisation of basaltic eucrites has been interpreted to have occurred relatively fast as suggested by different models of formation and thermal evolution of Vesta (Mandler and Elkins-Tanton, 2013; Neumann et al., 2014; Yamaguchi et al., 2009; Schiller et al., 2011; Boggard and Garrison, 2003, and others). The incompatible elements may not have been able to exsolve during this cooling and subsequent cooling after the impact might have been slow enough for the incompatible elements to exsolve in pyroxene and plagioclase. Clouding in pyroxene and plagioclase has been interpreted to be the result of the exsolution of minor components which became incompatible and crystallised on microfractures or healed cracks and other nucleation sites during post-brecciation meta-

morphism. These assemblages of coexisting phases cause clouding record temperature (T) and oxygen fugacity ( $f\text{O}_2$ ) conditions, and therefore it can be a useful indicator of post-crystallisation conditions.

## 2.7 References

- Almond. C. (1964) Metamorphism of Tertiary lavas in Strathaird, Skye. Trans. Roy. Soc.Edin. 65,413434.
- Armbrustmacher, T. J., & Banks, N. G. (1974). Clouded plagioclase in metadolerite dikes, southeastern Bighorn Mountains, Wyoming. American Mineralogist: Journal of Earth and Planetary Materials, 59(7-8), 656-665.
- Barrat, J. A., Blichert-Toft, J., Gillet, P., & Keller, F. (2000). The differentiation of eucrites: the role of in situ crystallisation. Meteoritics & Planetary Sci
- Barrat, J. A., Yamaguchi, A., Greenwood, R. C., Bohn, M., Cotten, J., Benoit, M., & Franchi, I. A. (2007). The Stannern trend eucrites: Contamination of main group eucritic magmas by crustal partial melts. Geochimica et Cosmochimica Acta, 71(16), 4108-4124.
- Bea, F. (1996). Residence of REE, Y, Th and U in granites and crustal protoliths; implications for the chemistry of crustal melts. Journal of petrology, 37(3), 521-552.
- Bogard, D. D., & Garrison, D. H. (2003).  $^{39}\text{Ar}$ - $^{40}\text{Ar}$  ages of eucrites and thermal history of asteroid 4 Vesta. Meteoritics & Planetary Science, 38(5), 669-710.
- Buchanan, P. C., Mittlefehldt, D. W., Hutchison, R., Koeberl, C., Lindstrom, D. J., & Pandit, M. K. (2000). Petrology of the Indian eucrite Piplia Kalan. Meteoritics & Planetary Science, 35(3), 609-615.
- Chattopadhyay., Rajawat R.S., Mathurk. N.,Gajanand And Dwivedi G. L. (1998) Lohawat Meteorite-A Howardite. J. Geol. Soc.India 51, 171-174
- Christophe Michel-Lévy, M., Bourot-Denise, M., Palme, H., Spettel, B., & Wänke, H. (1987). L'eucrite de Bouvante. Chimie, pétrologie et minéralogie. Bulletin de minéralogie, 110(4), 449-458.
- Cleverly, W. H., Jarosewich, E., & Mason, B. (1986). Camel Donga meteorite, a new eucrite from the Nullarbor Plain, Western Australia. Meteoritics, 21(3), 263-269.
- Duke, M. B. (1965). Metallic iron in basaltic achondrites. Journal of Geophysical Research, 70(6), 1523-1527.
- Duke, M. B., & Silver, L. T. (1967). Petrology of eucrites, howardites and Mesosiderites. Geochimica et Cosmochimica Acta, 31(10), 1637-1665.

Dymek, R. F., Albee, A. L., Chodos, A. A., & Wasserburg, G. J. (1976). Petrography of isotopically-dated clasts in the Kapoeta howardite and petrologic constraints on the evolution of its parent body. *Geochimica et Cosmochimica Acta*, 40(9), 1115-1130.

Ghosh, S., Pant, N. C., Rao, T. K., Mohana, C. R., Ghosh, J. B., Shome, S., ... & Suthar, K. M. (2000). The Vissannapeta eucrite. *Meteoritics & Planetary Science*, 35(5), 913-917.

Greenwood, R. C., Barrat, J. A., Yamaguchi, A., Franchi, I. A., Scott, E. R., Bottke, W. F., & Gibson, J. M. (2014). The oxygen isotope composition of diogenites: Evidence for early global melting on a single, compositionally diverse, HED parent body. *Earth and Planetary Science Letters*, 390, 165-174.

Greenwood, R. C., Franchi, I. A., Jambon, A., & Buchanan, P. C. (2005). Widespread magma oceans on asteroidal bodies in the early solar system. *Nature*, 435(7044), 916-918.

Haba, M. K., Yamaguchi, A., Horie, K., & Hidaka, H. (2014). Major and trace elements of zircons from basaltic eucrites: Implications for the formation of zircons on the eucrite parent body. *Earth and Planetary Science Letters*, 387, 10-21.

Harlow, G. E., & Klementidis, R. (1980). Clouding of pyroxene and plagioclase in eucritesImplications for post-crystallisation processing. In *Lunar and Planetary Science Conference Proceedings* (Vol. 11, pp. 1131-1143).

Hewins, R. H., & Newsom, H. E. (1988). Igneous activity in the early solar system. *Meteorites and the early solar system*, 73-101.

Hoskin, P. W. O., & Black, L. P. (2000). Metamorphic zircon formation by solid-state recrystallisation of protolith igneous zircon. *Journal of metamorphic Geology*, 18(4), 423-439.

Hsu, W., & Crozaz, G. (1996). Mineral chemistry and the petrogenesis of eucrites: I. Noncumulate eucrites. *Geochimica et Cosmochimica Acta*, 60(22), 4571-4591.

Hutchison, R., & Bevan, J. C. (1977). The Cuillin layered igneous complex—evidence for multiple intrusion and former presence of a picritic liquid. *Scottish Journal of Geology*, 13(3), 197-209.

Ikeda, Y., & Takeda, H. (1985). A model for the origin of basaltic achondrites based on the Yamato 7308 howardite. *Journal of Geophysical Research: Solid Earth*, 90(S02), C649-C663.

Ireland, T. R., & Wlotzka, F. (1992). The oldest zircons in the solar system. *Earth and Planetary Science Letters*, 109(1-2), 1-10.

Jarosewich, E. (1990). Chemical analyses of meteorites: A compilation of stony and iron meteorite analyses. *Meteoritics*, 25(4), 323-337.

Jérôme, D. Y., & Slodzian, G. (1971). Utilisation du microanalyseur ionique en géochimie. Application à la météorite de Juvinas. Bulletin de Minéralogie, 94(5), 538-548.

Lacroix, A. (1926). L'Eucrite de Béréba (Haute-Volta) et les météorites feldspathiques en général. Archives du Muséum national d'Histoire naturelle, 6ème série, 1(1), 15-55.

Lawrence, D. J., Peplowski, P. N., Prettyman, T. H., Feldman, W. C., Bazell, D., Mittlefehldt, D. W., ... & Yamashita, N. (2013). Constraints on Vesta's elemental composition: Fast neutron measurements by Dawn's gamma ray and neutron detector. Meteoritics & Planetary Science, 48(11), 2271-2288.

Ma, M. S., & Schmitt, R. A. (1979). Genesis of the cumulate eucrites Serra de Magé and Moore County: A geochemical study. Meteoritics, 14(1), 81-89.

Mahajan, R. R., Murty, S. V. S., & Ghosh, S. (2000). Exposure ages of Lohawat (howardite) and Vissannapeta (eucrite), the recent falls in India. Meteoritics and Planetary Science Supplement, 35, A101.Singh et al., 1998; Sisodia et al., 2001).

Mandler, B. E., & Elkins-Tanton, L. T. (2013). The origin of eucrites, diogenites, and olivine diogenites: Magma ocean crystallisation and shallow magma chamber processes on Vesta. Meteoritics & Planetary Science, 48(11), 2333-2349.

Mason, B., Jarosewich, E., & Nelen, J. A. (1979). The pyroxene-plagioclase achondrites. Smithson. Contrib. Earth Sci, 22, 27-45.

McCarthy, T. S., Erlank, A. J., & Willis, J. P. (1973). On the origin of eucrites and diogenites. Earth and Planetary Science Letters, 18(3), 433-442.

McCarthy, T. S., Erlank, A. J., Willis, J. P., & Ahrens, L. H. (1974). New chemical analyses of six achondrites and one chondrite. Meteoritics, 9(3), 215-221.

McSween Jr, H. Y., Binzel, R. P., De Sanctis, M. C., Ammannito, E., Prettyman, T. H., Beck, A. W., ... & Dawn Science Team. (2013). Dawn; the Vesta-HED connection; and the geologic context for eucrites, diogenites, and howardites. Meteoritics & Planetary Science, 48(11), 2090-2104.

Metzler K., Bobe K., Palme H., Spettel B., and Stoßfler D. (1995) Thermal and impact Metamorphism on the HED parent asteroid. Planet. Space Sci. 43, 499–525

Metzler, K., Bobe, K. D., Palme, H., Spettel, B., & Stöffler, D. (1995). Thermal and impact metamorphism on the HED parent asteroid. Planetary and Space Science, 43(3-4), 499-525.

Minster, J. F., & Allègre, C. J. (1978). Systematic use of trace elements in igneous processes. Contribuitons to Mineralogy and Petrology, 68, 37–52.

Misawa, K., Yamaguchi, A., & Kaiden, H. (2005). U-Pb and 207Pb-206Pb ages of

zircons from basaltic eucrites: Implications for early basaltic volcanism on the eucrite parent body. *Geochimica et Cosmochimica Acta*, 69(24), 5847-5861.

Mittlefehldt, D. W. (1979). Petrographic and chemical characterisation of igneous lithic clasts from mesosiderites and howardites and comparison with eucrites and diogenites. *Geochimica et Cosmochimica Acta*, 43(12), 1917-1935.

Mittlefehldt, D. W. (2015). Asteroid (4) Vesta: I. The howardite-eucrite-diogenite (HED) clan of meteorites. *Geochemistry*, 75(2), 155-183.

Mittlefehldt, D. W., & Lindstrom, M. M. (1991). Generation of abnormal trace element abundances in Antarctic eucrites by weathering processes. *Geochimica et Cosmochimica Acta*, 55(1), 77-87.

Mittlefehldt, D. W., & Lindstrom, M. M. (1998). Petrology and geochemistry of lodranite GRA 95209. *Meteoritics and Planetary Science Supplement*, 33, A111.

Mittlefehldt, D. W., Greenwood, R. C., Berger, E. L., Le, L., Peng, Z. X., & Ross, D. K. (2022). Eucrite-type achondrites: Petrology and oxygen isotope compositions. *Meteoritics & Planetary Science*, 57(2), 484-526.

Neumann, W., Breuer, D., & Spohn, T. (2014). Differentiation of Vesta: Implications for a shallow magma ocean. *Earth and Planetary Science Letters*, 395, 267-280.

Ohara, Y., Yoshida, T., Kato, Y. et al. Giant Megamullion in the Parece Vela Backarc Basin. *Marine Geophysical Researches* 22, 47–61 (2001).

Palme, H., Baddehausen, H. I. L. D. E. G. A. R. D., Blum, K., Cendales, M., Dreibus, G., Hofmeister, H., ... & Wänke, H. (1978). New data on lunar samples and achondrites and a comparison of the least fractionated samples from the Earth, the moon and the eucrite parent body. In *Lunar and Planetary Science Conference Proceedings* (Vol. 9, pp. 25-57).

Palme, H., Wlotzka, F., Spettel, B., Dreibus, G., & Weber, H. (1988). Camel Donga: a eucrite with high metal content. *Meteoritics*, 23(1), 49-57.

Papike, J. J., & White, C. (1979). Pyroxenes from planetary basalts: Characterisation of "other" than quadrilateral components. *Geophysical Research Letters*, 6(12), 913-916.

Poldervaart, A., & Gilkey, A. K. (1954). On clouded plagioclase. *American Mineralogist: Journal of Earth and Planetary Materials*, 39(1-2), 75-91.

Prinz, M. (1964). Geologic evolution of the Beartooth Mountains, Montana and Wyoming. Part 5. Mafic dike swarms of the southern Beartooth Mountains. *Geological Society of America Bulletin*, 75(12), 1217-1248.

Ray, D., & Ghosh, S. (2022). The unusual low Mg rock clasts from Lohawat Howardite, India: Petrogenetic implications. *Journal of Earth System Science*, 131(2), 125.Biggar

(1985)

Reed, S. J. B. (2005). Electron microprobe analysis and scanning electron microscopy in geology. Cambridge university press.

Righter, K., & Drake, M. J. (1997). A magma ocean on Vesta: Core formation and petrogenesis of eucrites and diogenites. *Meteoritics & Planetary Science*, 32(6), 929-944.

Rubin, A. E. (2004). Aluminian low-Ca pyroxene in a Ca-Al-rich chondrule from the Semarkona meteorite. *American Mineralogist*, 89(5-6), 867-872. Rubin, A. E., & Wasson, J. T. (1995). Variations of chondrite properties with heliocentric distance. *Meteoritics*, 30.

Rubin, A. E., Kallemeyn, G. W., & Wasson, J. T. (2002). A AB-complex iron meteorite containing low-Ca clinopyroxene: northwest Africa 468 and its relationship to lodranites and formation by impact melting. *Geochimica et Cosmochimica Acta*, 66(20), 3657-3671.

Russell, C. T., Raymond, C. A., Coradini, A., McSween, H. Y., Zuber, M. T., Nathues, A., & Titus, T. N. (2012). Dawn at Vesta: Testing the protoplanetary paradigm. *Science*, 336(6082), 684-686.

Ruzicka, A., Snyder, G. A., & Taylor, L. A. (1997). Vesta as the howardite, eucrite and diogenite parent body: Implications for the size of a core and for large-scale differentiation. *Meteoritics & Planetary Science*, 32(6), 825-840.

Sarbadhikari, A. B., Mahajan, R. R., Das, P., Chakraborty, S., Babu, E. V. S. S. K., Kumar, T. V., & Sisodia, M. S. (2017, August). New constraints of the petrogenesis of Piplia Kalan eucrite. In *METEORITICS & PLANETARY SCIENCE* (Vol. 52, Pp. A17-A17). 111 RIVER ST, HOBOKEN 07030-5774, NJ USA: WILEY.

Sawka, W. N. (1988). REE and trace element variations in accessory minerals and hornblende from the strongly zoned McMurry Meadows Pluton, California. *Earth and Environmental Science Transactions of The Royal Society of Edinburgh*, 79(2-3), 157-168.

Schiller, M., Baker, J., Creech, J., Paton, C., Millet, M. A., Irving, A., & Bizzarro, M. (2011). Rapid timescales for magma ocean crystallisation on the howardite–eucrite–diogenite parent body. *The Astrophysical Journal Letters*, 740(1), L22.

Shukla, A. D., Shukla, P. N., Suthar, K. M., Bhandari, N., Vaya, V. K., Sisodia, M. S., ... & Rajawat, R. S. (1997). Piplia Kalan eucrite: Fall, petrography and chemical characteristics. *Meteoritics & Planetary Science*, 32(5), 611-615.

Srinivasan, G. (2002, March). 26Al-26Mg Systematics in A881394 Eucrite. In *Lunar and Planetary Science Conference* (p. 1489).

Srinivasan, G., Goswami, J. N., & Bhandari, N. (1999). 26Al in eucrite Piplia Kalan:

- Plausible heat source and formation chronology. *Science*, 284(5418), 1348-1350.
- Srivastava, R. K. (2013). Petrography and petrogenesis of some Indian basaltic achondrites derived from the HED parent body: Insights from electron microprobe analyses. *Journal of Earth System Science*, 122, 729-741.
- Stolper, E. (1977). Experimental petrology of eucritic meteorites. *Geochimica et Cosmochimica Acta*, 41(5), 587-611.
- Takeda, H. (1997). Mineralogical records of early planetary processes on the howardite, eucrite, diogenite parent body with reference to Vesta. *Meteoritics & Planetary Sciences*, 32(2), 217-230.
- Takeda, H., & Graham, A. L. (1991). Degree of equilibration of eucritic pyroxenes and thermal metamorphism of the earliest planetary crust. *Meteoritics*, 26(2), 129-134.
- Takeda, H., Mori, H., Delaney, J. S., Prinz, M., Harlow, G. E., & Ishii, T. (1983). Mineralogical comparison of Antarctic and non-Antarctic HED (howardites-eucrites-diogenites) achondrites.
- Treiman, A. H. (1997). The parent magmas of the cumulate eucrites: A mass balance approach. *Meteoritics & Planetary Science*, 32(2), 217-230.
- Tschermark, G. (1923). Lehrbuch der mineralogie. Hölder-Pichler-Tempsky.
- Vayav. K., Mehtad. S., Bafnap. C., Sisodium. S. And Shrivastava K. L. (1996) The Pipliya Meteor Shower: A Preliminary Study. *Curr. Sci.* 71,253-257.
- Wänke H. et al. (1972) Multielement analyses of lunar samples and some implications of the results. *Proc. Lunar Sci. Conf.* 3rd, 1251-1268.
- Wänke, H., Baddehausen, H., Blum, K., Cendales, M., Dreibus, G., Hofmeister, H., ... & Vilcsek, E. (1977). On the chemistry of lunar samples and achondrites-Primary matter in the lunar highlands: A re-evaluation. In *Lunar and Planetary Science Conference Proceedings* (Vol. 8, pp. 2191-2213).
- Wänke, H., Palme, H., Baddehausen, H., Dreibus, G., Jagoutz, E., Kruse, H., ... & Thacker, R. (1974). Chemistry of Apollo 16 and 17 samples-Bulk composition, late stage accumulation and early differentiation of the moon. In *Lunar and Planetary Science Conference Proceedings* (Vol. 5, pp. 1307-1335).
- Warren, P. H. (1997). Magnesium oxide-iron oxide mass balance constraints and a more detailed model for the relationship between eucrites and diogenites. *Meteoritics & Planetary Science*, 32(6), 945-963.
- Warren, P. H., & Jerde, E. A. (1987). Composition and origin of Nuevo Laredo trend eucrites. *Geochimica et Cosmochimica Acta*, 51(3), 713-725.
- Warren, P. H., & Kallemeyn, G. W. (2001, March). Eucrite Bluewing 001: A Stannern-like bulk composition and its linkage with other unequilibrated HED basalts.

In 32nd Lunar and Planetary Science Conference (p. 2114).

Warren, P. H., Jerde, E. A., Migdisova, L. F., & Yaroshevsky, A. A. (1990). Pomozdinoan anomalous, high-MgO/FeO, yet REE-rich eucrite. In Lunar and Planetary Science Conference Proceedings (Vol. 20, pp. 281-297).

Warren, P. H., Kallemeijn, G. W., & Jerde, E. A. (1985). Geochemistry of Lakangaon, the Most Fe-Rich Eucrite. *Meteoritics*, 20, 779.

Yamaguchi, A., Barrat, J. A., Greenwood, R. C., Shirai, N., Okamoto, C., Setoyanagi, T., ... & Bohn, M. (2009). Crustal partial melting on Vesta: Evidence from highly metamorphosed eucrites. *Geochimica et Cosmochimica Acta*, 73(23), 7162-7182.

Yamaguchi, A., Takeda, H., Bogard, D. D., & Garrison, D. (1994). Textural variations and impact history of the Millbillillie eucrite. *Meteoritics*, 29(2), 237-245.

Yamaguchi, A., Taylor, G. J., & Keil, K. (1996). Global crustal metamorphism of the eucrite parent body. *Icarus*, 124(1), 97-112.

Yamaguchi, A., Taylor, G. J., Keil, K., Floss, C., Crozaz, G., Nyquist, L. E., ... & Shih, C. Y. (2001). Post-crystallisation reheating and partial melting of eucrite EET90020 by impact into the hot crust of asteroid 4Vesta 4.50 Ga ago. *Geochimica et Cosmochimica Acta*, 65(20), 3577-3599.

Zhang, A. C., Wang, R. C., Hsu, W. B., & Bartoschewitz, R. (2013). Record of S-rich vapors on asteroid 4 Vesta: Sulfurization in the Northwest Africa 2339 eucrite. *Geochimica et Cosmochimica Acta*, 109, 1-13.

# Chapter 3

## Bulk Major and Trace Element Composition

### 3.1 Analytical Methods

The three eucrite and one howardite samples were powdered using agate mortar and pestle. For the determination of elemental concentration, approximately 10 mg of sample powders were dissolved in 15 ml screw-cap Teflon vials from Savillex using a mixture of 1 ml concentrated  $\text{HNO}_3$  and 1 ml concentrated HF acids. After 48 hours, the acid mixture was evaporated, and a mixture of 1 ml concentrated  $\text{HNO}_3$ , and 1 ml concentrated  $\text{HCl}$  was added to the sample. After another 48 hours of reaction at 100 degree Celsius, the Teflon vials were opened for evaporation, and the residues were dissolved in 2 ml of  $\text{HNO}_3$ . Two separate 125 ml pre-cleaned HDPE bottles (from Tarsons) were used for each sample for making trace elements aliquots with a dilution factor of  $\sim 4,000$  and a major elements aliquot with a dilution factor of  $\sim 10,000$ . The dilution was carried out using 18.2 MΩ water. Sample preparation was executed in class 10k clean lab at the Centre for Earth Sciences (CEaS), Indian Institute of Science (IISc), Bangalore.

Elemental concentrations were measured using a quadrupole Inductively Coupled Plasma Mass Spectrometer (ICP-MS, Thermo Scientific X-Series II) at CEaS, IISc, equipped with skimmer cones. A CETAC ASX-520 auto-sampler was used. The up-take time for samples and standards was 50 seconds, while the rinse time was 90 seconds (in 2%  $\text{HNO}_3$ ). The  $\text{CeO}^+/\text{Ce}^+$  ratio was kept below 0.5% to minimise oxide-related interferences so as to eradicate the possibility of oxide-related interferences, which affect the measurements of some of the middle to heavy-REEs. All raw counts were corrected for the contribution from acid blanks. USGS rock standards BHVO-2 (Hawaiian basalt), AGV-2 (Guano Valley Andesite), and BCR-2 (Columbia River basalt). The accuracy of the data was tested by analysing USGS rock standard BIR-1 (Icelandic basalt) run as an

unknown. The reproducibility for trace and major element concentration data is better than 5% for most elements.

## 3.2 Whole-Rock Chemistry

### 3.2.1 Basaltic and Cumulate Eucrites

Eucrites are divided into cumulates and non-cumulates based on the chemical makeup of the whole meteorite. These two groups separate themselves in the  $\text{TiO}_2$  vs  $\text{FeO}^*/\text{MgO}$  diagram (Fig. 3.1). The plot further segregates the basaltic eucrites into two distinct trends, the Main-Group Nuevo Laredo (MGNL) trend and the Stannern trend (Barrat et al., 2003, Barrat et al., 2007). Although the eucrites from both trends exhibit similar  $\text{FeO}^*/\text{MgO}$  ratios, the percentage of  $\text{TiO}_2$  in the Stannern trend can be seen to be up to 1.4, whereas the MGNL trend eucrites show values of up to  $\sim 1.0$  for the same. The cumulate eucrites, on the other hand, show less  $\text{TiO}_2$  (up to  $\sim 0.5$ ) and  $\text{FeO}/\text{MgO}$  (up to  $\sim 2.5$ ) concentrations than the basaltic eucrites. Lakangaon and Piplia Kalan both fall under the MGNL trend of basaltic eucrite. Lakangaon, being known for its highest bulk Fe content shows greater values of  $\text{FeO}^*/\text{MgO}$  and  $\text{TiO}_2$  as compared to Piplia Kalan. Vissannapeta lies perfectly in the range of cumulate eucrites. The measured data for all four samples have been presented in Table 3.1.

Plotting an incompatible element like La against  $\text{FeO}^*/\text{MgO}$  or Sc also provides segregation between the MG-NL trend and Stannern trend of basaltic eucrites (Fig. 3.2 (a), (b)). In these plots, the Stannern trend eucrites have very similar major element composition ( $\text{FeO}^*/\text{MgO}$  and Sc) but a high concentration of La (incompatible element). In the La vs  $\text{FeO}^*/\text{MgO}$  plot (Fig. 3.2 (a)) too, we see that Lakangaon and Piplia Kalan are distant from each other even though they have quite similar trace element compositions (Table 3.1), and this is again because of high bulk Fe content of Lakangaon. La vs Sc plot (Fig. 3.2 (b)) further seems to divide the cumulate eucrites into two separate regions. Yamaguchi et al. (2009) proposed the bottom-right region ( $> 25$  ppm Sc and  $< 2$  ppm La) to be included as the third chemical group of basaltic eucrites and to be called as residual eucrites. As can be seen from the plot, this proposed group of basaltic eucrites will include some basaltic eucrites as well as cumulate eucrites that fall into that region. These residual eucrites are depleted in light REE contents and were probably deeply seated in the crust. This is said to be consistent with the model where the MGNL eucrite magmas are contaminated by partial melting of the crust, which explains the high incompatible trace element concentrations of the Stannern trend eucrites, put forward by Barrat et al. (2007).

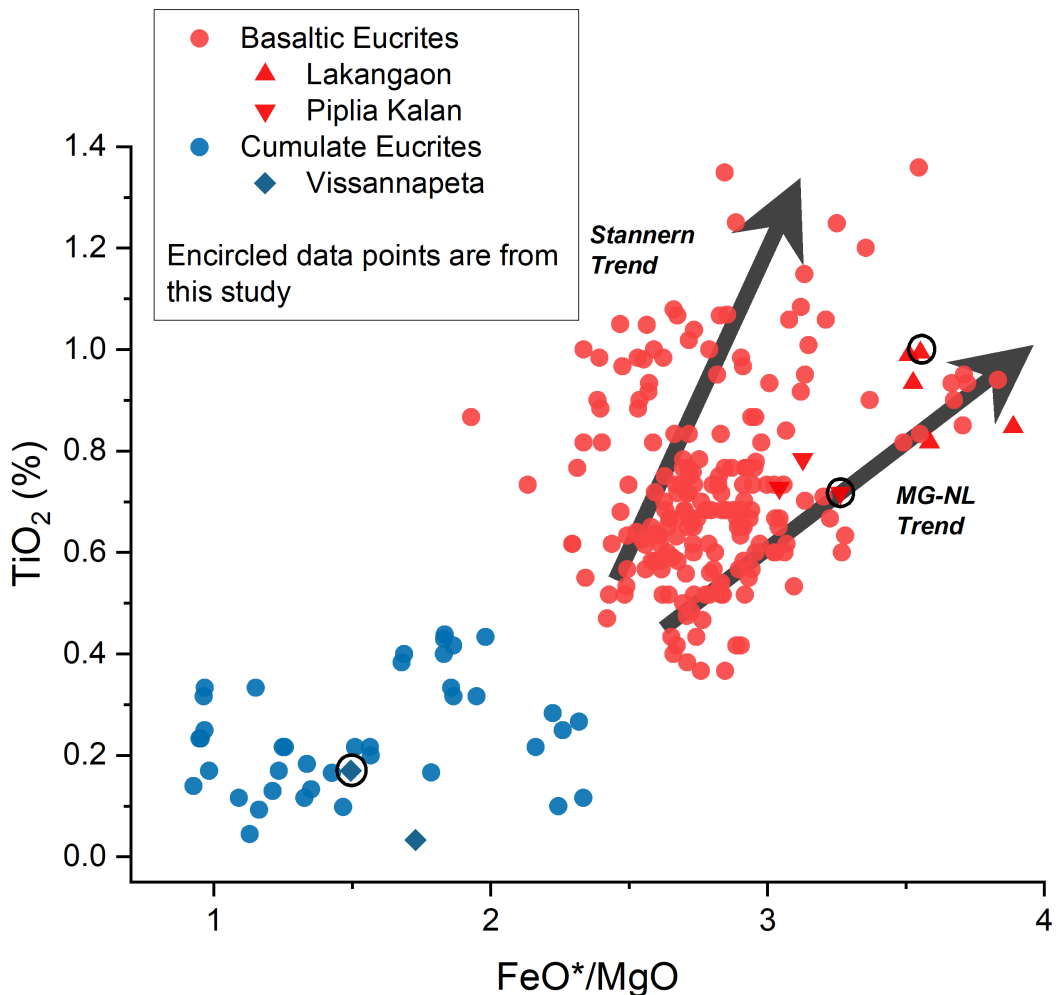


Figure 3.1:  $\text{TiO}_2$  vs  $\text{FeO}^*/\text{MgO}$  plot for cumulate and basaltic eucrites. The data points for this study are Lakangaon, Piplia Kalan, and Vissannapetra. The Stannern and MG-NL trend segregation can be observed. The cumulate eucrites also form a separate cluster with significantly less  $\text{FeO}^*/\text{MgO}$  and  $\text{TiO}_2$  concentration. The literature data (red and blue circles) have been taken from the data compiled by Mittlefehldt (2015) (which included hundreds of studies which are mentioned therein) and Dhaliwal et al. (2023).

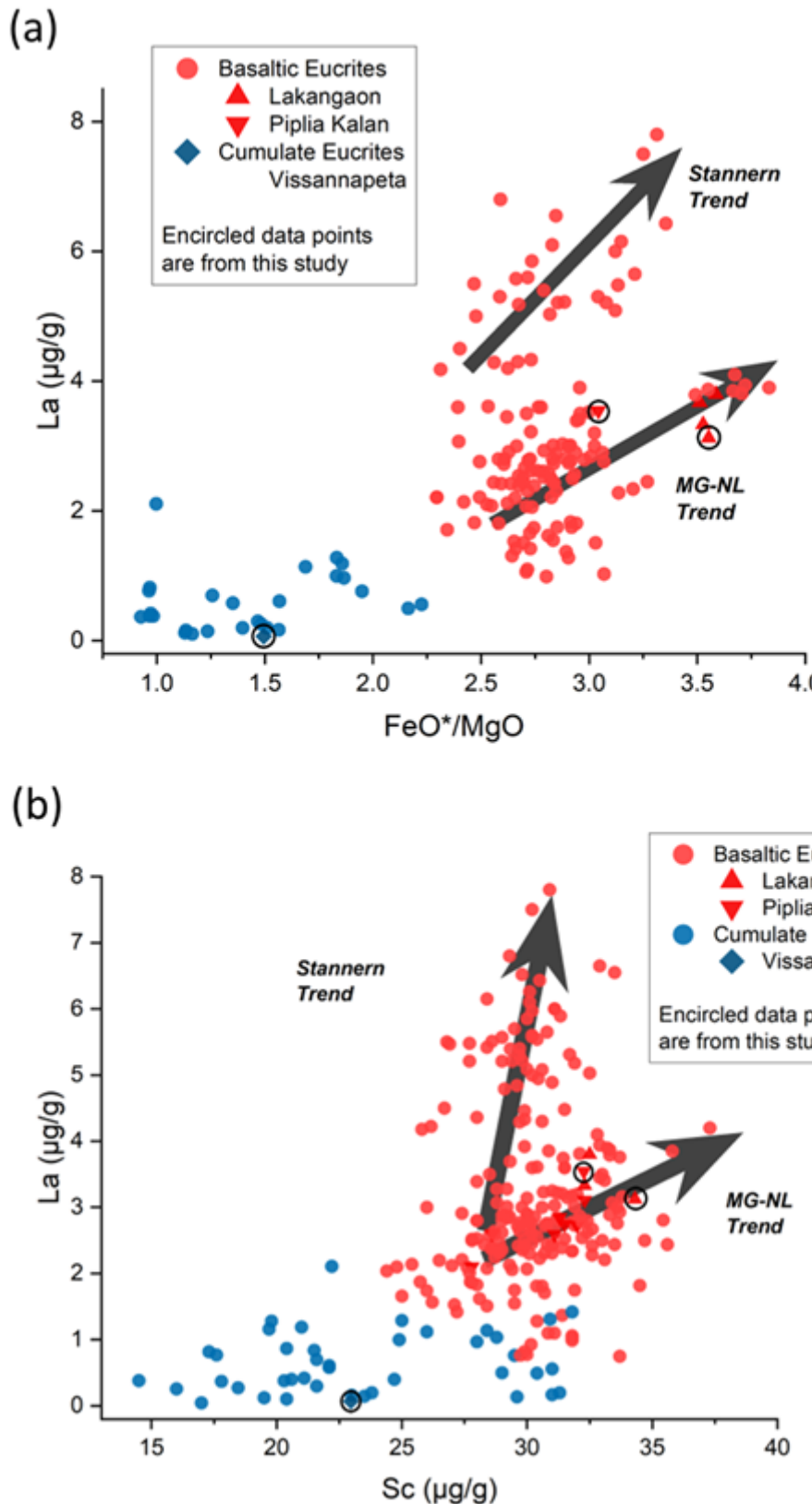


Figure 3.2: (a) La vs  $\text{FeO}^*/\text{MgO}$  plot, (b) La vs Sc Plot. The concentrations of La and Sc are in the order of ppm. The literature data (red and blue circles) have been taken from the data compiled by Mittlefehldt (2015) and Dhaliwal et al. (2023).

The reason for this segregation is based on the formation mechanisms of the Stannern and MGNL trend. The formation mechanisms still remain controversial even after half a century of rigorous studies. The genesis of the entire range of eucrites and a variety of cumulates is thought to have come from an early global magma ocean that occurred within the HED parent body (Ikeda and Takeda, 1985; Righter and Drake, 1997; Warren, 1997, Ruzicka et al., 1997; Greenwood et al., 2005). According to experimental studies and trace element systematics, the Main Group-Nuevo Laredo trend eucrites can be described as the result of a fractional crystallisation sequence (e.g., Warren and Jerde, 1987). Assuming early Main Group eucrites like Juvinas can be generated from the magma ocean, magma ocean models can explain the variety of compositions demonstrated by the Main Group-Nuevo Laredo trend eucrites. It is more difficult to understand where the Stannern trend eucrites came from. A complex scenario, including the interaction between eucritic and highly residual melts, is sufficient to explain the decoupling of major elements from incompatible trace elements using a magma ocean model (Barrat et al., 2000; Warren and Kallemeyn, 2001). Partly as a result of these difficulties, magma ocean models are not universally accepted, and instead, partial melting models have been suggested as a more effective way to explain the petrogenetic relationship between the Main Group and Stannern eucrites, particularly with regard to the incompatible components. Stannern trend eucrites may therefore have originated from the same mantle source as the main group eucrites, albeit at lower melting points and perhaps at somewhat different oxygen fugacities. Therefore, it is possible that some of the primary melt diversity from the parent body mantle can be seen in the diversity of the eucritic melts (e.g., Consolmagno and Drake, 1977; Stolper, 1977; Mittlefehldt, 1979; Mittlefehldt and Lindstrom, 2003).

The coarse-grained rocks known as cumulate eucrites have greater Mg-numbers and lower incompatible trace element abundances than basaltic eucrites. Additionally, their Rare-Earth Element (REE) patterns exhibit strong Eu anomalies, which is a characteristic compatible with plagioclase accumulation. The Mg-numbers ( $((\text{Mg}/(\text{Mg} + \text{Fe})) \times 100)$ ), Ti, and incompatible trace element abundances of the non-cumulate eucrites have been used to separate them into two compositional categories: the Main Group - Nuevo Laredo trend eucrites and the Stannern trend eucrites (e.g., Stolper, 1977).

The nature of the process governing the Nuevo Laredo and Stannern evolutionary trends has been of particular interest. According to some authors, igneous activity on the HED parent body produced a variety of cumulate rocks (the diogenites and the cumulate eucrites) as well as some more evolved liquids by giving birth to a variety of primary liquids. As a result, the different lithologies found in the HED meteorites may only be connected by proximity rather than necessarily being comagmatic. Some other authors believe that the eucrites and diogenites are the results of the crystallisation of a vast magma ocean, which would only need one initial melting event in the parent body's

early history.

Clearly, it can be observed that Lakangaon and Piplia Kalan fall in the MG-NL trend of eucrites, whereas Vissannapeta sits in the cumulate eucrites region. For the eucrites of the MG-NL trend, the abundance of Ti (Fig. 12a) (or any other incompatible element, such as La increases with the  $\text{FeO}^*/\text{MgO}$  ratio; in contrast, the eucrites on the Stannern trend have the highest abundances of incompatible elements, but these enrichments are unrelated to the  $\text{FeO}^*/\text{MgO}$  ratio. Both trends, as seen in Fig. 3.1, 3.2 (a), (b), have a common origin where a substantial concentration of non-cumulate eucrites (like Juvinas) are concentrated at  $\text{FeO}^*/\text{MgO}$  ratios and  $\text{TiO}_2$  abundances of around 2.5% and 0.6%, respectively. The Nuevo Laredo trend is largely acknowledged to be a trend of fractional crystallisation (e.g. Stolper, 1977; Warren and Jerde, 1987).

### 3.2.2 Rare Earth Elements (REE)

The 14 rare earth elements (REE), from La to Lu, and Y, on the periodic table (Pm lacks a stable isotope), are extremely useful tracers of silicate petrogenesis (e.g., Hess, 1989). Except for Eu and Ce, the majority of the elements in this group are trivalent, and from La to Lu, their solid-melt partition coefficients generally increase. For each element and silicate mineral phase (such as olivine, orthopyroxene, etc.), the partition coefficients ( $D_{solid-melt}$ ) for the REE are distinctive.  $D_{solid-melt} > 1$  signifies "compatible" in the mineral phase, whereas  $D_{solid-melt} < 1$  denotes "incompatibility". La, Ce, Pr, Nd, Sm, Eu, and Gd are examples of light rare earth elements (LREE), which are more incompatible during melting than heavy rare earth elements (HREE), which include Tb, Dy, Ho, Er, Tm, Yb, and Lu. This is demonstrated by the lower LREE partition coefficients for mafic mineral phases. For instance, during low degrees of partial melting, the LREE quickly partition into the melt and shows strong enrichments in the resulting crystallisation products; however, these effects are less pronounced during higher degrees of partial melting as incompatible elements become more enriched in the melt and depleted in the residue. This causes inter-element fractionation patterns that can be utilised to track the melting history of rock from its source reservoir due to the partitioning behaviour of the REE during melting.

Fig. 3.3 presents the REE patterns of the samples analysed in this study. Lakangaon shows a very slight increasing trend from La to Sm, a significant negative Eu anomaly ( $\text{Eu/Eu}^* = 0.78$ ), and then again a relatively flat pattern from Gd to Y while showing a small enrichment in Yb concentration. The pattern matches the data measured by Barrat et al., 2000. Lakangaon, along with Piplia Kalan, is a MGNL trend basaltic eucrite, as seen in the previous section. Piplia Kalan shows a decreasing trend from La to Sm, a very slight negative Eu anomaly ( $\text{Eu/Eu}^* = 0.92$ ) and the subsequent elements

(Gd to Y) exhibit a flat pattern and are depleted as compared to Lakangaon. The Yb enrichment looks similar to Lakangaon. Lakangaon and Piplia Kalan show  $\sim$  10-15 times the concentration of the chondritic value. As seen in Chapter 2, the Piplia Kalan eucrite possesses two distinct major lithologies and a minor lithology. Basu et al. (2016) presented the REE pattern for both the major lithologies of Piplia Kalan, and a positive Eu anomaly could be seen for the coarse fraction of the sample, whereas a negative Eu anomaly could be observed for the fine fraction. The reason for this was indicated to be chemical heterogeneity due to different petrogenetic processes. Moreover, the bulk data from that study showed an increasing trend for La to Sm, and then a decreasing trend after a small negative Eu anomaly. The differences in the studies can result from the modal percentages of plagioclase in the section of the sample used to measure the bulk composition. Basaltic rocks have been known to display slight to significant negative Eu anomalies. Even in the case of lunar rocks, basaltic rocks typically show negative Eu anomalies except in anorthosite-rich samples from some sites that are highly prone to impacts (Papike et al., 1998 and references therein).

The only significant bulk positive Eu anomalies are shown by cumulate eucrites due to plagioclase accumulation. Cumulate eucrites also have higher Mg-numbers and lower incompatible trace element abundances than basaltic eucrites. The same can be observed for Vissannapeta in Fig. 2. Vissannapeta, being a cumulate eucrite, is highly depleted in REE concentration as compared to the basaltic eucrites and also shows extremely huge positive Eu anomaly ( $\text{Eu/Eu}^* = 7.03$ ). The concentrations increase from La to Pr and then start to increase till Sm, and the positive Eu anomaly is followed by an increasing trend from Gd to Yb and then decreases for Lu and Y. The concentration of Vissannapeta lies in the range of 0.25 to 0.6 times the concentration of CI-chondrite, except for Eu, where it is  $\sim 2.4 \times$  CI-chondrite value.

Lohawat displays a relatively flat REE pattern with a marked negative Eu anomaly ( $\text{Eu/Eu}^* = 0.072$ ). The concentrations of the REE are also depleted ( $\sim 4$  to  $5 \times$  CI-chondrite) but not as much as in the case of Vissannapeta. The REE pattern from this study is similar to those observed in typical howardites but is completely different from the Lohawat bulk REE pattern from Sisodia et al. (2001) and slightly different from Basu et al. (2016). The negative Eu anomaly in Lohawat was attributed to glassy spherules observed in Lohawat (Basu et al., 2016). Sample heterogeneity is the most probable cause for the discrepancy of the data point from this study and Sisodia et al. (2001), as the Ni abundance in their chip was reported to be 217 ppm, whereas the Ni content in Lohawat from this study came out to be 16.61 ppm. It is possible that their chip which was powdered, contained a chondritic clast, which led to the extremely high Ni abundance.

Sample ID	Fall /Find	Lithology	Trend	Petrolog-ical Type	Na	Mg	Al	Ca
Lakangaon	Fall	Eucrite	MGNL	Monomict	3.42	35.73	55.68	65.83
Piplia Kalan	Fall	Eucrite	MGNL	Monomict	3.30	37.43	63.04	64.89
Vissan-napeta	Fall	Eucrite	-		1.64	55.81	69.79	61.65
Lohawat	Fall	Howardite	-		0.84	900.1	187.1	38.71
Sc	Ti	V	Cr	Mn	Fe	Co	Ni	Zn
µg/g	mg/g	ug/g	mg/g	mg/g	mg/g	ug/g	µg/g	ug/g
34.31	5.96	54.02	1.65	4.671	163.6	5.056	5.514	17.29
32.27	4.36	55.77	1.591	4.355	146.8	4.721	3.944	11.12
22.97	1.019	64.29	1.21	3.838	107.5	6.181	30.71	1.634
18.78	3.341	66.5	2.55	3.313	109.8	12.05	16.61	4.531
Ga	Rb	Sr	Y	Zr	Nb	Ba	La	Ce
µg/g	ng/g	µg/g	µg/g	µg/g	µg/g	ug/g	ug/g	ug/g
1.634	511	66.75	19.78	40.55	4.289	33.82	3.124	8.01
2.183	12.9	73.44	15.84	26.86	3.381	46.25	3.546	8.445
1.118	0.066	36.59	0.749	0.88	0.075	2.004	0.069	0.161
0.764	1000	61.39	6.765	13.77	1.089	15.28	1.01	2.501
Pr	Nd	Sm	Eu	Gd	Tb	Dy	Ho	Er
ug/g	ug/g	ug/g	ug/g	ug/g	ug/g	ug/g	ug/g	ug/g
1.19	5.886	1.993	0.549	2.33	0.464	3.369	0.744	2.156
1.16	5.348	1.728	0.56	1.994	0.373	2.69	0.593	1.732
0.024	0.12	0.052	0.134	0.065	0.015	0.113	0.027	0.083
0.37	1.805	0.621	0.165	0.775	0.15	1.144	0.256	0.758
Tm	Yb	Lu	Hf	Pb	Th	U	Eu/Eu*	#Mg
ug/g	ug/g	ug/g	ug/g	ng/g	ng/g	ng/g		
0.325	2.256	0.311	1.182	781	386	77	0.78	33.40
0.26	1.807	0.244	0.846	1982	913.3	112.8	0.92	36.93
0.013	0.096	0.013	0.026	302	8.088	1.494	7.03	54.38
0.114	0.804	0.116	0.424	1119	174.4	68.7	0.72	94.96

Table 3.1: Bulk composition of the four samples from this study, along with their Eu anomaly ( $\text{Eu}/\text{Eu}^* = [\text{Eu}]_n / \sqrt{([\text{Sm}]_n \times [\text{Gd}]_n)}$ , where  $[ ]_n$  denotes normalization with respect to CI chondrite) and Mg numbers ( $\#Mg = (\text{MgO}/(\text{FeO}+\text{MgO})) * 100$  (molar)).

Lohawat consists of diogenite clasts, basaltic eucrite clasts, as well as cumulate eucrite clasts (Chapter 2). The diogenite clasts consist mostly of low-Ca and high-Mg pyroxenes which are known to be depleted in REEs as compared to other phases from basaltic/cumulate eucrites. The major and trace element data for these four samples, along with Eu/Eu\* data and Mg-numbers, is presented in Table 3.1.

### 3.2.3 Impact Contamination

The discussion on the influence of chondritic composition on the HED meteorites, especially howardites, is not uncommon and new. According to Jérôme and Goles (1971), in a simple mixing model of eucrites and diogenites, the observed Ni and Co values are typically greater than the estimated values. This excess was explained by the presence of chondritic components. Bunch (1975) and Wilkening (1973) identified carbonaceous chondritic clasts in the Jodzie howardite and rare bits of carbonaceous chondrites in the Kapoeta howardite, respectively. In addition, Chou et al. (1976) reported that the abundances of the siderophile elements Ni, Ge, Ru, Ir, and Au indicated that these elements were contributed by  $\sim 2.4$  and 3.3% of the carbonaceous chondritic materials in howardites. In their descriptions of carbonaceous clasts from the Kapoeta howardite, Wilkening (1973) and Pun et al. (1992) came to the conclusion that these fragments were primarily made of CM2 chondrite material, with smaller amounts of CI-like materials. According to Zolensky et al. (1992), the carbonaceous clasts in the LEW 85300 eucrite were distinct in composition but most comparable mineralogically to CV3 chondrites. According to Buchanan et al. (1993), the majority of carbonaceous clasts in the EET 87513 and Bholghati howardites appear to be heated CM2 chondrites, while the remaining clasts from Bholghati were likely heated CI or CR materials. Zolensky et al. (1996) reported CR clasts in four howardites: Bholghati, Jodzie, Kapoeta, and Y 793497. Moreover, according to Zolensky et al. (1996), almost 80% of the carbonaceous chondrite clasts found in the HED meteorites belong to CM2 class. There are plenty more studies which provide a solid reason to believe that the event that caused the HED meteorites to eject from the surface of Vesta was due to a chondritic impactor.

Although no chondritic clast was found in any of the samples analysed during the course of this study, certain criterion such as low Ni/Co ratios and low abundances of siderophile elements can be used as tracers in order to understand impactor contamination. During core segregation and planetary differentiation, the moderately siderophile elements Ni and Co are prone to metal-silicate partitioning but are also incorporated into the silicate phase. These elements have  $0.2 \times$  CI-chondrite abundances in the terrestrial mantle, and oxygen fugacity, temperature, and pressure conditions further regulate how they partition into metal-silicates (Chou, 1978).

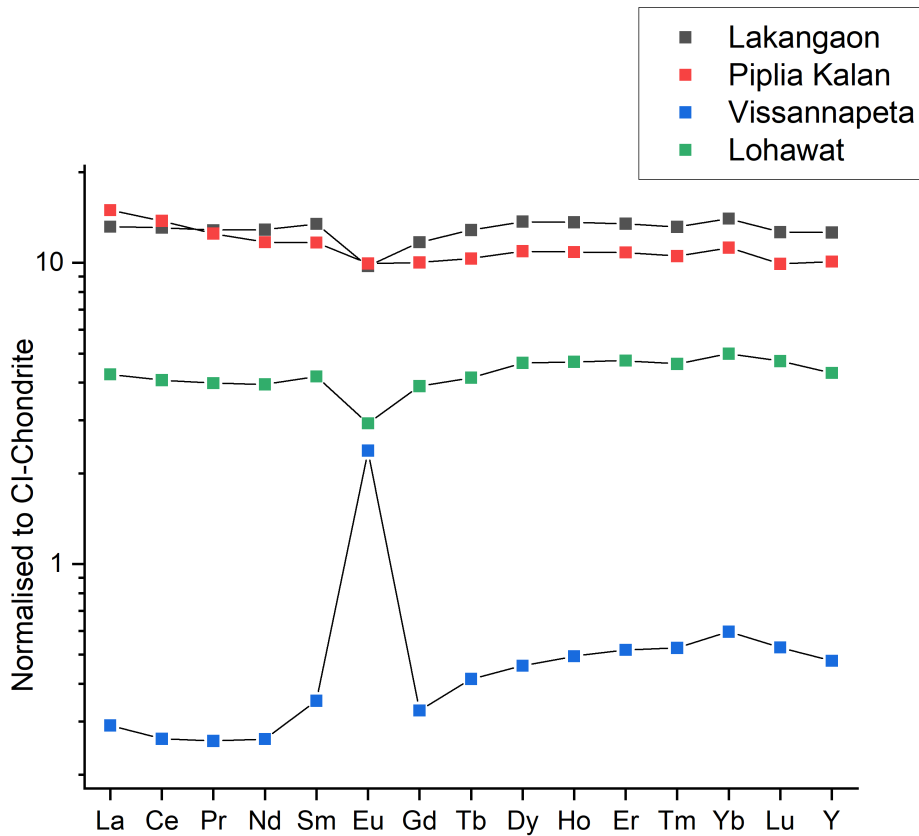


Figure 3.3: REE patterns for Lakangaon, Piplia Kalan, Vissannapeta, and Lohawat, were normalised with respect to CI chondrite. The reference CI chondrite is from McDonough and Sun (1995).

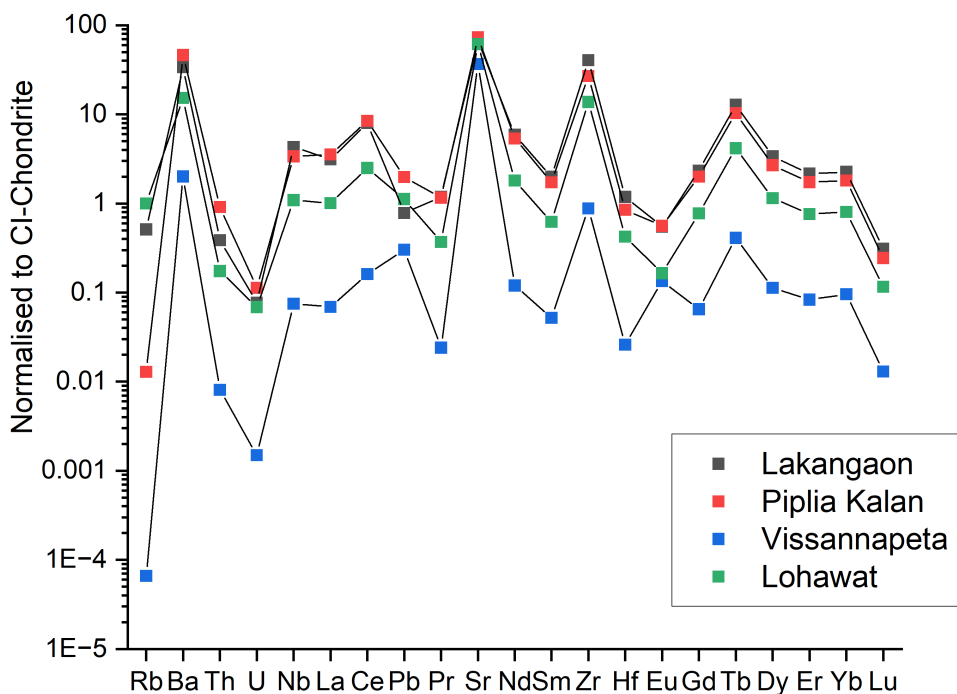


Figure 3.4: Compatible to Incompatible trace element spider plot normalized to CI chondrite (the data for CI chondrites was taken from McDonough and Sun, 1995).

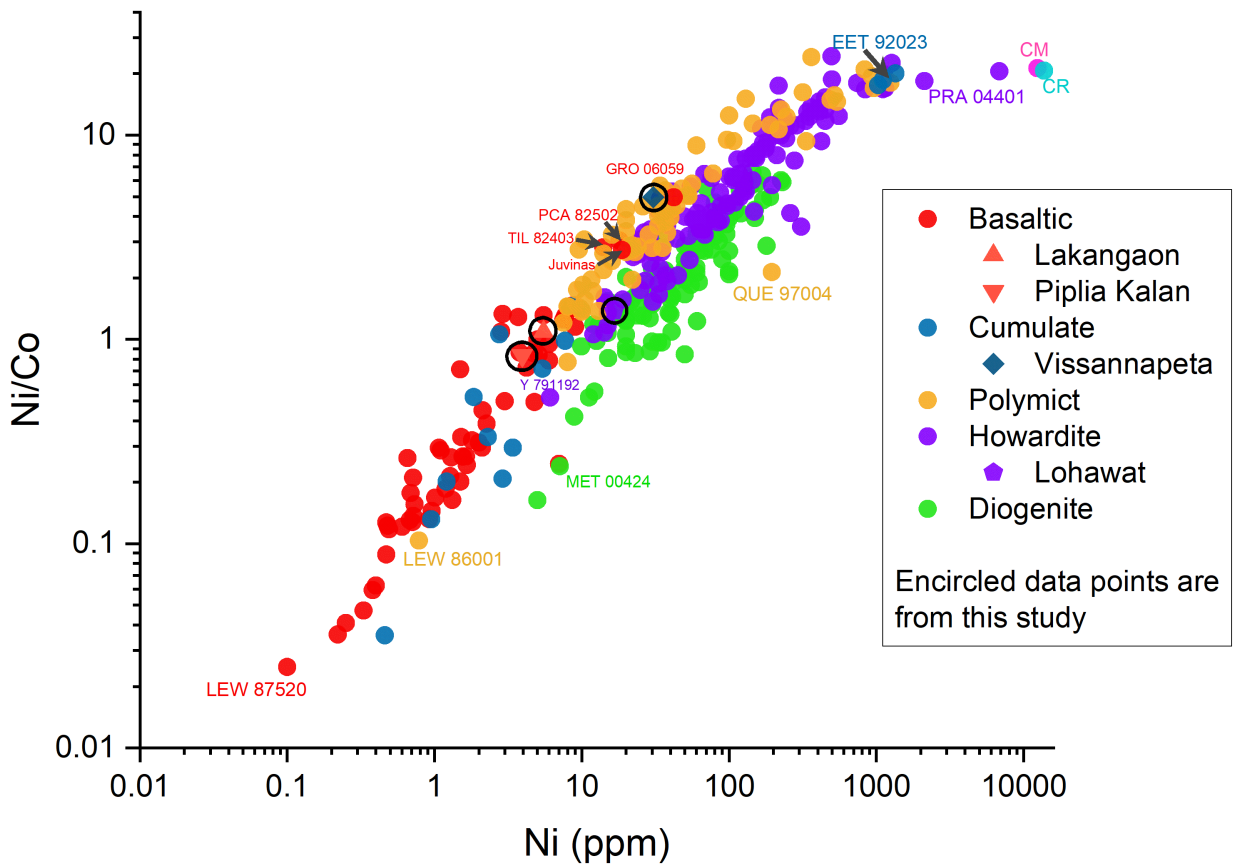


Figure 3.5: Ni/Co vs Ni plot for HEDs and CM and CR chondrites. Other than the four encircled data points which are from this study, the literature values have been taken from Dhaliwal et al. (2023) and the extensive data compiled by Mittlefehldt (2015) and the references therein.

Because impactor material is often rich in Fe-Ni metal, samples that have been contaminated by impact tend to display higher Ni/Co ratios as a result of the addition of Ni. This measure has been used in the past to distinguish lunar polymict breccias, which have been susceptible to impact mixing, with pristine lunar rocks, which have a Ni/Co ratio of less than two (Ryder et al., 1980).

Projectile material characterization using siderophile components can be quite effective (e.g., Norman et al., 2002). Because these elements are strongly partitioned into metallic phases during core-mantle formation, siderophile elements are significantly depleted in Vesta's pristine silicate areas (e.g., Dale et al., 2012). Siderophile element abundances for chondrites are several orders of magnitude higher than those for (pristine) crustal materials. As a result, the inclusion of meteoritic components to pristine crustal materials is what causes the enrichment of siderophile element abundances in brecciated HED meteorites. Hence, the type of impactors affects the relative abundances of siderophile elements. Refractory and volatile siderophile components were studied in earlier studies too, to identify impactors (Anders et al., 1973, for instance).

Moreover, the Ni content has been used to assess the level of brecciation in HED meteorites, particularly the howardites, and suggests that even in 'breccias,' there are very different Ni concentrations (Warren et al., 2009). Moreover, Warren et al. (2009) demonstrated that polymict eucrites had varying and occasionally low siderophile contents, indicating that several influences on the HED parent body were necessary to considerably enhance siderophile element inventories. The HED meteorites were subjected to detailed analyses of HSE abundances and Os-isotope ratios in order to identify specimens with the most primitive (i.e., late-accretion/impact contamination free) signatures. This criterion of Ni content ( $< 1$  ppm) was applied by Dhaliwal et al. (2023) to the HED meteorites for the preliminary identification of pristine eucrite samples.

The effect of impact contamination in some samples is shown by the notable enrichments in Ni content in select samples when compared to Co concentrations. According to petrographic data, samples with Ni contents  $> 8$  ppm are thought to show impact addition (e.g., Dhaliwal and Day, 2014). Ni content can also be used to classify the samples into very low ( $< 1$  ppm), low (1-5 ppm), intermediate (5-10 ppm), and high ( $> 10$  ppm) categories (Dhaliwal et al., 2016).

Fig. 3.4 shows the Ni/Co plots for the literature data and the data from this study. The segregation between different classes and chemical types can be clearly observed. The basaltic and cumulate eucrites separate themselves in a region (where Ni  $< 10$  ppm and Ni/Co  $< 2$ ), the polymict eucrites, howardites, and diogenites mark their presence starting from 10 ppm Ni with Ni/Co ratios above 1. Over the years, it has been understood that there is a continuum from unbreciated eucrites to monomict eucrites and polymict eucrite breccias, followed by howardites and unbreciated diogenites (McSween

et al., 2012). Fig. 3.4 shows that above the basaltic and cumulate eucrites, the polymict eucrites and howardites are quite indistinguishable and do not segregate. This is expected as any polymict eucrite which has more than 10% of diogenitic clasts is by definition a howardite. This definition makes it hard to distinguish polymict eucrites and howardites in a geochemical plot. However, the diogenites in this plot are still distinguishable as they show a bit more Ni content for comparable Ni concentrations in polymict eucrites and howardites.

Piplia Kalan can be classified in the low Ni category (< 5 ppm), whereas Lakan-gaon, with slightly more Ni content, makes it to the intermediate Ni category (5-10 ppm). All the basaltic eucrites lie below the 2.0 mark for Ni/Co except PCA 82502, TIL 82403, Juvinas (one out of six data points), and GRO 06059. PCA 82502 was deemed as an impact-melt product, and it also shows a positive Ce-anomaly, which is strange for basaltic eucrites (Warren et al., 2009). That may be indicative of terrestrial contamination. TIL 82404 is deemed as siderophile-rich and probably polymict, by Warren et al. (2009). Out of six data points for Juvinas (with the concentration data for Ni as well as Co) by Barrat et al. (2007) and Dhaliwal et al. (2023), only one data point from the latter showed a high Ni content (18.75 ppm), which was attributed to sample heterogeneity due to inhomogeneous impactor contamination. The aliquot with low Ni content also showed high Os concentration and vice versa. The other five data points lie in the basaltic and cumulate eucrite range (i.e. < 10 ppm Ni and Co). When it comes to GRO 06059, Mittlefehldt et al. (2016) have indicated to be cautious while interpreting the data as it displays some similarity to Ibitira, which is a well-known anomalous eucrite. GRO 06059 is a breccia which contains different lithologic components, including impact-melt clasts, and thus it may be a polymict eucrite (Mittlefehldt et al., 2016). GRO 06059, being a polymict eucrite, will justify the high Ni/Co ratio in our plot.

We are then presented with the curious case of Vissannapeta. It also has an anomalous oxygen isotopic composition (Greenwood et al., 2012). Whereas, Vissannapeta is well established as a cumulate eucrite and there are no such anomalies in its texture.

Lohawat is a fragmental howardite, and it lies at the low Ni/Co extreme of the howardite region in the Ni vs Co plot (Fig. 3.3). This indicates that Lohawat displays a feeble amount of impact contamination, and this is also the reason why no chondritic clasts were found during the petrographic analysis during this study (Chapter 2) and also by Ray and Ghosh (2022). For example, the Bholghati howardite is well known for showcasing chondritic clasts (Buchanan et al., 1993; Zolensky et al., 1992; Reid et al., 1990; Laul, 1990), and in the Ni/Co plot, Bholghati lies among the howardites with the highest Ni/Co ratio (data from Laul and Gosselin, 1990). An example of a polymict eucrites would be LEW 85300, which has been observed to contain chondritic clasts (Zolensky et al., 1992) and also displays a high Ni/Co ratio.

The polymict eucrite LEW 86001 extremely less Nickel as compared to the typical values for other polymict eucrites. Although the mixing diagrams of Zr, Nb, Ba, Hf, and Ta with Al displayed no evidence of significant contribution from Stannern trend eucrites to Mittlefehldt et al. (2012), LEW 86001 proved to be an exception, being dominated by Stannern-trend basaltic debris. Polymict breccia QUE 97004, similar to TIL 82403, appears to be exceptionally rich in Co (Warren et al., 2009).

EET 87520 (studied by Warren et al., 2009) can be assumed to represent the pristine eucritic material with low Co and Ni abundances (Shirai et al., 2016). The data point for Vissannapeta shows a Ni content of 30.71 ppm, which is at least three times higher than the other cumulate eucrites, except EET 92023. EET 92023 lies in the extreme range of howardites as its Ni and Co concentrations are 1000-1350 ppm and 58-68 ppm, respectively (Mittlefehldt and Lindstrom, 2003; Warren et al., 2009). Both these studies deemed it as an exceptionally siderophile-rich sample due to the unusually high abundance of coarse metal. A short overview of EET 92023 was provided by Kaneda and Warren (1998) and Yamaguchi et al. (2017) performed a detailed study. Moreover, the  $\Delta^{17}\text{O}$  isotopic composition of EET 92023 deviates significantly from normal eucrites (Sanborn et al., 2016; Yamaguchi et al., 2017). Yamaguchi et al. (2017) concluded from oxygen isotopic data and Fe-Ni metal aggregates that it is a cumulate eucrite contaminated by iron meteorite (chemically similar to IAB and IVA). However, some authors (Mittlefehldt et al., 2016; Barrett et al., 2017) also say that EET 92023 might as well be from another asteroid. EET 92023 is also regarded by Mittlefehldt and Lindstrom (1993) as an anomalous metal-rich cumulate eucrite.

The diogenite MET 00424 exhibits a low Ni/Co ratio. According to Mittlefelhldt (2002), MET 00424 has very low Sm content, the amount of a trapped melt component must be very low and thus, we can assume that MET 00424 (along with MET 00425, Shalka, and Tatahouine) preserve the clearest cumulate signature and their Sc-Mg# is correlation is compatible with igneous fractionation. The most contaminated howardite we see on this graph is PRA 04401. Herrin et al. (2010) reported that it consists of 60-70% chondritic clasts, that resemble CM2. This explains why it lies so close to the data points for CM chondrites.

Out of the four samples studied in this study, the two eucrites (Lakangaon and Piplia Kalan) and one howardite (Lohawat) lie perfectly in their respective regions in the Ni/Co vs Ni plot except Vissannapeta. Vissannapeta and EET 92023 are the two cumulate eucrites that show anomalously high Ni/Co ratios as well as Ni content as compared to the average of cumulate eucrites. EET 92023 is moderately shocked (Yamaguchi et al., 2017) whereas Vissannapeta is extremely brecciated.

From	Sample Name	Type of Sample	Percentage of Impacto- r Contamination	Potential Impactors
Chou et al., 1976	Bholghati	Howardite	3.3%	CM
	Bununu		2.6%	
	Kapoeta		2.6%	
	Malvern		2.4%	
	Johnstown		1.0%	
	Le Teilleul		0.45%	
Buchanan and Mittlefehldt, 2003	EET 87513	Howardite	2-3%	CM2 (Murchi- son)
Yamaguchi et al., 2017	EET 92023	Cumulate Eucrite	12-17%	Ordinary Chondrite
Shirai et al., 2016	ALH 76005	Polymict Eucrite	0.035%	Chondrites
	EET 92003	Basaltic Eucrite	0.36%	
	GRO 95633	Howardite	0.18%	
	LEW 85300	Polymict Eucrite	0.002%	
	LEW 87026	Polymict Eucrite	0.033%	Meteorites
Herrin et al., 2011	PRA 04401	Howardite	35%	CM/CR
	SCO 06040	Howardite	5%	CM/CR
This Study	Vissannapeta	Cumulate Eucrite	0.37%	CM/CR

Table 3.2: Compilation of Impactor Contamination from different studies and the potential impactors which were used to calculate the percentage of impactor contamination. Vissannapeta from this study suggests at least 0.37% contamination assuming a CM/CR impactor.

No Fe-Ni metal were observed in the Vissannapeta sample during the course of this study (Chapter 2). Like several studies mentioned in this section, no carbonaceous chondrite clasts were found in the thin section of Vissannapeta used in this study. It is possible that a tiny amount of CM is present as sub-microscopic particles between individual mineral and lithic fragments in the matrix, just like in the case of EET 87513 (Buchanan and Mittlefehldt., 2003) (Table 3.2). Some diogenetic and/or basaltic eucrite material can also get incorporated ,along with the impactor material, into the matrix as very fine debris resulting from the impacts on the surface.

Several studies such as Chou et al. (1976), Zolensky et al. (1996), Buchanan and Mittlefehldt (2003), have tried to model the contribution of impactor in the contamination of individual polymict eucrites and howardites (Table 3.2). Similar modelling based on Ni/Co ratio for Vissannapeta, assuming a chondritic impactor (specifically CM type; CR is also a contender, but the Ni and Co values of average CM and CR are not very different) has been carried out in this study. Contribution from the chondritic impactor came out to be at least 0.37%. The average Ni and Co abundances for CM chondrites were taken from Tagle and Berlin (2008).

### 3.3 Partial Melting and Fractional Crystallisation

An essential process that facilitates the differentiation and evolution of the Earth is the partial melting of planetary (and Earth) materials. To comprehend the melt formation and segregation process and to interpret the chemical composition of primary melts, partial melting modelling utilising trace element concentrations can often be essential. Applications of mathematics can be applied to the behaviours of trace elements during partial melting.

There are three general models based on the extent of chemical equilibrium between the solid and melt: batch, fractional (Schilling and Winchester, 1967; Gast, 1968; Shaw, 1970) and dynamic melting (Langmuir et al., 1977; McKenzie, 1985; Zou, 1998;Zou, 2000; Zou and Reid, 2001). The batch melting model, one of the three general models, assumes that melt stays in equilibrium with the solid throughout the melting event, while the fractional melting model assumes that melt is removed from the initial source as it is formed and that only the last drop of melt is in equilibrium with the residue, and that there is no residual melt. In the case of dynamic melting, the retention of a key fraction of the melt in the mantle residue is crucial.

Given below is the derivation of the batch melting equation:

Since it is a closed system, by conservation of Mass,  $M_o = M_s + M_m$ , where  $M_o$  is the

total mass and  $M_s$  and  $M_m$  are the masses of the solid and melt fractions, respectively.

$$X_s = M_s/M_o$$

$$X_m = M_m/M_o = F$$

Therefore,

$$X_s + X_m = 1$$

Let total concentration of an element be  $C_o$  in the total Mass  $M_o$ ,

Therefore,

$$C_o M_o = C_s M_s + C_m M_m$$

Dividing the whole equation with  $M_o$  and rewriting the above equation in terms of F gives us,

$$C_o = C_s(1 - F) + C_m F$$

Let the partition coefficient of the element be D ( $C_s/C_m$ ). If D is  $> 1$ , the element is compatible, and if D is  $< 1$ , the element will be deemed incompatible.

Writing the equation in terms of  $C_o$  and  $C_m$ ,

$$C_o = DC_m(1 - F) + C_m F$$

Rewriting gives:

$$\frac{C_m}{C_o} = \frac{1}{D + F(1 - D)}$$

And, for the solid residue,

$$\frac{C_s}{C_o} = \frac{D}{D + F(1 - D)}$$

The generated melt can crystallise through a process known as fraction crystallisation. The process of fractional crystallisation involves the removal and segregation of mineral precipitates from a melt; unless unusual circumstances apply, the removal of the crystals alters the composition of the magma. Fractional crystallisation, in its simplest form, is the removal of newly created crystals from an initially homogenous magma (for instance, by gravity settling) in order to stop these crystals from reacting further with the remaining melt. A series of distinct minerals precipitate as a result of the composition of the residual melt becoming relatively enriched in some components and deficient in others.

Melts become enriched in incompatible components as a result of the fractional crys-

tallisation process. Therefore, understanding the process of crystallisation is essential to comprehending how melt compositions change. As Bowen's response series showed in the early 1900s, the textures of rocks can provide information. The intergranular (also known as intercumulus) textures that appear whenever a mineral crystallises later than the surrounding matrix, thus filling the unfilled interstitial space, are an example of such texture, which is connected to fractioned crystallisation. Various oxides of chromium, iron and titanium show such textures, such as intergranular chromite in a siliceous matrix. Since such chromites have been observed in the eucrites analysed in this study, it becomes necessary to use the concept of fractional crystallisation for modelling the formation of basaltic eucrites. The modelling equation for fractional crystallisation can be derived as follows:

If  $W$  is the initial weight or mass of the melt, and crystallization removes a melt increment of mass  $dW$ , then the mass of an element put into crystals in each increment is  $C_s dW$ . In order to maintain mass balance, this amount going into crystals has to be equal to the amount of the element removed from the liquid.

$$C_s dW = d(C_i W)$$

Differentiating,

$$C_s dW = C_s dW + W dC_m$$

Rearranging,

$$\frac{dW}{W} = \frac{dC_l}{(C_s - C_l)}$$

Integrating,

$$\int_{W^o}^W \frac{dW}{W} = \int_{C_o}^{C_l} \frac{dC_l}{(C_s - C_l)} = \int \frac{dC_l}{(DC_l - C_l)}$$

$$\ln \frac{W}{W^o} = \frac{1}{(D-1)} \ln \frac{C_l}{C_o}$$

Since  $W/W^o = F =$  the proportion of the residual liquid,

$$F^{(D-1)} = \frac{C_s}{C_o}$$

This can be rewritten as,

$$F^{D-1} = \frac{C_l}{C_o}$$

Or, for the changes in concentration of the solid phase ( $C_o$ )

$$DF^{D-1} = \frac{C_s}{C_o}$$

### 3.3.1 Batch Melting and Fractional Crystallisation Modelling

In numerous studies, eucrites have been referred to as a product of partial melting of a chondritic source. Stolper (1977) argued that eucrites are initial partial melts of the parent body, a process that necessitates minimal heating of the asteroid. Bartels and Grove (1992) and Barrat (2004) supported this work by proposing that diogenites developed from distinct batches of parental magmas (Mittlefehldt, 1994; Fowler et al., 1995; Shearer et al., 1997). Longhi and Pan (1988) also favoured a concept in which the diogenites formed by remelting the eucritic source, which had a relatively low Mg content, whereas the eucrites formed by partial melting of this source.

Studies on eucrites using the ratios of  $^{147}\text{Sm}/^{143}\text{Nd}$  and  $^{176}\text{Lu}/^{176}\text{Hf}$  show that cumulate eucrites are 100 Ma younger than basaltic eucrites and that basaltic eucrites are roughly the same age as the Solar System (Blichert-Toft et al., 2002). Also, it is believed that eucrites are partial melts and not residual magmas due to the wide range of variation and significant correlation of the Lu/Hf and Sm/Nd ratios (Blichert-Toft et al., 2002). Furthermore, Blichert-Toft et al. (2002) mark that the ratio of plagioclase to mafic minerals in the residue controls the relative Lu/Hf and Sm/Nd fractionation; as a result, they interpret the strong correlation between the Lu/Hf and Sm/Nd ratios as being caused by an increase in plagioclase saturation in the low-gravity field of the eucrite parent body. Blichert-Toft et al. (2002) suggest that ilmenite in cumulate eucrites plays this role as this mineral can accommodate sufficient amounts of Hf. They also conclude that basaltic eucrites most likely formed as large-degree melts of an original chondritic source because cumulate eucrites have enhanced Lu/Hf fractionation, which requires a process to remove Hf from the melt.

In this study, an attempt has been made to model the basaltic eucrites using a two stage model (and a single stage model for cumulate eucrites) based on the rare-earth element compositions assuming a chondritic (CI) precursor. For the modelling, the mineral modes of the samples studied are required so as to calculate the bulk D (partition coefficient). Since no X-ray mapping was conducted during this study, the accurate mineral mode data was unavailable for these samples. Thus, to get an approximation of the mineral modes, the mosaics of these samples were processed using ImageJ software which uses the K means clustering algorithm to segment an image based on the gray values. The thresholds can then be manually adjusted. Table 3.3. shows the rough average modes of the multiple thin and thick sections analysed in this study.

Sample	Opx (%)	Cpx (%)	Plg (%)	Total (%)
Piplia Kalan Thick	19.78	17.64	61.96	99.38
Piplia Kalan Thin_A	23.66	17.32	59.46	100.44
Piplia Kalan Thin_B	26.43	16.10	60.05	102.58
Piplia Kalan Average	23.29	17.02	60.49	100.80
<hr/>				
Lakangaon Thick_A	16.92	24.85	60.46	102.24
Lakangaon Thick_B	27.99	18.23	55.55	101.77
Lakangaon Average	22.45	21.54	58.01	102.00
<hr/>				
Vissannapeta	25.80	16.26	61.34	103.41

Table 3.3: Representative modes of orthopyroxene, clinopyroxene, and plagioclase of multiple thin and thick sections of Lakangaon, Piplia Kalan, and Vissannapeta. The average data for multiple sections of Lakangaon and Piplia Kalan was used for modelling calculation.

Rare Earth Elements	Opx	Cpx	Plg
La	0.03	0.056	0.148
Ce	0.02	0.092	0.082
Nd	0.03	0.23	0.055
Sm	0.05	0.445	0.039
Eu	0.05	0.474	0.1/1.5*
Dy	0.15	0.582	0.023
Er	0.23	0.583	0.02
Yb	0.34	0.542	0.023

Table 3.4: Partition coefficient (D) values from Rollinson (1993). \*The Europium values are denoted as  $\text{Eu}^{3+}/\text{Eu}^{2+}$  for plagioclase.  $\text{Eu}^{3+}$  values have been used for modelling in this study.

The bulk partition coefficient ( $D$ ) was calculated as a weighted average using the calculated modes (Table 3.3) and the partition coefficients of the rare earth elements taken from Rollinson (1993). The CI chondrite values were taken from McDonough and Sun (1995). Interestingly, Eu shows two different partition coefficients for plagioclase for  $\text{Eu}^{3+}$  and  $\text{Eu}^{2+}$  because  $\text{Eu}^{2+}$  is significantly more compatible in plagioclase than  $\text{Eu}^{3+}$  (and other REEs). The true bulk partition coefficient for Eu is therefore a function of the ratio of  $\text{Eu}^{2+}$  and  $\text{Eu}^{3+}$  in the liquid, which ultimately is the function of oxygen fugacity and temperature (Weill and Drake, 1973; Drake and Weill, 1975; Toplis, 2005). Therefore, Eu in magmatic rocks can be seen as a potential in-situ sensor of the redox conditions at the time of crystallisation. However, only the partition coefficient of  $\text{Eu}^{3+}$  in plagioclase is used while calculating the bulk partition coefficient for the model.

The REE pattern of cumulate eucrite Vissannapeta can be generated through 21% partial melting ( $F = 0.21$ ) of CI chondrite precursor. Such low REE abundances can be acquired assuming Vissannapeta to be a residue during the partial melting event. Fig. 3.5 displays the REE values for Vissannapeta and the modelled values for the residue generated after 21% partial melting. Clearly, the Eu concentration in Vissannapeta is  $\sim 5-5.5 \times$  the modelled value. This also correlates with the fact that Visannapeta shows a huge positive Eu anomaly in the CI-normalised REE plot (Fig. 3.3). This excess Eu may have incorporated at a later stage (possibly during impact melting) into the plagioclase as  $\text{Eu}^{2+}$  as  $\text{Eu}^{3+}$ . The positive Eu anomaly in cumulate eucrites is generally explained by plagioclase accumulation, which is consistent with a greater modal abundance of plagioclase as compared to basaltic eucrites.

In the case of Lakangaon and Piplia Kalan, the REE concentrations are  $> 10 \times$  CI chondrites (Fig. 3.3). Therefore, to accommodate for this much enrichment, the two-stage model describes partial melting followed by the melt undergoing fractional crystallisation. For Lakangaon, which is a highly evolved basaltic eucrite, the partial melting can be up to 44%. Following that, fractional crystallisation up to 90% is plausible ( $X_s = 0.90$ ) (Fig. 3.6). Similarly, for Piplia Kalan, Stage I would be partial melting up to 33% followed by Stage II being 84% fractional crystallisation (Fig. 3.6). It can be seen in Fig. 3.6, 3.7, and 3.8 that the model result patterns are pretty good for Vissannapeta and Piplia Kalan but seems a bit off for Lakangaon. As can be seen in Table 3.3., the modes of different sections of Piplia Kalan are very consistent, but the modes of the two sections of Lakangaon do not match very well, probably due to sample bias. This might be why the modelling result of Lakangaon is a bit off compared to Piplia Kalan. However, the modelling result for Vissannapeta is good even though the mode of only one sample was measured, maybe due to no sample bias.

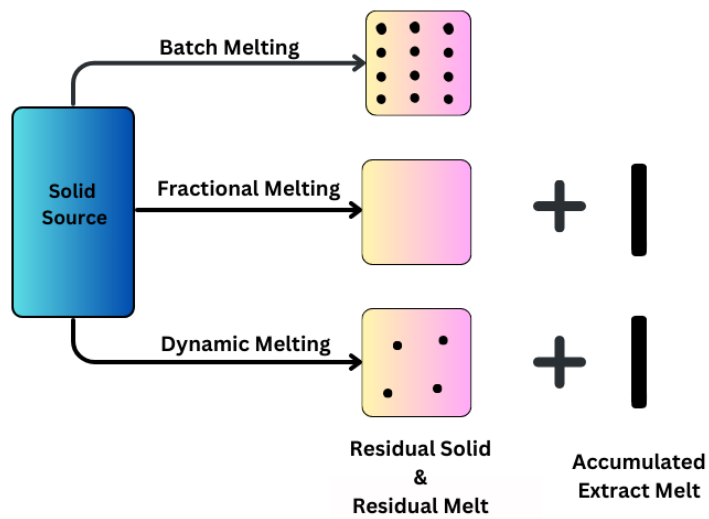


Figure 3.6: A sample diagram showing batch, fractional, and dynamic melting models. Filled circles represent melts in equilibrium with the residual solid. There is no residual melt for the fractional melting model.

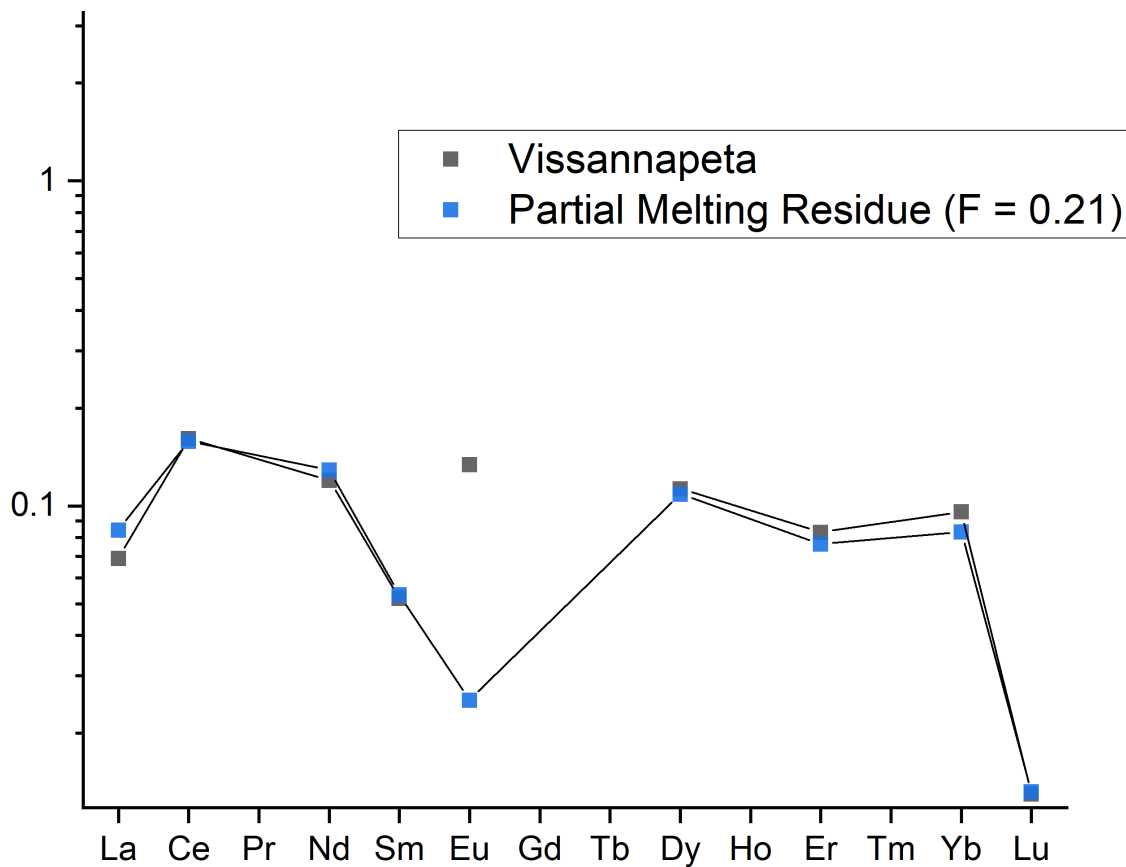


Figure 3.7: Vissannapeta REE concentrations based on a single stage model.  $F$  is the melt fraction that is produced after partial melting of 21%.

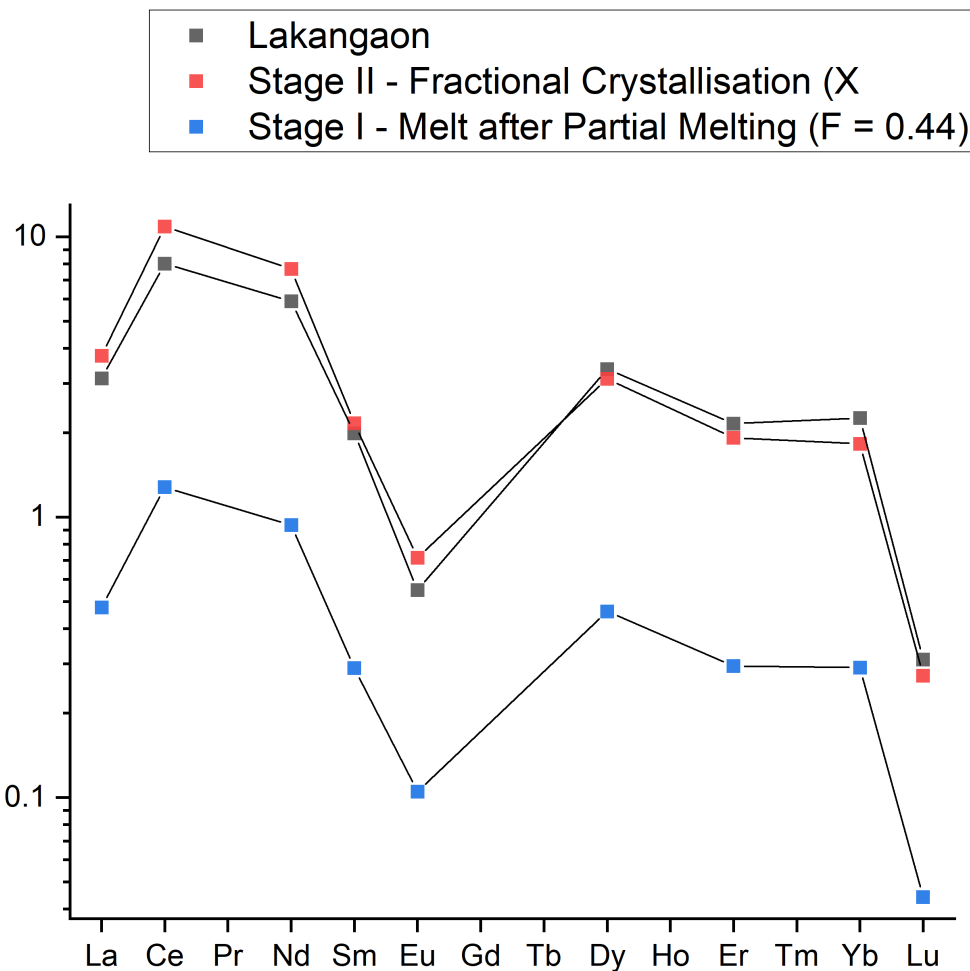


Figure 3.8: Lakangaon REE concentrations based on a two-stage model. The blue line represents the concentration of the melt generated after partial melting of 44%. When this melt crystallizes to 90% solid, Lakangaon-like REE concentrations are formed.

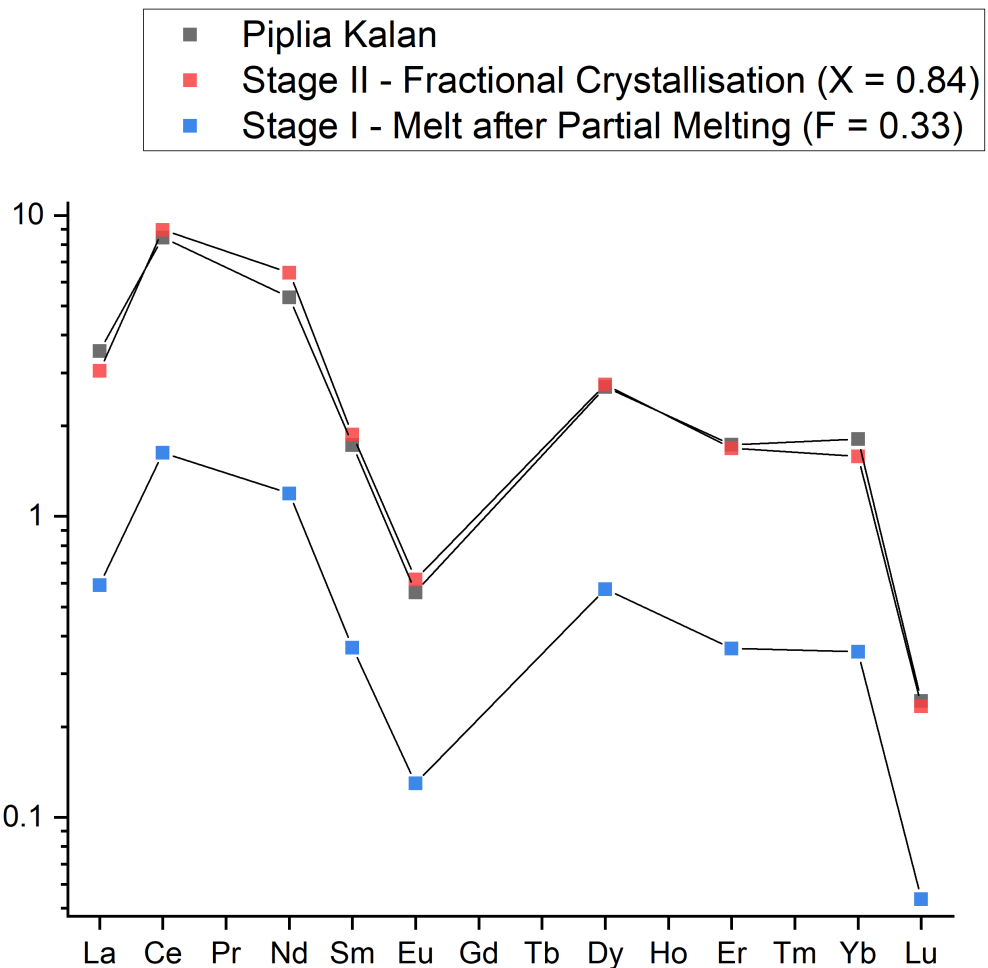


Figure 3.9: REE concentrations in Piplia Kalan based on a two-stage model. The blue line shows the concentration of the melt that was produced after a 33% partial melting. REE concentrations resembling Piplia Kalan are created when this melt crystallises to about 84% solid.

### 3.4 Conclusions

Eucrites can be divided into two petrographic types, basaltic and cumulate. The basaltic eucrites can also be divided into two major chemical types – Stannern trend eucrites and MGNL (Main Group Nuevo Laredo) trend eucrites, and there also can be a minor chemical type – residual eucrites. The cumulate eucrites show greater Mg-numbers and lower incompatible trace element abundances than basaltic eucrites and vice versa for the basaltic eucrites. Two of the samples studied, Lakangaon and Piplia Kalan, show similarity in geochemical plots as they both belong to the MGNL trend of basaltic eucrites. With respect to these two eucrites, Lohawat, which is a howardite, displays significant REE depletion. Vissannapeta is even more depleted as compared to Lohawat and shows an extreme positive Eu anomaly which is attributed to plagioclase accumulation.

A closer look into the Ni/Co plot reveals that the diogenites, polymict eucrites, and howardites have higher Ni/Co ratios than the monomict basaltic and cumulate eucrites. This correlates with the fact that many of these polymict eucrites and howardites have been observed to have chondritic clasts (mostly CM2 and CR2) within them. Similarly, it is possible that a few rare monomict eucrites like Vissannapeta are also contaminated by the impactor, to a lesser degree.

Partial Melting (Batch Melting) and fractional crystallisation modelling show that the REE compositions of the cumulate eucrite (Vissannapeta) and the basaltic eucrites (Lakangaon and Piplia Kalan) can be generated through a single-stage partial melting model, and a two-stage partial melting and fractional crystallisation model, respectively. The excess Eu in Visannapeta can be attributed to plagioclase accumulation at a later stage, such as impact melting.

### 3.5 References

Anders, E., Ganapathy, R., Krähenbühl, U., & Morgan, J. W. (1973). Meteoritic material on the Moon. *The moon*, 8, 3-24.

BARRAT, J. A. (2004). Determination of parental magmas of HED cumulates: The effects of interstitial melts. *Meteoritics & Planetary Science*, 39(11), 1767-1779.

Barrat, J. A., Blichert-Toft, J., Gillet, P., & Keller, F. (2000). The differentiation of eucrites: the role of in situ crystallisation. *Meteoritics & Planetary Science*, 35(5), 1087-1100.

Barrat, J. A., Jambon, A., Bohn, M., Blichert-Toft, J., Sautter, V., Göpel, C., ... & Keller, F. (2003). Petrology and geochemistry of the unbreciated achondrite Northwest

Africa 1240 (NWA 1240): An HED parent body impact melt. *Geochimica et Cosmochimica Acta*, 67(20), 3959-3970.

Barrat, J. A., Yamaguchi, A., Greenwood, R. C., Bohn, M., Cotten, J., Benoit, M., & Franchi, I. A. (2007). The Stannern trend eucrites: Contamination of main group eucritic magmas by crustal partial melts. *Geochimica et Cosmochimica Acta*, 71(16), 4108-4124.

Blichert-Toft, J., Boyet, M., Télouk, P., & Albarède, F. (2002).  $^{147}\text{Sm}$ - $^{143}\text{Nd}$  and  $^{176}\text{Lu}$ - $^{176}\text{Hf}$  in eucrites and the differentiation of the HED parent body. *Earth and Planetary Science Letters*, 204(1-2), 167-181.

Buchanan, P. C., Zolensky, M. E., & Reid, A. M. (1993). Carbonaceous chondrite clasts in the howardites Bholghati and EET87513. *Meteoritics*, 28(5), 659-669.

Bunch, T. E. (1975). Petrography and petrology of basaltic achondrite polymict breccias/Howardites. In In: Lunar Science Conference, 6th, Houston, Tex., March 17-21, 1975, Proceedings. Volume 1.(A78-46603 21-91) New York, Pergamon Press, Inc., 1975, p. 469-492. (Vol. 6, pp. 469-492).

Chou, C. L. (1978). Fractionation of siderophile elements in the Earth's upper mantle. In IN: PROCEEDINGS OF THE 9TH LUNAR AND PLANETARY SCIENCE CONFERENCE, vol. 1, 219-230. Proceedings Paper. (Vol. 9).

Chou, C. L., BoYNTON, W. V., Bild, R. W., Kimberlin, J., & Wasson, J. T. (1976, April). Trace element evidence regarding a chondritic component in howardite meteorites. In Lunar and Planetary Science Conference Proceedings (Vol. 7, pp. 3501-3518).

Dale, C. W., Burton, K. W., Greenwood, R. C., Gannoun, A., Wade, J., Wood, B. J., & Pearson, D. G. (2012). Late accretion on the earliest planetesimals revealed by the highly siderophile elements. *Science*, 336(6077), 72-75.

Dhaliwal, J. K. (2016). Geochemical Constraints for Mechanisms of Planetary Differentiation and Volatile Depletion. University of California, San Diego. Dhaliwal, J. K., & Day, J. M. D. (2014). Insights into the Pristinity of Unbrecciated Eucrites. In Lunar and Planetary Science Conference, 45, # 2833.

Dhaliwal, J. K., Day, J. M., & Tait, K. T. (2023). Pristinity and petrogenesis of eucrites. *Meteoritics & Planetary Science*.

Drake, M. J., & Consolmagno, G. J. (1977, March). Asteroid 4 Vesta: Possible bulk composition deduced from geochemistry of eucrites. In Lunar and Planetary Science Conference (Vol. 8).

Fowler, G. W., Shearer, C. K., Papike, J. J., & Layne, G. D. (1995). Diogenites as asteroidal cumulates: Insights from orthopyroxene trace element chemistry. *Geochimica et Cosmochimica Acta*, 59(14), 3071-3084.

Greenwood, R. C., Franchi, I. A., Gibson, J. M., & Benedix, G. K. (2012). Oxygen isotope variation in primitive achondrites: The influence of primordial, asteroidal and terrestrial processes. *Geochimica et Cosmochimica Acta*, 94, 146-163.

Greenwood, R. C., Franchi, I. A., Jambon, A., & Buchanan, P. C. (2005). Widespread magma oceans on asteroidal bodies in the early solar system. *Nature*, 435(7044), 916-918.

Grove, T. L., & Bartels, K. S. (1992). The relation between diogenite cumulates and eucrite magmas. In IN: Proceedings of Lunar and Planetary Science, Volume 22; Conference, Houston, TX, Mar. 18-22, 1991 (A92-30851 12-91). Houston, TX, Lunar and Planetary Institute, 1992, p. 437-445. (Vol. 22, pp. 437-445).

Herrin, J. S., Zolensky, M. E., & Mittlefehldt, D. W. (2010, July). A Carbonaceous Chondrite Dominated Lithology from the HED Parent; PRA 04401. In 73rd Annual Meeting of the Meteoritical Society (No. JSC-CN-21143).

Herrin, J. S., Zolensky, M. E., Cartwright, J. A., Mittlefehldt, D. W., & Ross, D. K. (2011, March). Carbonaceous chondrite-rich howardites; the potential for hydrous lithologies on the HED parent. In 42nd Lunar and Planetary Science Conference (No. JSC-CN-22726).

Hess, P. C. (1989). Highly evolved liquids from the fractionation of mare and nonmare basalts. In Moon in Transition: Apollo 14, KREEP, and Evolved Lunar Rocks (pp. 46-52).

Ikeda, Y., & Takeda, H. (1985). A model for the origin of basaltic achondrites based on the Yamato 7308 howardite. *Journal of Geophysical Research: Solid Earth*, 90(S02), C649-C663.

Jerome, D. Y., & Goles, G. G. (1971, January). A re-examination of relationships among pyroxene-plagioclase achondrites. In Activation analysis in geochemistry and cosmochemistry; Advanced Study Institute.

Kaneda, K., & Warren, P. H. (1998). Iron-Nickel Metal Bearing Unique Eucrite Elephant Moraine 92023: Its Petrography, Siderophile Concentrations, and Petrogenesis. *Meteoritics and Planetary Science Supplement*, 33, A81.

L. L. Wilkening, "Foreign Inclusions in Stony Meteorites—I. Carbonaceous Chondritic Xenoliths in the Kapoeta Howardite," *Geochim. Cosmochim. Acta* 37, 1985–1989 (1973)  
Laul, J. C. (1990). The Bholghati (howardite) consortium: An overview. *Geochimica et Cosmochimica Acta*, 54(8), 2155-2159.

Laul, J. C., & Gosselin, D. C. (1990). The Bholghati howardite: chemical study. *Geochimica et Cosmochimica Acta*, 54(8), 2167-2175.

McDonough, W. F., & Sun, S. S. (1995). The composition of the Earth. *Chemical geology*, 120(3-4), 223-253.

McSween, H. Y., Mittlefehldt, D. W., Beck, A. W., Mayne, R. G., & McCoy, T. J. (2012). HED meteorites and their relationship to the geology of Vesta and the Dawn mission. *The Dawn mission to minor planets 4 Vesta and 1 Ceres*, 141-174.

Mittlefehldt, D. W. (1979). Petrographic and chemical characterisation of igneous lithic clasts from mesosiderites and howardites and comparison with eucrites and diogenites. *Geochimica et Cosmochimica Acta*, 43(12), 1917-1935.

Mittlefehldt, D. W. (2015). Asteroid (4) Vesta: I. The howardite-eucrite-diogenite (HED) clan of meteorites. *Geochemistry*, 75(2), 155-183.

Mittlefehldt, D. W., & Lindstrom, M. M. (1993, May). Geochemistry and petrology of a suite of ten Yamato HED meteorites. In *Seventeenth Symposium on Antarctic Meteorites*. Proceedings of the NIPR Symposium, No. 6, held August 19-21, 1992, at the National Institute of Polar Research, Tokyo. Editor in Chief, Keizo Yanai, with Hideyasu Kojima, Keiji Misawa, Nobuo Takaoka, and Yoshio Yoshida. Published by the National Institute of Polar Research, 1993, p. 268 (Vol. 6, p. 268).

Mittlefehldt, D. W., & Lindstrom, M. M. (2003). Geochemistry of eucrites: Genesis of basaltic eucrites, and Hf and Ta as petrogenetic indicators for altered Antarctic eucrites. *Geochimica et Cosmochimica Acta*, 67(10), 1911-1934.

Mittlefehldt, D. W., & Lindstrom, M. M. (2003). Geochemistry of eucrites: Genesis of basaltic eucrites, and Hf and Ta as petrogenetic indicators for altered Antarctic eucrites. *Geochimica et Cosmochimica Acta*, 67(10), 1911-1934.

Mittlefehldt, D. W., Greenwood, R. C., Peng, Z. X., Ross, D. K., Berger, E. L., & Barrett, T. J. (2016). Petrologic and oxygen-isotopic investigations of eucritic and anomalous mafic achondrites.

Mittlefehldt, D. W., Greenwood, R. C., Peng, Z. X., Ross, D. K., Berger, E. L., & Barrett, T. J. (2016). Petrologic and oxygen-isotopic investigations of eucritic and anomalous mafic achondrites.

Palme, H., Wlotzka, F., Spettel, B., Dreibus, G., & Weber, H. (1988). Camel Donga: a eucrite with high metal content. *Meteoritics*, 23(1), 49-57.

Papike, J. J., Ryder, G. & Shearer, C. K. (1998). Lunar materials. In: Papike, J. J. (ed.)

Planetary Materials. Mineralogical Society of America, *Reviews in Mineralogy* 36, 5.1-5.234.

Pun, A., Shearer, C. K., & Papike, J. J. (1992). A comparison of the trace element chemistries of pyroxenes between two unequilibrated eucrite clasts: A eucrite from the Kapoeta howardite and the Pasamonte eucrite. *Meteoritics*, 27.

Ray, D., & Ghosh, S. (2022). The unusual low Mg rock clasts from Lohawat Howardite, India: Petrogenetic implications. *Journal of Earth System Science*, 131(2), 125.

Reid, A. M., Buchanan, P., Zolensky, M. E., & Barrett, R. A. (1990). The Bholghati howardite: Petrography and mineral chemistry. *Geochimica et Cosmochimica Acta*, 54(8), 2161-2166.

Righter, K., & Drake, M. J. (1997). A magma ocean on Vesta: Core formation and petrogenesis of eucrites and diogenites. *Meteoritics & Planetary Science*, 32(6), 929-944.

Rollinson, H. R. (2014). Using geochemical data: evaluation, presentation, interpretation. Routledge.

Ruzicka, A., Snyder, G. A., & Taylor, L. A. (1997). Vesta as the howardite, eucrite and diogenite parent body: Implications for the size of a core and for large-scale differentiation. *Meteoritics & Planetary Science*, 32(6), 825-840.

Ryder, G., Norman, M. D., and Score, R. A. 1980. The Distinction of Pristine from Meteorite-Contaminated Highlands Rocks Using Metal Compositions (Abstract). 11th Lunar and Planetary Science Conference Proceedings. pp. 11471-9

Sarbadhikari, E. A. B. Multiple stages of early evolution of heterogeneous type-7 piplia kalan.

Shearer, C. K., Fowler, G. W., & Papike, J. J. (1997). Petrogenetic models for magmatism on the eucrite parent body: Evidence from orthopyroxene in diogenites. *Meteoritics & Planetary Science*, 32(6), 877-889.

Shirai, N., Okamoto, C., Yamaguchi, A., & Ebihara, M. (2016). Siderophile elements in brecciated HED meteorites and the nature of projectile materials in HED meteorites. *Earth and Planetary Science Letters*, 437, 57-65.

Sisodia, M. S., Shukla, A. D., Suthar, K. M., Mahajan, R. R., Murty, S. V. S., Shukla, P. N., ... & Natarajan, R. (2001). The Lohawat howardite: Mineralogy, chemistry and cosmogenic effects. *Meteoritics & Planetary Science*, 36(11), 1457-1466.

Stolper, E. (1977). Experimental petrology of eucritic meteorites. *Geochimica et Cosmochimica Acta*, 41(5), 587-611.

Tagle, R., & Berlin, J. (2008). A database of chondrite analyses including platinum group elements, Ni, Co, Au, and Cr: Implications for the identification of chondritic projectiles. *Meteoritics & Planetary Science*, 43(3), 541-559.

Warren, P. H. (1997). Magnesium oxide-iron oxide mass balance constraints and a more detailed model for the relationship between eucrites and diogenites. *Meteoritics & Planetary Science*, 32(6), 945-963.

Warren, P. H., & Jerde, E. A. (1987). Composition and origin of Nuevo Laredo trend

eucrites. *Geochimica et Cosmochimica Acta*, 51(3), 713-725.

Warren, P. H., & Kallemeyn, G. W. (2001, March). Eucrite Bluewing 001: A Stannern-like bulk composition and its linkage with other unequilibrated HED basalts. In 32nd Lunar and Planetary Science Conference (p. 2114).

Warren, P. H., Kallemeyn, G. W., Huber, H., Ulff-Møller, F., & Choe, W. (2009). Siderophile and other geochemical constraints on mixing relationships among HED-meteoritic breccias. *Geochimica et Cosmochimica Acta*, 73(19), 5918-5943.

Yamaguchi, A., Barrat, J. A., Greenwood, R. C., Shirai, N., Okamoto, C., Setoyanagi, T., ... & Bohn, M. (2009). Crustal partial melting on Vesta: Evidence from highly metamorphosed eucrites. *Geochimica et Cosmochimica Acta*, 73(23), 7162-7182.

Yamaguchi, A., Shirai, N., Okamoto, C., & Ebihara, M. (2017). Petrogenesis of the EET 92023 achondrite and implications for early impact events. *Meteoritics & Planetary Science*, 52(4), 709-721.

Zolensky, M. E., Hewins, R. H., Mittlefehldt, D. W., Lindstrom, M. M., Xiao, X., & Lipschutz, M. E. (1992). Mineralogy, petrology and geochemistry of carbonaceous chondritic clasts in the LEW 85300 polymict eucrite. *Meteoritics*, 27(5), 596-604.

Zolensky, M. E., Weisberg, M. K., Buchanan, P. C., & Mittlefehldt, D. W. (1996). Mineralogy of carbonaceous chondrite clasts in HED achondrites and the Moon. *Meteoritics & Planetary Science*, 31(4), 518-537.

# Chapter 4

## Future Outlooks

### 4.1 Ca Isotopic Analyses

Ca is a refractory lithophile element, which means that its stable isotopes do not fractionate during other planetary processes like metal crystallisation, core formation, and volatile depletion. Instead, these processes are anticipated to have little effect on Ca's isotope composition. The genetic links between typical eucrites, anomalous eucrites, howardites and the silicate components of mesosiderites, as well as the chondritic precursor material for Vesta, can therefore be tested using Ca isotopes as a tracer. Mass-dependent isotope fractionation of calcium is a reliable proxy for examining the evolution of planetary magmatism and determining the genetic connections between the Solar System materials. Zhu et al. (2023) measured the mass-dependent Ca isotope compositions of HEDs and mesosiderites using MC-ICP-MS. According to the data, eucrites and diogenites showed distinct Ca isotope compositions, which is predicted to be caused by crystallization of orthopyroxene which is isotopically heavy. This Ca isotope data supports the model where the diogenites crystallized from an eucritic melt. Vesta's main constituent of calcium are eucrites, hence its  $\delta^{44}/{}^{40}\text{Ca}$  values (relative to NIST 915a) are the closest to that of the bulk silicate on Vesta ( $0.83 \pm 0.04$ ). This figure is not the same as the figures for the bulk Earth ( $0.94 \pm 0.05$ ) and Mars ( $1.04 \pm 0.07$ ), indicating that there is significant Ca isotope variability between inner solar system entities.

The bulk Earth's and Mars'  $\delta^{44}/{}^{40}\text{Ca}$  values have been reported as  $0.94 \pm 0.05$  (Kang et al., 2017) and  $1.04 \pm 0.09$  (Magna et al., 2015), respectively. In case of the moon, the lack of mantle-derived rocks makes it difficult to estimate the bulk  $\delta^{44}/{}^{40}\text{Ca}$  value accurately. Vesta certainly has a distinct  $\delta^{44}/{}^{40}\text{Ca}$  value from Earth and Mars, despite the fact that there is a fair amount of uncertainty surrounding the  $\delta^{44}/{}^{40}\text{Ca}$  value for Mars. Hence, Earth, Mars, and Vesta, the three inner solar system worlds, may have differing mass-dependent Ca isotope compositions. A reliable fingerprint to evaluate the

relationships between the Solar System constituents is the nucleosynthetic anomaly of the  $^{48}\text{Ca}$  isotope (Dauphas et al., 2014; Moynier et al., 2010; Schiller et al., 2018; Schiller et al., 2015; Zhu et al., 2023). In reality, Earth, Mars, and Vesta have distinct mass-independent  $^{48}\text{Ca}/^{44}\text{Ca}$  signatures that are in line with their mass-dependent Ca isotope differences Dauphas et al., 2014; Schiller et al., 2018). It is possible that this is due to the differing origins of the two Ca isotope fractionation processes, namely mass-dependent isotope fractionation and nucleosynthesis, because  $\delta^{44/40}\text{Ca}$  and the mass-independent  $^{48}\text{Ca}/^{44}\text{Ca}$  compositions of Earth, Mars, and Vesta do not correlate with one another.

Volatile depletion is a crucial stage of planetary development (Allègre et al., 2001) that can result in the fractionation of isotopes, even for certain more refractory elements as Si (Pringle et al., 2014), Ca, and Ti (Zhang et al., 2014). Vesta is more depleted in volatile elements than Earth and Mars, as shown by its lower Rb/Sr and K/U ratios (Davis, 2006). This volatile depletion of Vesta has been traced by Zn (Paniello et al., 2012), K (Tian et al., 2019), and Cr stable isotope observations (Zhu et al., 2019). The Ca isotope difference is most likely not the result of Ca evaporation during a volatile loss because kinetic isotope fractionation during element evaporation would enrich the heavy isotopes in the residue, which is inconsistent with the isotopically lighter Ca of Vesta relative to those of Earth and Mars. As no other planetary processes are anticipated to fractionate the Ca isotopes, their differences in isotope composition can represent the distinct source materials they formed from and may also indicate Ca isotopic heterogeneities in the inner solar system. The Ca isotope discrepancy between Earth, Moon, and Vesta indicates that their precursor materials underwent different condensation histories since they accreted in separate parts of the inner solar system.

## 4.2 Sm-Nd Systematics

When dating the achondrite meteorites, it is more difficult using the Rb-Sr method as compared to the chondritic meteorites. Low Rb/Sr ratios in bulk samples typically result in ages with low precision, but isolated minerals in many achondrites produce Rb-Sr ages below 4.5 Ga, a sign of disturbance. Better age estimations can be obtained from separated minerals from achondrites because their Sm-Nd systems are less susceptible to resetting.

Sm-Nd systematics are composed of two decay schemes: the extinct  $^{146}\text{Sm}-^{142}\text{Nd}$  ( $T_{1/2}=103$  Ma) and the long-lived  $^{147}\text{Sm}-^{143}\text{Nd}$  chronometers ( $T_{1/2}=106$  Ga). Absolute ages can be known using the  $^{147}\text{Sm}-^{143}\text{Nd}$  system. Similar to  $^{26}\text{Al}-^{26}\text{Mg}$  ( $T_{1/2}=0.73$  Ma),  $^{146}\text{Sm}-^{142}\text{Nd}$  also involves refractory lithophile elements, but due to  $^{146}\text{Sm}$ 's longer lifetime, it is better able to constrain the silicate evolution of planetary bodies formed within the first 100 Ma of the history of the solar system. The Sm-Nd system is not

just another chronometer; it is a chronometer whose parent and daughter nuclides are incompatible, lithophile, and refractory at the same time. The siderophile properties of Os (and maybe Pb) isotopes and the volatile properties of  $^{87}\text{Rb}$  and Pb (and possibly Re) isotopes are absent from the Sm–Nd system. The pair becomes even more incompatible upon differentiation of a planetary object such as Vesta, where low gravity does not allow for garnet stability.

Plagioclase and clinopyroxene, the two primary mineral phases of cumulate eucrites, exhibit a wide range of Sm/Nd ratios that differ by a factor of 4 (Wadhwa and Lugmair., 1996). The  $^{146}\text{Sm}/^{144}\text{Sm}$  ratio during meteorite formation should be more precisely estimated according to new, high-precision Sm-Nd observations of these phases. These findings will be contrasted with earlier calculations of this ratio based on internal isochrons from various achondrite groups in order to better constrain the initial  $^{146}\text{Sm}/^{144}\text{Sm}$  ratio for the Solar System, address the initial Sm-Nd isotopic homogeneity during accretion of planetary objects in the Solar System, and to better comprehend the chronology of Vestan differentiation and, in particular, its crustal evolution (Boyett et al., 2010).

Blichert-Toft et al. (2002), derived age information using 18 eucrites from the composite cumulate-basaltic eucrite isochron, which gave an age of  $4464 \pm 75$  Ma. The three eucrites (Caldera, Moama, and Pasamonte) that fall on the  $^{147}\text{Sm}-^{144}\text{Nd}$  isochron clearly correspond to three of the four eucrites that have been proven to have noticeably higher  $^{17}\text{O}$  than other eucrites (Wiechert et al., 2002). Ibitira, the fourth eucrite with an abnormal oxygen isotope composition, is normal for Sm-Nd. These atypical eucrites may have incorporated significant amounts of the impactor, according to the oxygen isotope data. The current  $^{147}\text{Sm}-^{144}\text{Nd}$  isochron age is supported by the remarkable coincidence between anomalous oxygen and Sm– Nd isotopic ratios, as well as the fact that Pasamonte is strongly brecciated while Caldera is a highly recrystallised impact melt (Wadhwa and Lugmair., 1996).

Boyett et al. (2010) analysed short-lived  $^{146}\text{Sm}-^{142}\text{Nd}$  and long-lived  $^{147}\text{Sm}-^{143}\text{Nd}$  chronometers in three cumulate eucrites (Binda, Moore County and Moama). Plagioclase and pyroxene, the two main mineral phases found in these achondrites, exhibit a wide range of Sm/Nd ratios that enable well-resolved Sm-Nd isochrons. This set of meteorites is thus suitable to better constrain the Solar System’s initial  $^{146}\text{Sm}/^{144}\text{Sm}$  ratio. According to data from Binda and Moore County, the last Sm-Nd isotopic closure took place at around 4547 Ma. The ages obtained from Hf-W internal isochron studies on eucrites are fully consistent with this event, which cannot be linked to the HED planetesimal melting that appears to have taken place during the first 5 Ma of the solar system’s history as identified from studies of very shortlived chronometers in eucrites. The initial radiogenic Nd isotope composition and range of Sm-Nd ages show that Moama’s history is more complicated and that its evolution likely took place over several stages.

The  $^{146}\text{Sm}/^{144}\text{Sm}$  ratios determined for Binda and Moore County agree with earlier calculations based on internal isochrons from angrite, eucrite, and mesosiderite. The best estimate of the solar system's  $^{146}\text{Sm}/^{144}\text{Sm}$  ratio at 4568 Ma has been produced by Boyet et al. (2010) by meticulously compiling and analysing all the  $^{146}\text{Sm}-^{142}\text{Nd}$  literature data acquired on internal isochrons of achondrites. According to this study, Sm and Nd were homogeneously distributed and isotopically uniform throughout the solar system at the planetary scale, at least where the achondrites and terrestrial planets formed.

### 4.3 Oxygen Isotopic Compositions

Although meteorites belonging to the howardite, eucrite, and diogenite (HED) clan are frequently referred to as Vesta meteorites, there is still some debate about whether Vesta is the only parent body for HEDs. In earlier investigations of oxygen isotopes, several estimates of the number of HED parent asteroids have been made. The fundamental point of contention is whether Vesta's intrinsic isotopic heterogeneity or other causes, such as terrestrial weathering, the addition of exogenous material during brecciation, or heterogeneous oxygen isotopic compositions in specific HEDs, are to blame. The oxygen isotopic data can be used to reassess whether all HED meteorites originate from the same parent body or to limit the number of possibly multiple parent asteroids.

Recently, it was discovered that some V-type asteroids do not have a dynamic relationship with Vesta (Florczak et al., 2002; Sykes and Vilas, 2001; Wasson, 2013). Magnya and 1995WC7 are two recently found basaltic asteroids in the asteroid belt that have no relationship to Vesta and have distinct reflectance spectra (De Sanctis et al., 2011; Pieters et al., 2005). Furthermore, according to Wasson (2013)'s analysis of iron meteorites, at least 26 distinct asteroids could be the origin of igneous achondrites that resemble the HED meteorites. Thus, a growing number of studies indicate that Vesta may not be the only region where HED meteorites are formed, despite the fact that it ejected V-type asteroids into space.

Since R.N. Clayton first suggested using oxygen isotopes to classify meteorites (Clayton et al., 1976), the difference in  $^{17}\text{O}$ , or the offset from the terrestrial fractionation line in an oxygen three isotope diagram, has been an effective indicator of which meteorites cannot have come from the same parent body (Clayton and Mayeda, 1983, 1996; Greenwood et al., 2006, 2017). Nine eucrites were the subject of an oxygen isotope analysis by Clayton and Mayeda in 1983, who discovered that they had consistent oxygen isotopic compositions and that their  $^{17}\text{O}$  values differed significantly from those of Earth and the terrestrial planets. Later studies revealed that the oxygen isotope compositions of all HED meteorites were uniform (Clayton and Mayeda, 1996; Wiechert et al., 2004). However, oxygen isotope analysis was unable to distinguish the HED meteorites from angrites

and pallasites due to the limits of analytical methods at the time (Clayton and Mayeda, 1996). The precision of oxygen isotope analysis has greatly increased recently with the use of infrared laser fluorination technology. As a result, the oxygen isotopic compositions of HED meteorites ( $^{17}\text{O} \pm 0.24$ ), which can be totally separated from angrites ( $^{17}\text{O} \pm 0.07$ ), pallasites ( $^{17}\text{O} \pm 0.19$ ), and Earth rocks ( $^{17}\text{O} \pm 14.0$ ) (Greenwood et al., 2005, 2006, 2014; Scott et al., 2009), are realisable. However, according to Greenwood et al. (2017), the present analytical methods are still unable to separate the oxygen isotope compositions of HEDs from mesosiderites ( $^{17}\text{O} \pm 0.25$ ). However, the complexity of the oxygen isotopic compositions of the HED meteorites has increased with the development of analytical tools to gather high-quality data. When measured by high-precision analytical techniques, some meteorites (such as Ibitira), which were previously thought to be HED meteorites with "normal" oxygen isotopic compositions (i.e.,  $^{17}\text{O} \pm 0.24$ ), reveal  $^{17}\text{O}$  values significantly different from this "normal" HED value (Clayton and Mayeda, 1996; Scott et al., 2009). These HEDs are referred to as "anomalous oxygen isotope HEDs" when their  $^{17}\text{O}$  values deviate by  $3\sigma$  from the overall HED trend (Greenwood et al., 2012; Sanborn et al., 2016; Scott et al., 2009). Three different hypotheses have been proposed in response to the intense debate surrounding the interpretation of these HED meteorites with aberrant oxygen isotopes.

1. Oxygen isotope anomalies are caused by elements outside of their igneous development, such as brecciation on their parent body or terrestrial weathering. In this model, the analysed samples either contain exogenous components from the breccia-forming impacts or are combined with terrestrial weathering products (Greenwood et al., 2008, 2013; Janots et al., 2012).
2. Since oxygen isotope anomalous HEDs are thought to have formed in a particular region of Vesta, it is likely that their parent asteroid's inhomogeneities are what caused the anomalies in the first place (Delaney, 2010; Wiechert et al., 2004). (Benedix et al., 2014; Scott et al., 2009)
3. The mass-independent HED meteorites are not all from the same parent body; instead, they are differentiation products from multiple, comparable asteroids. This means that Vesta is not the only source of the HED meteorites.

It is possible to distinguish between various meteorite groups using the oxygen isotope composition of the meteorites (Clayton and Mayeda, 1996). In order to identify the parent body of HED meteorites, especially those HED meteorites with anomalous oxygen isotopes, it is crucial to understand their oxygen isotopic composition. 34 HED meteorites' oxygen isotopes were measured by Wiechert et al. (2004), who made the case that all HEDs share a parent body (Vesta) and that Vesta's fundamental isotopic

heterogeneity is responsible for 4 HEDs' abnormal oxygen isotopic compositions. Similar to this, Greenwood et al. (2005), who examined 18 HEDs, hypothesise that all HED meteorites come from Vesta and explain the oxygen isotope abnormalities in 2 HEDs as contamination by external impact debris. Scott et al. (2009), who examined 22 HED meteorites, claim, however, that six eucrites with abnormal oxygen isotopic compositions are thought to have come from five different asteroids. Greenwood et al. (2017) contend that there is still a great deal of uncertainty regarding the formation of HEDs with abnormal oxygen isotope compositions. Even though they contend that 10 eucrites with oxygen isotope anomalies may have originated from 4 separate asteroids, if a high isotopic heterogeneity or impact-related processes were assumed, only two parent bodies would be required for all HEDs. Therefore, it is still debatable and worth arguing whether or not all HED meteorites derive from a single parent body or how many separate asteroids.

## 4.4 Rb-Sr Chronology of Volatile Depletion

One distinguishing aspect of the overall chemical composition of planetary bodies in the inner solar system is the depletion of volatile elements. According to the composition of CI chondrites and the Sun, all massive planets, including the Earth, Moon, and to a lesser extent Mars, are somewhat depleted in volatile elements (e.g., Davis, 2006; Humayun and Cassen, 2000). These depletions extend to moderately volatile elements (i.e., elements predicted to condense from  $\sim$ 1250 to 650 K), and the strongest depletions have been documented for the parent bodies of angrites and eucrites (Lugmair and Galer, 1992, Nyquist et al., 1994, Papanastassiou and Wasserburg, 1969, Wasserburg et al., 1977), the IVA and IVB iron meteorites (e.g., Scott and Wasson, 1975), and for the Moon (e.g., Anders, 1977). According to Palme et al. (1988) and Wasson and Chou (1974), the majority of chondrites likewise exhibit lower volatile element abundances than CI chondrites, demonstrating that volatile element depletion is a typical characteristic of planetary bodies regardless of planet size and temperature history.

According to Humayun and Clayton (1995), Larimer and Anders (1967), Wasson and Chou (1974), Halliday (2004), and Mittlefehldt (1987), and Ringwood (1966), the depletion of volatile elements may be due to their incomplete condensation at the time of planetary accretion or it may reflect later evaporative losses during protracted accretion and differentiation. The systematics of the  $^{87}\text{Rb}$ - $^{87}\text{Sr}$  isotope can be used to obtain constraints on the timescales of volatile depletion. Rubidium is moderately volatile ( $T_C=800$  K) and separates from Sr, which is refractory ( $T_C=1464$  K), during volatile loss. The time of volatile loss is thus revealed by variations in the initial  $^{87}\text{Sr}/^{87}\text{Sr}$  ratios of volatile-poor materials. Papanastassiou and Wasserburg (1969) demonstrated in their pioneering Rb-Sr study on basaltic meteorites that basaltic eucrites define a Rb-Sr isochron and

a primitive initial  $^{87}\text{Sr}/^{87}\text{Sr}$  at the time of parent body differentiation that they named BABI (Basaltic Achondrite Best Initial).

Sr isotope data will be essential for precisely defining the early  $^{87}\text{Sr}/^{87}\text{Sr}$  ratios of eucrites and for identifying any nucleosynthetic isotope variability between basaltic achondrites and CAI. The timelines and origin of volatile element depletion in protoplanets can be assessed based on the new Rb-Sr data.

## 4.5 In-Situ Trace Element Analyses

Eucrites are among the oldest basalts in the Solar System, composed primarily of plagioclase and pigeonite, which together account for only 5 to 10% of the whole rock LREE abundances, 55 to 75% of the Eu, and 10 to 20% of the HREE abundances (Hsu and Crozaz., 1996). Eucrites can generally display a variety of textural characteristics, such as remnant primary grains, granoblastic regions with numerous triple connections, vitrophyric groundmass, mesostasis, and disturbed regions with opaque phases, such as sulphide, spinel, and chromite grains. An LA-ICP-MS would help in characterising every mineral (high & low calcium pyroxenes, plagioclase) with respect to their trace element concentrations. This will help in solving these outstanding problems:

1. Ce anomaly – A product of terrestrial weathering or impact-related processes on the Vesta.

A convincing argument is made in some studies that REE mobilisation occurs in Antarctic conditions as well as hot Sahara. This is because Cerium anomalies have been found to be present in the in situ analyses of three out of seven Antarctic eucrites (Crozaz et al., 2003), as well as in  $\sim 61\%$  of bulk rock analyses (Mittlefehldt and Lindstrom., 1991). Cerium, in Antarctic conditions, partially oxidises to  $\text{Ce}^{+4}$ , which is more insoluble than the other REE, allowing for separation from the other REE. The Ce anomalies were also observed in the individual grains of other groups of meteorites such as shergottites, nakhlites, lunar meteorites, angrites, and acapulcoites, but eucrites are the only group of cold desert meteorites that show Ce anomaly that is so prevalent in their whole rock samples (Crozaz et al., 2003).

The reason that was given is that although Ca-phosphate in the eucrites is so rich in REEs, their high U and Th concentrations must have led to the radiation damage to their crystals, and it is thus likely that most phosphates from the Antarctic eucrites must have been completely dissolved with their REEs getting mobilised (Crozaz et al., 2003; Crozaz and Plachy., 1976). The same study also emphasises the fact that the difference between the eucrites that exhibit Ce anomalies and the ones do not, is the presence of network of shock-induced fractures and cracks. For example, ALHA

76005, which majorly comprises of pyroxene and plagioclase that show Ce-anomaly, also possesses an extensive network of shock-induced microcracks (Hsu and Crozaz., 1996; Floss and Crozaz., 1991).

On the other hand, Dhaliwal et al. (2023) note that among the Antarctic eucrites they analysed, ALHA 81001 and PCA 82502 show positive Ce anomaly and both these two eucrites show vitrophyric textures, shock darkening, and evidence of remelting, which suggests that the Ce anomalies could also be attributed to impact-related processes on the Vesta. The evidence for impact contamination in eucrite meteorites are also present. The Highly Siderophile elements (HSE) are sensitive tracers of impactor contamination in samples which have low initial abundances of these elements. The data for HSE abundances in eucrites and diogenites shows HSE abundances as low as  $\sim 10\text{-}5 \times \text{CI-chondrite}$ , and elevated HSE abundances are observed for some diogenites and eucrites (Dale et al., 2012; Day et al., 2012). The compositions of these diogenites have been shown to suggest contamination by chondritic impactor material.

These studies that analysed the *in situ* trace element compositions of eucrites were performed only on eucrites that were finds. The eucrite samples that we have (Lakanagaon, Vissannapeta, and Piplia Kalan) are all falls and it would be very interesting to see how whether we detect any positive, negative, or no Ce anomaly in their low-Ca, high-Ca, and plagioclase grains. Moreover, the howardite Lohawat also presents us with cumulate eucrite, basaltic eucrite, as well as diogenetic clasts. It too being a fall will help in the inquiry of Ce anomalies and if they relate with the degree of thermal metamorphism.

## 2. The "Pristinity" of Eucrites

When it comes to eucrites, for which a thorough thermal metamorphism scheme has been put forward (Takeda and Graham., 1991), there is no established mechanism for figuring out the impact's effects through addition or volatile loss. Since the first eucrites were described, a rich diversity in petrogenetic textures and levels of brecciation have been observed in samples, and these observations, combined with the variable HSE contents of eucrites measured to date have shown the need for a eucrite-specific pristinity filter to evaluate potential impact effects. Dhaliwal et al. (2023) describe a pristinity filter, where one of the three basic criteria for classification of unbrecciated eucrites as pristine is that the interstitial metal and sulfide grains should have a low Ni/Co ratio. Moreover, one of the four expanded requirements is to have low absolute abundances of HSE (in whole-rock as well as *in situ*).

For bulk rocks, typically the low concentrations of the siderophile elements, Ni and Co ( $\sim 10\text{-}4 \times \text{CI-Chondrite}$ ), reflect the severe depletion of siderophile elements, which is predicted of the Vestan mantle by metal–silicate partitioning (Righter and

Drake., 1997). The dynamics of Ni and Co suggest that Ni in basaltic eucrites is a close proxy of impact contamination and can be used as a proxy, even in unbreciated eucrites. The pristinity filter will come in handy as such a filter is likely to help when interpreting siderophile, HSE (e.g., Os, W, Mo, Ru), volatile, and moderately volatile element (e.g., Zn, Cu) abundances and isotopic compositions that can be affected by impactor contamination, metamorphism, or shock processes.

Although these differences are not clearly correlated to thermal metamorphism, they are related to the new pristinity filter that is applied to eucrites. For instance, the isotopically lightest Zn in eucrites with high Zn concentrations likewise correlates with higher Ni/Co (Dhaliwal et al., 2023). These results indicate that only eucrites with low Ni/Co are more likely to correctly record the  $^{66}\text{Zn}/^{64}\text{Zn}$  of their sources, and that such sources are typically isotopically heavy. This example gives rise to the notion that any eucrites evaluated for these kinds of volatile investigations can be screened for "pristinity."

3. In order to better comprehend how volatile, MVE, and other elements may be distributed inside eucrite meteorites, our samples must be explored for wide range of geochemical and petrological variation. In order to estimate the total inventories of trace elements in these phases, and to estimate the total parental melt compositions of the eucrites, one important objective can be to characterise these samples for trace element distributions in the main silicate mineral phases, pyroxene and plagioclase. These results can clarify some of the crucial characteristics of mineral phases in eucrites for comprehending planetesimal volatile depletion histories when compared with bulk rock MVE concentrations.

## 4.6 References

Allègre, C., Manhès, G., & Lewin, É. (2001). Chemical composition of the Earth and the volatility control on planetary genetics. *Earth and Planetary Science Letters*, 185(1-2), 49-69.

Anders, E. (1977). Chemical compositions of the Moon, Earth, and eucrite parent body. *Philosophical Transactions of the Royal Society of London. Series A, Mathematical and Physical Sciences*, 285(1327), 23-40.

Benedix, G.K., Bland, P.A., Friedrich, J.M., Mittlefehldt, D.W., Sanborn, M.E., Yin, Q.Z., Greenwood, R.C., Franchi, I.A., Bevan, A.W.R., Towner, M.C., 2014. Bunburra Rockhole: exploring the geology of a new differentiated basaltic asteroid. In: *Lunar and Planetary Science Conference*, p. 1650.

Blichert-Toft, J., Boyet, M., Télouk, P., Albarède, F., 2002.  $^{147}\text{Sm}$ - $^{143}\text{Nd}$  and  $^{176}\text{Lu}$ - $^{176}\text{Hf}$  in eucrites and the differentiation of the HED parent body. *Earth Planet. Sci. Lett.* 204, 167–181.

Boyet, M., Carlson, R. W., & Horan, M. (2010). Old Sm–Nd ages for cumulate eucrites and redetermination of the solar system initial  $^{146}\text{Sm}/^{144}\text{Sm}$  ratio. *Earth and Planetary Science Letters*, 291(1-4), 172-181.

Clayton, R. N., & Mayeda, T. K. (1996). Oxygen isotope studies of achondrites. *Geochimica et Cosmochimica Acta*, 60(11), 1999-2017.

Clayton, R. N., Mayeda, T. K., & Rubin, A. E. (1984). Oxygen isotopic compositions of enstatite chondrites and aubrites. *Journal of Geophysical Research: Solid Earth*, 89(S01), C245-C249.

Clayton, R. N., Onuma, N., & Mayeda, T. K. (1976). A classification of meteorites based on oxygen isotopes. *Earth and Planetary Science Letters*, 30(1), 10-18.

Crozaz, G., & Plachy, A. L. (1976, April). Origin of the Apollo 17 deep drill coarse-grained layer. In *Lunar and Planetary Science Conference Proceedings* (Vol. 7, pp. 123-131).

Crozaz, G., Floss, C., & Wadhwa, M. (2003). Chemical alteration and REE mobilisation in meteorites from hot and cold deserts. *Geochimica et Cosmochimica Acta*, 67(24), 4727-4741.

Dale, C. W., Burton, K. W., Greenwood, R. C., Gannoun, A., Wade, J., Wood, B. J., & Pearson, D. G. (2012). Late accretion on the earliest planetesimals revealed by the highly siderophile elements. *Science*, 336(6077), 72-75.

Dauphas, N., Chen, J. H., Zhang, J., Papanastassiou, D. A., Davis, A. M., & Travaglio, C. (2014). Calcium-48 isotopic anomalies in bulk chondrites and achondrites: Evidence for a uniform isotopic reservoir in the inner protoplanetary disk. *Earth and Planetary Science Letters*, 407, 96-108.

Davis, A. M. (2006). Volatile evolution and loss. *Meteorites and the Early Solar System II*, 1, 295–307

Day, J. M., Walker, R. J., Qin, L., & Rumble III, D. (2012). Late accretion as a natural consequence of planetary growth. *Nature Geoscience*, 5(9), 614-617.

De Sanctis, M. C., Migliorini, A., Jasmin, F. L., Lazzaro, D., Filacchione, G., Marchi, S., ... & Capria, M. T. (2011). Spectral and mineralogical characterization of inner main-belt V-type asteroids. *Astronomy & Astrophysics*, 533, A77.

Dhaliwal, J. K., Day, J. M., & Tait, K. T. (2023). Pristinity and petrogenesis of eucrites. *Meteoritics & Planetary Science*.

- Florczak, M., Lazzaro, D., & Duffard, R. (2002). Discovering new V-type asteroids in the vicinity of 4 Vesta. *Icarus*, 159(1), 178-182.
- Floss, C., & Crozaz, G. (1991). Ce anomalies in the LEW85300 eucrite: evidence for REE mobilisation during Antarctic weathering. *Earth and Planetary Science Letters*, 107(1), 13-24.
- Greenwood, R. C., Burbine, T. H., Miller, M. F., & Franchi, I. A. (2017). Melting and differentiation of early-formed asteroids: The perspective from high precision oxygen isotope studies. *Geochemistry*, 77(1), 1-43.
- Greenwood, R. C., Franchi, I. A., Gibson, J. M., & Benedix, G. K. (2012). Oxygen isotope variation in primitive achondrites: The influence of primordial, asteroidal and terrestrial processes. *Geochimica et Cosmochimica Acta*, 94, 146-163.
- Greenwood, R. C., Franchi, I. A., Jambon, A., & Buchanan, P. C. (2005). Widespread magma oceans on asteroidal bodies in the early solar system. *Nature*, 435(7044), 916-918.
- Greenwood, R. C., Franchi, I. A., Jambon, A., Barrat, J. A., & Burbine, T. H. (2006). Oxygen isotope variation in stony-iron meteorites. *Science*, 313(5794), 1763-1765.
- Greenwood, R. C., Gibson, J. M., & Franchi, I. A. (2008, July). Hot and cold weathering: Determining the oxygen isotope composition of achondrites. In *Meteoritics & Planetary Science* (Vol. 43, No. 7, pp. A182-A182). DEPT CHEMISTRY/BIOCHEMISTRY, UNIV ARKANSAS, FAYETTEVILLE, AR 72701 USA: METEORITICAL SOC.
- Greenwood, R., Barrat, J.-A., Scott, E.R.D., Franchi, I.A., Yamaguchi, A., Gibson, J.M., Haack, H., Lorenz, C.A., Ivanova, M.A., Bevan, A., 2013. Large-scale melting and impact mixing on early-formed asteroids: evidence from high-precision oxygen isotope studies. In: 44th Lunar and Planetary Science Conference. Lunar and Planetary Institute, Houston, p. 3048.
- Halliday, A. N. (2004). Mixing, volatile loss and compositional change during impact-driven accretion of the Earth. *Nature*, 427(6974), 505-509.
- Hsu, W., & Crozaz, G. (1996). Mineral chemistry and the petrogenesis of eucrites: I. Noncumulate eucrites. *Geochimica et Cosmochimica Acta*, 60(22), 4571-4591. Humayun, M., & Cassen, P. (2000). 1. SOLAR NEBULA THERMAL STRUCTURE. Origin of the Earth and Moon, 30, 3.
- Humayun, M., & Clayton, R. N. (1995). Potassium isotope cosmochemistry: Genetic implications of volatile element depletion. *Geochimica et Cosmochimica Acta*, 59(10), 2131-2148.
- Janots, E., Gnos, E., Hofmann, B.A., Greenwood, R.C., Franchi, I.A., Bermingham, K., Netwing, V., 2012. Jiddat al Harasis 556: a howardite impact melt breccia with an H chondrite component. *Meteoritics Planet Sci.* 47, 1558–1574.

- Kang, J. T., Ionov, D. A., Liu, F., Zhang, C. L., Golovin, A. V., Qin, L. P., ... & Huang, F. (2017). Calcium isotopic fractionation in mantle peridotites by melting and metasomatism and Ca isotope composition of the Bulk Silicate Earth. *Earth and Planetary Science Letters*, 474, 128-137.
- Larimer, J. W., & Anders, E. (1967). Chemical fractionations in meteorites—II. Abundance patterns and their interpretation. *Geochimica et Cosmochimica Acta*, 31(8), 1239-1270.
- Lugmair, G. W., & Galer, S. J. G. (1992). Age and isotopic relationships among the angrites Lewis Cliff 86010 and Angra dos Reis. *Geochimica et Cosmochimica Acta*, 56(4), 1673-1694.
- Magna, T., Gussone, N., & Mezger, K. (2015). The calcium isotope systematics of Mars. *Earth and Planetary Science Letters*, 430, 86-94.
- Mittlefehldt, D. W. (1987). Volatile degassing of basaltic achondrite parent bodies: Evidence from alkali elements and phosphorus. *Geochimica et Cosmochimica Acta*, 51(2), 267-278.
- Mittlefehldt, D. W., & Lindstrom, M. M. (1991). Generation of abnormal trace element abundances in Antarctic eucrites by weathering processes. *Geochimica et Cosmochimica Acta*, 55(1), 77-87.
- Moynier, F., Agranier, A., Hezel, D. C., & Bouvier, A. (2010). Sr stable isotope composition of Earth, the Moon, Mars, Vesta and meteorites. *Earth and Planetary Science Letters*, 300(3-4), 359-366.
- Nyquist, L. E., Bansal, B., Wiesmann, H., & Shih, C. Y. (1994). Neodymium, strontium and chromium isotopic studies of the LEW86010 and Angra dos Reis meteorites and the chronology of the angrite parent body. *Meteoritics*, 29(6), 872-885.
- Palme, H., Wlotzka, F., Spettel, B., Dreibus, G., & Weber, H. (1988). Camel Donga: a eucrite with high metal content. *Meteoritics*, 23(1), 49-57.
- Paniello, R. C., Moynier, F., Beck, P., Barrat, J. A., Podosek, F. A., & Pichat, S. (2012). Zinc isotopes in HEDs: Clues to the formation of 4-Vesta, and the unique composition of Pecora Escarpment 82502. *Geochimica et Cosmochimica Acta*, 86, 76-87.
- Papanastassiou, D. A., & Wasserburg, G. J. (1968). Initial strontium isotopic abundances and the resolution of small time differences in the formation of planetary objects. *Earth and Planetary Science Letters*, 5, 361-376.
- Pieters, C. M., Binzel, R. P., Bogard, D., Hiroi, T., Mittlefehldt, D. W., Nyquist, L., ... & Takeda, H. (2005). Asteroid-meteorite links: The Vesta conundrum (s). *Proceedings of the International Astronomical Union*, 1(S229), 273-288.

Pringle, E. A., Moynier, F., Savage, P. S., Badro, J., & Barrat, J. A. (2014). Silicon isotopes in angrites and volatile loss in planetesimals. *Proceedings of the National Academy of Sciences*, 111(48), 17029-17032.

Righter, K., & Drake, M. J. (1997). A magma ocean on Vesta: Core formation and petrogenesis of eucrites and diogenites. *Meteoritics & Planetary Science*, 32(6), 929-944.

Ringwood, A. E. (1966). Chemical evolution of the terrestrial planets. *Geochimica et Cosmochimica Acta*, 30(1), 41-104 . Sanborn, M. E., Yin, Q. Z., & Mittlefehldt, D. W. (2016, March). The diversity of anomalous HEDs: isotopic constraints on the connection of EET 92023, GRA 98098, and Dhofar 700 with Vesta. In *Lunar and Planetary Science Conference* (No. JSC-CN-35242).

Schiller, M., Bizzarro, M., & Fernandes, V. A. (2018). Isotopic evolution of the protoplanetary disk and the building blocks of Earth and the Moon. *Nature*, 555(7697), 507-510.

Schiller, M., Connelly, J. N., Glad, A. C., Mikouchi, T., & Bizzarro, M. (2015). Early accretion of protoplanets inferred from a reduced inner solar system  $^{26}\text{Al}$  inventory. *Earth and Planetary Science Letters*, 420, 45-54.

Scott, E. R., & Wasson, J. T. (1975). Classification and properties of iron meteorites. *Reviews of Geophysics*, 13(4), 527-546.

Scott, E. R., Greenwood, R. C., Franchi, I. A., & Sanders, I. S. (2009). Oxygen isotopic constraints on the origin and parent bodies of eucrites, diogenites, and howardites. *Geochimica et Cosmochimica Acta*, 73(19), 5835-5853.

Sykes, M. V., & Vilas, F. (2001). Closing in on HED meteorite sources. *Earth, planets and space*, 53, 1077-1083.

Takeda, H., & Graham, A. L. (1991). Degree of equilibration of eucritic pyroxenes and thermal metamorphism of the earliest planetary crust. *Meteoritics*, 26(2), 129-134.

Tian, Z., Chen, H., Fegley Jr, B., Lodders, K., Barrat, J. A., Day, J. M., & Wang, K. (2019). Potassium isotopic compositions of howardite-eucrite-diogenite meteorites. *Geochimica et Cosmochimica Acta*, 266, 611-632.

U. Wiechert, A.N. Halliday, H. Palme, D. RumbleIII, Oxygen isotopic heterogeneity among eucrites, *Geochim. Cosmochim. Acta* 66 (2002) A834.

Wadhwa, M., & Lugmair, G. W. (1996). Age of the eucrite "Caldera" from convergence of long-lived and short-lived chronometers. *Geochimica et Cosmochimica Acta*, 60(23), 4889-4893.

Wasserburg, G. J., Tera, F., Papanastassiou, D. A., & Hunkele, J. C. (1977). Isotopic and chemical investigations on Angra dos Reis. *Earth and Planetary Science Letters*,

35(2), 294-316.

Wasson, J. T. (2013). Vesta and extensively melted asteroids: Why HED meteorites are probably not from Vesta. *Earth and Planetary Science Letters*, 381, 138-146. Wasson, J. T., & Chou, C. L. (1974). Fractionation of moderately volatile elements in ordinary chondrites. *Meteoritics*, 9(1), 69-84.

Wiechert, U. H., Halliday, A. N., Palme, H., & Rumble, D. (2004). Oxygen isotope evidence for rapid mixing of the HED meteorite parent body. *Earth and Planetary Science Letters*, 221(1-4), 373-382.

Zhang, J., Huang, S., Davis, A. M., Dauphas, N., Hashimoto, A., & Jacobsen, S. B. (2014). Calcium and titanium isotopic fractionations during evaporation. *Geochimica et Cosmochimica Acta*, 140, 365-380.

Zhu, K., Hui, H., Klaver, M., Li, S. J., Chen, L., & Hsu, W. (2023). Calcium isotope evolution during differentiation of Vesta and calcium isotopic heterogeneities in the inner solar system. *Geophysical Research Letters*, 50(4), e2022GL102179.

Zhu, K., Schiller, M., Moynier, F., Groen, M., Alexander, C. M. O. D., Davidson, J., et al. (2023). Chondrite diversity revealed by chromium, calcium, and magnesium isotopes. *Geochimica et Cosmochimica Acta*, 342, 156–168

Zhu, K., Sossi, P. A., Siebert, J., & Moynier, F. (2019). Tracking the volatile and magmatic history of Vesta from chromium stable isotope variations in eucrite and diogenite meteorites. *Geochimica et Cosmochimica Acta*, 266, 598-610.